

8-30-2018

Investigation of Flow Mechanisms in Gas-Assisted Gravity Drainage Process

Iskandar Dzulkarnain

Louisiana State University and Agricultural and Mechanical College

Follow this and additional works at: https://digitalcommons.lsu.edu/gradschool_dissertations



Part of the [Petroleum Engineering Commons](#)

Recommended Citation

Dzulkarnain, Iskandar, "Investigation of Flow Mechanisms in Gas-Assisted Gravity Drainage Process" (2018). *LSU Doctoral Dissertations*. 4700.

https://digitalcommons.lsu.edu/gradschool_dissertations/4700

This Dissertation is brought to you for free and open access by the Graduate School at LSU Digital Commons. It has been accepted for inclusion in LSU Doctoral Dissertations by an authorized graduate school editor of LSU Digital Commons. For more information, please contact gradetd@lsu.edu.

INVESTIGATION OF FLOW MECHANISMS IN GAS-ASSISTED GRAVITY
DRAINAGE PROCESS

A Dissertation

Submitted to the Graduate Faculty of the
Louisiana State University and
Agricultural and Mechanical College
in partial fulfillment of the
requirements for the degree of
Doctor of Philosophy

in

The Craft & Hawkins Department of Petroleum Engineering

by

Iskandar Dzulkarnain

B.Eng., University of Technology PETRONAS, 2007

M.S., University of Technology PETRONAS & Heriot-Watt University, 2010

December 2018

Acknowledgments

This work would not be possible without the guidance and patience from my advisor, Dr. Dandina Rao. He has a way of interacting with his students that make them feel appreciated, inspired and always motivated to push more, and when the time gets tough, to endure and persevere over the course of their graduate study to see to it until its eventual completion. To him I would say thank you and extend my heartfelt gratitude.

I would also like to thank my former advisor, Dr. Seung Kam for his guidance in the beginning of my doctoral study. He is the role model I seek to emulate when it comes to teaching and research.

I thank my committee members, Dr. Mehdi Zeidouni, Dr. Mayank Tyagi and Dr. Samuel Snow for their support and useful comments as my committee members. My thank also goes to Dr. Mileva Radonjic who was on my committee initially and had provided valuable suggestions during the Proposal Defense.

I would like to acknowledge the funding received toward completion of this study which came from two sources. Craft and Hawkins Department of Petroleum Engineering has given me the opportunity as graduate teaching assistant during the duration of my study while University of Technology PETRONAS provided me with financial support under their Staff Development Program.

I would also take this opportunity to thank the members of Enhanced Oil recovery group past and present including Dr. Mohamed Al Riyami, Dr. Bikash D. Saikia, Dr. Paulina Mwangi, Dr. Watheq Al-Mudhafar, Mohammad Foad Haeri, Alok Shah and Abdullah At-Tamimi.

Many thanks also go to the Malaysian and Indonesian communities in Lafayette, Baton Rouge and New Orleans for their hospitality and many memorable moments shared during our frequent gatherings. I would like to mention Melati Tessier and Aunt Rubaiyah for their kindness and help during our stay in Baton Rouge. It was also due to them that we are introduced to Louisiana dishes such as crawfish etouffee, gumbo and jambalaya. This

work is dedicated to my parents and to my beloved wife Norashikin Mohd Said and our children: Mushab, Wafa, Abdullah and Asma.

Table of Contents

ACKNOWLEDGMENTS	ii
LIST OF TABLES	vi
LIST OF FIGURES	vii
ABSTRACT	xi
CHAPTER	
1 INTRODUCTION	1
1.1 Background of the research	1
1.2 Problem statement and motivation of research	4
1.3 Aim and scope of the research	5
1.4 Significance of the research	5
1.5 Overview of the dissertation	6
2 LITERATURE REVIEW	7
2.1 Pioneering study	7
2.2 Investigation of displacement mechanism	10
2.3 Modeling studies for gravity drainage	25
3 EXPERIMENTAL SETUP, MATERIAL, AND PROCEDURE	28
3.1 Experimental setup	28
3.2 The material	33
3.3 Experimental procedures	34
4 GRAVITY DRAINAGE EXPERIMENTS FOR SPREAD- ING AND NON-SPREADING SYSTEMS	42
4.1 Experimental results	42
4.2 Pore-scale mechanisms	81
4.3 Analysis of results with dimensionless groups	97
5 EVALUATION OF EXISTING GRAVITY DRAINAGE MODELS	118
5.1 Goodness-of-fit parameter for gravity drainage models	118
5.2 Dykstra model	120
5.3 Schechter-Guo model	127
5.4 Li-Horne model	135
5.5 Discussion and summary	141
6 CONCLUSIONS AND RECOMMENDATIONS	146
REFERENCES	150

APPENDIX	
A	PROGRAM CODES FOR SCHECHTER-GUO MODEL 156
B	PROGRAM CODES FOR DYKSTRA MODEL 158
C	PROGRAM CODES FOR LI-HORNE MODEL 163
VITA 165

List of Tables

2.1	Residual oil saturation (S_{org}) after gravity drainage under various spreading and wetting conditions.....	15
3.1	Fluid systems used in experiments.	33
3.2	Fluid densities and viscosities used in experiments.	33
3.3	Matrix of experimental work	34
4.1	Summary of experimental results for free-fall gravity drainage, secondary controlled gravity drainage and tertiary controlled gravity drainage.....	43
4.2	Pore scale configurations and oil recoveries for gravity drainage experiments.	89
5.1	Performance of Dykstra model in FGD, secondary GAGD and tertiary GAGD experiments.....	126
5.2	Performance of Schechter-Guo model in FGD, secondary GAGD and tertiary GAGD experiments.	134
5.3	Performance of Li and Horne model in FGD, secondary GAGD and tertiary GAGD experiments.	140
5.4	Best curve fit results from Dykstra, Schechter and Guo and Li and Horne models for FGD, secondary GAGD and tertiary GAGD experiments.....	141

List of Figures

1.1	Schematic of Gas-Assisted Gravity Drainage (GAGD) process	3
2.1	Three phases fluid configuration on a water-wet surface	11
2.2	Spreading oil covering water-wet surface	12
2.3	Geometry model showing formation of oil layer in wedge-shaped pore	22
3.1	Experimental setup for water injection.	29
3.2	Experimental setup for oil injection.	29
3.3	Experimental setup for gas injection.....	30
3.4	Procedures to measure contact angle of oil-wet sand.	37
3.5	The steps performed during each experiment with water-wet sand.....	39
3.6	The steps performed during each experiment with oil-wet sand.....	39
4.1	Recovery profile of FGD, secondary CGD and tertiary CGD in water-wet sand.....	44
4.2	Time-lapsed photos of water-wet GAGD in FGD mode	46
4.3	Time-lapsed photos of water-wet GAGD in secondary CGD mode	47
4.4	Time-lapsed photos of water-wet GAGD in tertiary CGD mode.....	48
4.5	Recovery profile for secondary CGD in water-wet sand with spreading oil (Soltrol), showing regions of bulk flow and layer flow	51
4.6	Gas velocity profiles for all injection modes of GAGD in water-wet sand.	53
4.7	Recovery profile of FGD, secondary CGD and tertiary CGD in oil-wet sand.	55
4.8	Time-lapsed photos of FGD in oil-wet sand.....	57
4.9	Time-lapsed photos of secondary CGD in oil-wet sand.	58
4.10	Time-lapsed photos of tertiary CGD in oil-wet sand.	59
4.11	Gas velocity profiles for all injection modes of GAGD in oil-wet sand.	61

4.12	Recovery profile of FGD, secondary CGD and tertiary CGD in fractional-wet sand.	63
4.13	Time-lapsed photos of FGD in fractional-wet sand.	65
4.14	Time-lapsed photos of secondary CGD in fractional-wet sand.	66
4.15	Time-lapsed photos of tertiary CGD in fractional-wet sand.	67
4.16	Gas velocity profile for FGD experiments in fractional-wet sand.	69
4.17	Gas velocity profiles for secondary CGD in fractional-wet sand.	71
4.18	Gas velocity and liquid production profile for tertiary CGD in fractional-wet sand.	71
4.19	Flow-regime for FGD experiments in fractional-wet sand.	73
4.20	Oil recovery for GAGD under FGD and secondary CGD mode with all wettability conditions.	76
4.21	Oil recovery for GAGD under tertiary CGD mode with all wettability conditions	77
4.22	Ternary diagrams showing saturation paths for tertiary CGD experiments under all wettability conditions.	79
4.23	Configuration A	84
4.24	Configuration B	85
4.25	Configuration C	85
4.26	Pore scale fluid configuration in water-wet experiments	91
4.27	Pore scale fluid configuration in oil-wet experiments with Soltrol- based fluid system.	93
4.28	Pore scale fluid configuration in oil-wet experiments with low viscosity, non-spreading Decane	94
4.29	Pore scale fluid configuration in fractional-wet experiments	96
4.30	Profile of Bond Number, N_B for FGD experiments in water- wet, oil-wet and fractional-wet sand.	99
4.31	Effect of Bond Number, N_B on oil recovery for FGD experi- ments in water-wet, oil-wet and fractional-wet sand.	101

4.32	Profile of Capillary Number N_C for FGD experiments in water-wet, oil-wet and fractional-wet sand.	104
4.33	Effect of Capillary Number, N_C on oil recovery for FGD experiments in water-wet, oil-wet and fractional-wet sand.	105
4.34	Profile of Gravity Number, N_G for FGD experiments in water-wet, oil-wet and fractional-wet sand.	107
4.35	Effect of Gravity Number, N_G on oil recovery for FGD experiments in water-wet, oil-wet and fractional-wet sand.	108
4.36	Effect of N_B , N_C and N_G on liquid production in tertiary CGD experiments in water-wet, oil-wet and fractional-wet sand for both spreading and non-spreading fluid system.	111
4.37	Gas velocity as a function of time during FGD experiments in water-wet, oil-wet and fractional-wet sand showing the extent where flow is dominated either by capillary, viscous or gravity force.	113
5.1	Curve fit results using data from FGD experiments for Dykstra model.	122
5.2	Curve fit results using data from secondary GAGD experiments for Dykstra model.	123
5.3	Curve fit results using data from tertiary GAGD experiments for Dykstra model.	124
5.4	MATLAB GUI for solving Schechter and Guo (1996) model	129
5.5	Curve fit results using data from FGD experiments for Schechter-Guo model.	130
5.6	Curve fit results using data from secondary GAGD experiments for Schechter-Guo model.	131
5.7	Curve fit results using data from tertiary GAGD experiments for Schechter-Guo model.	132
5.8	Curve fit results using data from FGD experiments for Li-Horne model.	137
5.9	Curve fit results using data from secondary GAGD experiments for Li-Horne model.	138
5.10	Curve fit results using data from tertiary GAGD experiments for Li-Horne model.	139

5.11	Performance comparison between Schechter-Guo and Li-Horne model in tertiary GAGD of fractional-wet sand for both spreading and non-spreading system	142
------	---	-----

Abstract

In this study we investigate displacement mechanism for oil recovered using Gas-Assisted Gravity Drainage (GAGD) method. For a typical oil recovery under gravity drainage, the recovery profile can be characterized by an initial bulk flow which occurs rapidly and a later film flow that extends for a longer duration. It is the latter period where film spreading, the ability of oil to spread above water in the presence of gas, is identified as the displacement mechanism responsible for recovering the remaining oil in gravity drainage process.

Literature survey indicates that mathematical models for gravity drainage do not account for film spreading mechanism adequately. To address this knowledge gap in the literature, we would conduct experiments and simulation of mathematical model. The experiments aim to understand the role of film spreading in gravity drainage recovery. This is achieved by using spreading and non-spreading oils in sand packs, where the sand is either water-wet, oil-wet or fractional-wet. We would then evaluate the existing models to account for the observations obtained from these experiments.

The experimental results show that oil recovery is higher in spreading fluid system in water-wet sands. In oil-wet sands recovery from non-spreading fluid system is higher than that of spreading fluid. For fractional-wet sands, the recovery trend is similar to that of oil-wet experiments in that the non-spreading fluid produces more oil than spreading fluid system. We explain the results in terms of pore scale mechanism and investigate the role of gravity, capillary and viscous forces during gravity drainage experiment. Curve fitting of the experimental data with gravity drainage models show that the model which incorporates film flow mechanism in its formulations is able to match most of the experimental data.

Chapter 1

Introduction

In this chapter we will present the background of the project, problem statement, aim and scope of the project, and significance of the study. Toward the end, we will give an overview of the chapters to follow.

1.1 Background of the research

Enhanced oil recovery (EOR) is the umbrella term used to describe various processes to recover additional oil from a reservoir after the reservoir undergoes natural depletion or water flooding stage. The processes that encompass EOR can fall under chemical, gas, thermal, or microbial. One common theme that unites these processes are that they employ external agents in their operations. For gas injection EOR, gases such as carbon dioxide (CO_2), nitrogen (N_2), flue gas (hot gases coming out from factory stacks) or hydrocarbon gas are the agents injected into the reservoir to effect recovery.

Under gas EOR, processes that are commonly used are continuous gas injection (CGI), water alternating gas (WAG) and Gas-Assisted Gravity Drainage (GAGD). Both CGI and WAG propagate gas horizontally through the payzone to sweep oil to the producer well. Gas-Assisted Gravity Drainage (GAGD) injects gas at the top of the payzone through a vertical well and produces the oil through horizontal well at the bottom of the payzone.

CGI commonly uses CO_2 as its injectant to take advantage of the miscible condition that develops when the injection pressure is above miscibility pressure. In this condition, CO_2 behaves as oil phase, which facilitates mass transfer of light and intermediate components in the oil into gas. Repeated contacts between CO_2 and oil enables this extraction process to continue throughout the payzone until a point is reached, where the lighter density CO_2 , laden with the extracted oil components, is produced. This process works at the microscopic level; however, due to the density difference gas tends to override, which limits the number of contacts required to make this process successful. Furthermore, macroscopic

sweep is further hampered due to viscous fingering as a consequence of adverse mobility ratio inherent in this process.

One method to improve mobility ratio in gas injection EOR is to inject water alternately with gas. This is the basic concept of WAG. Since the viscosity of water is greater than gas and oil, the mobility ratio is reduced and the displacement front travels uniformly with less fingering. Consequently, the microscopic sweep efficiency is improved.

Nonetheless, despite its supposed improvement, Rao et al. (2004) noted that in actual implementation it is difficult to maintain a uniform displacement front throughout the payzone. This is because density difference is still prevalent, leading to gas override and water underdrive in a typical WAG process. This creates an unswept region where the oil is bypassed by either gas or water. In terms of performance, this accounts for meager additional recovery of 5-10% as reported by Rao et al. (2004). In addition, if the reservoir is waterflooded for a long time prior to WAG, the excess water will contribute to water blocking effect. This effect blocks the gas from contacting oil, thus reduces the extraction process described earlier.

GAGD aims to overcome the limitation posed by CGI and WAG by using the density difference between oil and gas to its advantage. Since in nature gas tends to override, GAGD allows this to happen so that eventually a gas dome is formed at the top of the payzone (see Figure 1.1). This dome gradually descends to the bottom, replaces the pore space initially occupied by oil while the oil drains by gravity to the horizontal producer well. Rao et al. (2004) showed that the gravity stabilized displacement front achieved by GAGD can recover more oil than the previous processes.

One advantage of GAGD is that it can deliver better performance over CGI and WAG regardless whether the injection gas is miscible or immiscible with oil. Since not all reservoirs could withstand the high injection pressure required to develop miscibility; and likewise not all fields have ready access to CO₂, immiscible gas injection with GAGD would be the preferred method to realize the benefits of GAGD to a wider range of reservoirs.

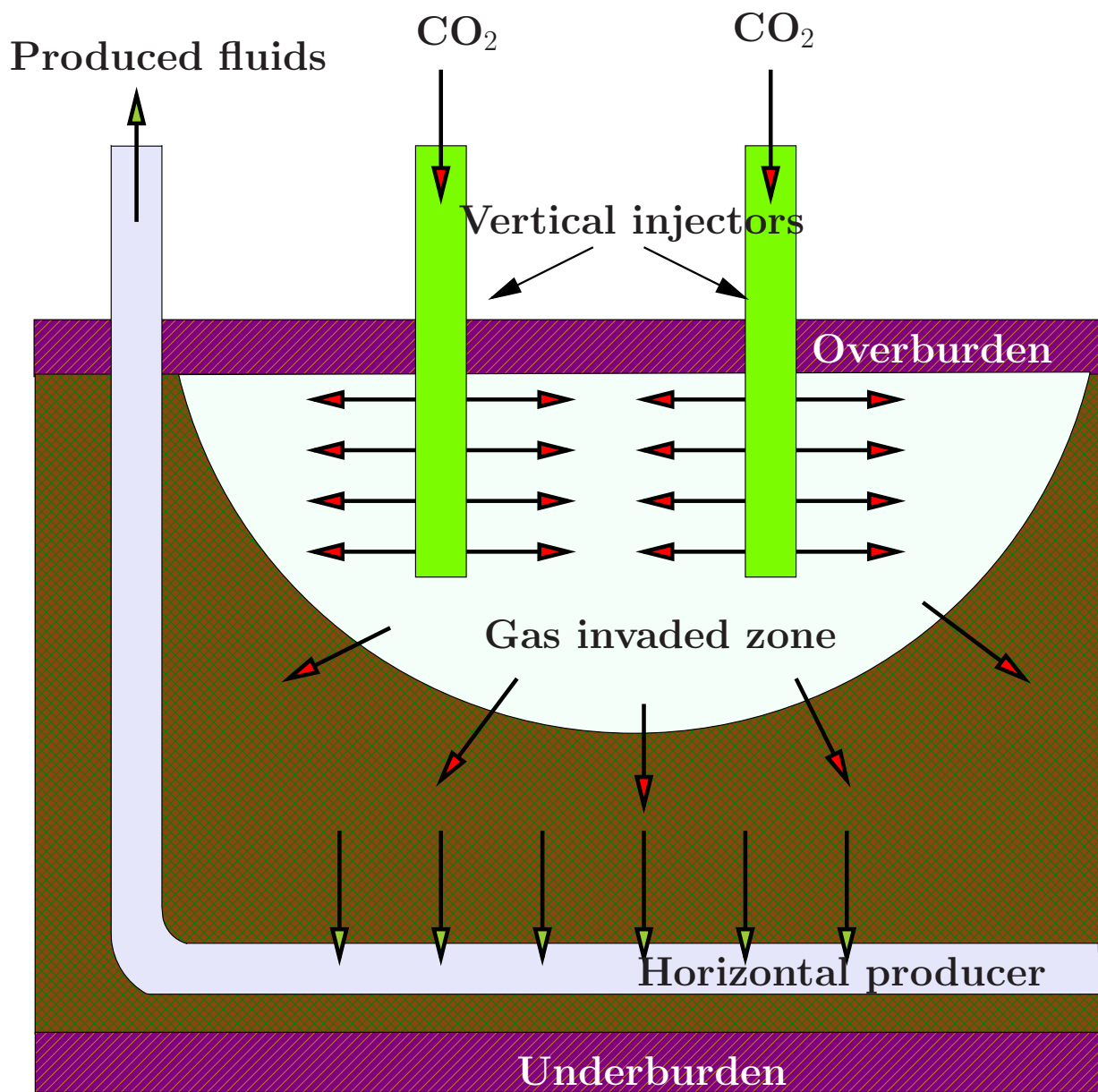


Figure 1.1: Schematic of Gas-Assisted Gravity Drainage (GAGD) process

On a pore-scale level, immiscible gravity drainage works by creating oil bank ahead of the displacement front which is then produced at the bottom of the payzone. This oil bank is formed after some time when the isolated oil blobs are reconnected through spreading film. In a water-wet rock, the oil can spread over water in the presence of the injected gas. This spreading film forms the bridge linking the bypassed oil blobs which eventually coalesce to form oil bank.

In literature, a few mathematical models have been developed for gravity drainage. However, not all models incorporate the spreading phenomenon described earlier. This leads to the model over-predicting or under-predicting the oil recovery when compared with experimental data. Furthermore, it is not known whether the existing models could match experimental data from rocks other than water-wet system. In this work the experimental results will be presented and the existing models will be evaluated to gauge their performance in characterizing gravity drainage process.

1.2 Problem statement and motivation of research

Although the literature suggests that spreading film influences oil recovery in gravity drainage, it seems paradoxical that systematic experimental investigation to understand this phenomenon is lacking. In the course of this research, we are motivated to answer the following questions:

- How would GAGD perform in water-wet, oil-wet and fractional-wet media?
- How would GAGD perform in the above conditions with spreading and non-spreading oil?
- Do the existing models account for spreading film mechanism?; and if they do,
- How would the models perform when matching gravity drainage experiments with the conditions above?

We hope the answers to the above questions illuminated by this research would help to advance understanding of oil recovery using gravity drainage process.

1.3 Aim and scope of the research

The present work aims to investigate the flow mechanisms operating in gravity drainage that experiments. As such we will run gravity drainage experiments with spreading and non-spreading oil, using sets of sand packs that are water-wet, oil-wet, and fractional-wet respectively. Specifically, we would like to achieve the following objectives:

1. To investigate effect of spreading and non-spreading behavior on oil recovery during gravity drainage in porous media with water-wet, oil-wet, and fractional-wet system.
2. To analyze and compare the results with existing literature.
3. To evaluate existing analytical models using experimental data obtained above.

To ensure successful completion of this research we limit the scope of investigation to immiscible GAGD. This is because miscibility requires high pressure, which is not possible using the setup in our laboratory. Therefore we will use nitrogen (N_2) which will be injected at low pressure. To test the spreading film behavior, we will use two types of oil; decane and Soltrol. From literature, combination of air, decane, and deionized water gives a non-spreading system; whereas air, Soltrol, and deionized water gives a spreading system. To run the experiments, we will use sand pack as the porous medium. Sand is preferable in our case since we can change the wettability by chemical treatment.

1.4 Significance of the research

This research is significant because it will help to refine our understanding of gravity drainage under various wetting and spreading conditions. The understanding gained from this study will fill the gap we found in the literature concerning the performance of gravity drainage with the conditions above since the data is sparse. On a practical level, having such

understanding will help engineers to understand interplay of various elements in gravity drainage process. This understanding will give them insights in designing field project for GAGD.

1.5 Overview of the dissertation

This study consists of six chapters. In Chapter 2, we position the research within the current literature and identify gaps that need to be addressed, particularly on the experimental aspect. By identifying the gaps we can better design the experiments and evaluate the existing models. The experimental design is the subject of Chapter 3. In that chapter we present the experimental setup, the materials used and the procedures to run the experiments. The experimental results are presented in Chapter 4. This also marks the beginning of our contribution to this research. Apart from presenting the results, we also analyze and discuss the results in light of existing literature. In Chapter 5 we used the experimental data as inputs to gravity drainage models to test their performance. Finally, Chapter 6 presents the conclusion and recommendations for future work.

Chapter 2

Literature Review

In this chapter we review the literature to identify opportunities for research. We begin with the earliest study on gravity drainage to see the extent of research during that period. Understanding research activities on gravity drainage during this time helps to set the context chronologically for later studies. This is followed by review of existing experimental studies in subsequent years.

The experimental studies we reviewed cover both the core and pore level. At the core level we look at gravity drainage experiments conducted either in sand packs or coreflood apparatus. By looking at these experimental studies, we can find areas where experimental results are lacking. These insights can be used later on when we carry out the experiments and compare the results.

Review of studies at the pore level covers experimental work using micromodels with three-phase fluids: water, oil and gas. Since we are particularly interested to understand mechanism of gravity drainage, pore level experimental work helps to understand both fluid-fluid and fluid-rock interactions occurring during three-phase flow. Such understanding establish the framework for explaining the results of experimental work at the core scale.

We then review the models that describe recovery from gravity drainage process. Our motivation here is to learn how far the existing models incorporate the mechanisms revealed from experimental work. Toward this end we will cover analytical models existing in the literature. The end of the chapter summarizes key opportunities for further investigation and outline our plan to address the knowledge gaps found in the literature, particularly with respect to experimental work and modeling study.

2.1 Pioneering study

The first reported systematic work to investigate gravity drainage as viable oil recovery method was the experimental work performed by Stahl et al. (1943). In their work Stahl et al. (1943) observed that some mature reservoirs in Oklahoma City field developed gravity

segregation and produced oil through gravity drainage. They initiated experimental study using a vertical sand pack filled with Wilcox sand to verify their observation in the field. They measured the transient and equilibrium liquid saturation distribution in the sand column and found that the liquid recovery ranged from 50 to 75 percent.

The following year Lewis (1944) published his work discussing the concept of gravity drainage in oil reservoirs and highlighted the state of the art extant at the time. Lewis work delineates the difference between gas-drive and gravity drainage conditions. In his paper he defined gravity drainage as the "self-propulsion of oil downward in the reservoir rock". This can be achieved by properly controlling the pressure reduction and withdrawal rate so that gravity segregation occurs deliberately followed by counter-current flow of gas and oil. Gas that flows to the top of the reservoir is allowed to expand as the pressure declines, creating gas cap in the process. The expanding gas cap slowly forms gas-oil front with the displaced oil forming oil bank ahead of the front. At the core of this principle is the concept of voidage replacement where gas occupies the voids left by the displaced oil as the gas cap expands. He explained that one way to gauge gravity drainage condition is taking place is by monitoring the gas-oil ratio. In a typical gas-drive displacement the GOR increases steadily and reaches maximum as the ultimate recovery is achieved which is then followed by GOR decline. For a gravity drainage condition, the GOR increases gradually towards solution GOR before it suddenly rises as the gas-oil front reaches the production well. In presenting several field examples operating under gravity drainage he suggested that more studies should be conducted to better understand the mechanism and inform operators of the possibility of producing their fields using gravity drainage.

Publication of the work above initiated work by Cardwell and Parsons (1949). They were motivated to find analytical solution to gravity drainage since the body of work concerning gravity drainage was limited to experimental study. Their derivation started with the equivalent expression for Darcy velocities of the unsaturated and saturated region in a column. Unsaturated region is at the top of the column where gas has displaced

most of the oil. The bottom of the column is the saturated region where the displaced oil accumulated before it is produced. By solving the continuity equation they formulated a partial differential equation (p.d.e) which is second order and non-linear. Since the solution is difficult they simplified the model by neglecting capillary pressure term to make the p.d.e quasilinear. The model uses empirical permeability-saturation relationship and equilibrium saturation height to predict the trajectory of gas-oil front over time. The model was validated using the experimental data from Stahl et al. (1943).

Subsequent work on gravity drainage also focused on mathematical modeling. Terwilliger et al. (1951) were motivated to investigate the effect of drainage rate on gravity drainage performance. It was understood that gravity drainage condition would develop when a suitable reservoir is drained at low rate but there was no practical method to calculate the rate at which gravity drainage is most effective. They approached this problem by conducting experiment in a vertical sand pack and measuring the conductivity over time to determine the brine saturation distribution in the column. By repeating the experiment at different drainage rate they were able to compare the saturation profiles. Their experiments showed that at low drainage rate the individual curve in the saturation profile traveled at the same rate and maintain its shape until breakthrough. The almost piston-like curve was called "stabilized zone". It was under the stabilized zone condition that most of the brine was displaced. They used Buckley and Leverett (1942) solution to calculate the saturation profile and found close match with experimental data. Their work showed the practical use of Buckley-Leverett solution to calculate the saturation profile in gravity drainage experiment and determine which drainage rate would lead to a stabilized zone.

In the 1950's publications from several workers further extend our understanding of gravity drainage. Marx (1956) showed that centrifuge experiment can be used to replicate gravity drainage recovery in consolidated porous media. Matthews and Lefkovits (1956) conducted gravity drainage experiments and analyzed the results using hyperbolic decline

curve. Essley et al. (1958) discussed application of gravity drainage in steeply dipping reservoir and presented calculations to predict gravity drainage performance.

So far the pertinent aspect of gravity drainage recovery, which is the spreading film mechanism has not been addressed in the literature. One exception is the work from Nenniger and Storrow (1958). They presented a model to calculate the saturation-time profile for liquid drainage in a packed bed under gravity. The differential equation is solved using a series solution. The effect of film drainage on the packed bed is incorporated using integration of Navier-Stokes approximate solution for film drainage down a vertical plane.

2.2 Investigation of displacement mechanism

In the previous section it was revealed that only one work incorporated film mechanism in their mathematical model (Nenniger and Storrow, 1958). However the film described in their model is not formed because of spreading or wetting phenomenon. This is because the volume of fluid contributed by the film does not distinguish whether it comes from a spreading film (fluid-fluid interaction) or wetting film (fluid-rock interaction). The lack of distinction between the film formed was because the experimental studies conducted so far had limited ability to make the spreading and wetting phenomena manifest in the experiments. This was perhaps due to the design of the experiment itself or the limited capability of the equipment used.

Only in later years, as technology improved researchers began to direct their focus to understanding the mechanisms at the physical level which contribute to gravity drainage recovery. As we will see later more experiments were conducted, both at core and pore levels to gain insights on the recovery mechanism. In the following core level refers to macroscale experimental work while pore level concerns with investigation at the microscale.

2.2.1 Experimental studies at core scale

The underlying mechanism operating in gravity drainage recovery was first identified by Dumore and Schols (1974). They conducted gravity drainage experiment by using

immiscible gas to displace oil at connate water saturation and found that the oil can be drained to very low saturation. They suggested that the residual oil was drained through spreading film. Later work by Kantzas et al. (1988a) also showed the same behavior in their experiments using consolidated and unconsolidated samples. They reported recovery of 99% for gravity drainage experiment conducted using unconsolidated sample at residual water condition. For condition at residual oil the recovery was 94%. In both cases the oil phase was Soltrol, which is a spreading oil.

The ability of oil to spread and form film over water in the presence of gas is a three-phase flow phenomenon involving interaction of the fluid-rock (wettability) and fluid-fluid (interfacial and surface tensions). This effect is commonly characterized by the parameter known as the spreading coefficient. In water-wet porous media Adamson and Gast (1997) defined this parameter as

$$S_{ow} = \sigma_{gw} - \sigma_{ow} - \sigma_{go} \quad (2.1)$$

where σ_{gw} , σ_{ow} and σ_{go} are the interfacial tensions of gas-water, oil-water and gas-oil fluid pairs respectively. Consider the fluids configuration on a water-wet surface in Figure 2.1.

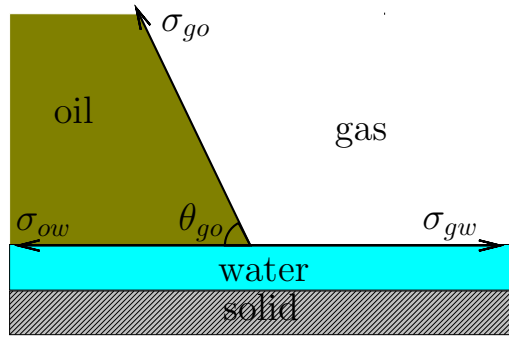


Figure 2.1: Three phases fluid configuration on a water-wet surface

A horizontal balance projection gives Equation 2.2:

$$\sigma_{go} \cos \theta_{go} + \sigma_{ow} = \sigma_{gw}. \quad (2.2)$$

A manipulation of Equation 2.1 and 2.2 shows that the spreading coefficient S_{ow} can be related to gas-oil contact angle θ_{go} (Kalaydjian and Tixier, 1991):

$$\cos \theta_{go} = 1 + \frac{S_{ow}}{\sigma_{go}}. \quad (2.3)$$

From Equation 2.2 equilibrium is possible when the spreading coefficient is negative because $|\cos \theta_{go}| \leq 1$. Therefore oil phase forms droplet or lens on the water surface when S_{ow} becomes less than $-2\sigma_{go}$.

A positive spreading coefficient, $S_{ow} > 0$ means gas-water interfacial tension, σ_{gw} is greater than the sum of oil-water and gas-oil interfacial tensions ($\sigma_{ow} + \sigma_{go}$). As such the surface tension σ_{go} becomes the dominant force per unit length over the sum of σ_{ow} and σ_{go} that is pulling the three-phase contact line in Figure 2.1. On a flat surface covered with water the oil spreads over water spontaneously in the presence of gas, as shown in Figure 2.2.

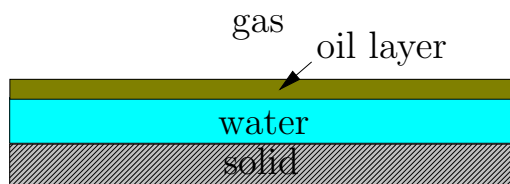


Figure 2.2: Spreading oil covering water-wet surface

The spreading oil film helps to maintain the hydraulic conductivity of the oil phase down to very low saturation (Zhou and Blunt, 1997). Kantzas et al. (1988a) explained that in a gas-assisted gravity drainage method, condition where oil as the intermediate phase is able to spread between the water-wet rock and air is favorable for oil recovery. This is because as air propagates and bypasses some of the oil, the isolated oil blobs can be reconnected to the bulk phase through the continuous path provided by the spreading film. Oil recovery is enhanced because of reduction in residual oil saturation as the reconnected oil is eventually produced at the outlet. However, when the oil is non-spreading (i.e. has negative S_{ow}) any bypassed oil remains stranded because there is no continuous path to

reconnect the oil to the bulk phase. Consequently the residual oil saturation is higher for water-wet rock with non-spreading oil.

At the core level experimental work can be broadly categorized into free-fall gravity drainage (FGD) and controlled gravity drainage (CGD) (Schechter and Guo, 1996). In FGD system the top column is open to atmosphere and ambient air is used to displace the oil. It is called free-fall because the column is drained due to the height of the saturated fluid in the column. This system replicates the gravity drainage occurring in naturally fractured rock, specifically the drainage of oil from the matrix and fracture. CGD system injects gas at fixed pressure or rate to simulate gas injection process in a typical reservoir. In most cases gas is injected at constant pressure since it is desirable for the operator to maintain the reservoir condition such that the oil phase is undersaturated and the solution gas does not evolve out of the oil phase. As Lewis (1944) explained earlier, the condition for gravity stabilized drainage can be achieved in the reservoir by simultaneously controlling both the gas injection pressure and the fluid withdrawal rate.

Experimental work by Vizika and Lombard (1996), Ren et al. (2004) and Ren et al. (2005) showed typical characteristic of film flow mechanism in action during gravity drainage. In their experimental work they observed two recovery stages characterized by time before and after break through. They reported that in the early stage of the experiment significant amount of oil is produced within a short period “bulk flow” until the gas breaks through. After break through, the oil production rate reduces dramatically over a long period “film flow” until the recovery curve reaches asymptote. It is during this second phase that the role of spreading film becomes dominant in draining residual oil behind the gas-oil front.

Since the effect of film flow becomes dominant later in the life of the reservoir, experimental work investigating the effect of film flow were often conducted under the condition of residual oil saturation. This is evident from experimental work performed by Kantzas et al. (1988a), Dullien et al. (1991), Chatzis and Ayatollahi (1993), Catalan et al. (1994), Skurdal et al. (1995), Paidin and Rao (2007), Sharma and Rao (2008), Maeda and Okatsu

(2008) and Parsaei and Chatzis (2011). This means the gas-assisted gravity drainage method is implemented as tertiary recovery after waterflooding to manifest the effect of film flow. Nevertheless experimental studies for gravity drainage under residual water saturation have also been performed by most of the authors cited above. Both setups create three-phase flow condition where water, oil and gas exist simultaneously which is a prerequisite as shown in Equation 2.1. Typically investigators would compare the oil recovery or residual oil saturation between spreading and non-spreading oil after gravity drainage experiment. Higher oil recovery or lower residual oil saturation is often attributed to the spreading oil film (Kantzas et al., 1988a; Chatzis and Ayatollahi, 1993; Vizika, 1993; Vizika and Lombard, 1996; Ren et al., 2004).

Water-wet media is typically used in experimental work investigating gravity drainage. This is because apart from spreading of the intermediate phase, another factor that influences oil recovery in three-phase flow is the wettability condition of the porous media (Vizika and Lombard, 1996). Hence in three-phase flow, such as the condition created under GAGD, both fluid-fluid interaction (spreading effect) and fluid-rock interaction (wettability effect) underlie the principal mechanism for oil recovery.

However, there still exists the need to study the oil recovery mechanism using spreading and non-spreading fluids in wettability conditions other than water-wet. We have compiled the experimental studies on gravity drainage in chronological order in Table 2.1. From the table it is seen that most of the experimental work on gravity drainage over the years concerned mainly with displacement in water-wet porous media using spreading or non-spreading oil. Based on the residual oil saturations tabulated, it is not possible to make an unambiguous conclusion regarding the performance of gravity drainage in water-wet media. Although higher recovery (lower residual oil saturation) is attributed to gravity drainage with spreading fluid in water-wet system, it is suspected that the duration of the experiment itself determines the lower bound of residual oil saturation that can be achieved after termination of the experiment. For example experimental work by Zhou

Table 2.1: Residual oil saturation (S_{org}) after gravity drainage under various spreading and wetting conditions

References	Porous media	Gravity drainage mode	S_{org} (% PV)			
			Water-wet		Oil-wet	
			Spreading ($S_{\text{ow}} > 0$)	Non-spreading ($S_{\text{ow}} < 0$)	Spreading ($S_{\text{ow}} > 0$)	Non-spreading ($S_{\text{ow}} < 0$)
Dumore and Schols (1974)	Bentheimer sandstone	N/A	2.9	3.2		
Kantzas et al. (1988a)	Bead pack	Controlled Free-fall	0.6 to 1.9 3.3 to 9.1			
Dullien et al. (1991)	Bead pack	Controlled Free-fall	2	16.9	12.7	
Chatzis and Ayatollahi (1993)	Bead pack (250-420 μm)	Controlled	1.6 to 13			
		Free-fall	14			
	Bead pack (600-710 μm)	Controlled Free-fall	1 to 7 16			
Catalan et al. (1994)	Bead pack	Controlled	2	16.9		
		Free-fall			12.7	
	Berea sandstone	Controlled	11.5 to 27.1		13.8	
	Pembina sandstone	Controlled			14.2 & 32.1	
Blunt et al. (1994)	Sand pack	Free-fall/Controlled	4 & 10.5			
Blunt et al. (1995)	Sand pack (long column)	Free-fall/Controlled	7.6 to 14	16.3		
	Sand pack (short column)	Free-fall/Controlled	14.5 to 20.6	21.8		
Catalan and Dullien (1995)	Sand pack (homogenous)	Controlled	6.1			
	Sand pack (heterogenous)	Controlled	10.7			
Skurdal et al. (1995)	Bentheimer sandstone	Controlled	4.7	6.7	12.6	1.1
Vizika and Lombard (1996)	Sand pack	Free-fall	11	23	21	22
Zhou and Blunt (1997)	Sand pack (purified sand)	Free-fall	0.13	1.13 & 1.49		
	Sand pack (red sand)	Free-fall	0.35	3.11 & 5.25		
Kulkarni and Rao (2006a)	Berea sandstone	Controlled		22 to 39.1		
Maeda and Okatsu (2008)	Berea sandstone	Controlled	34.2			
Parsaei and Chatzis (2011)	Bead pack	Controlled	3.98 to 11.3			

and Blunt (1997) showed very low residual oil saturation ($S_{\text{org}} = 0.13$ %PV) for spreading system compared to non-spreading system after the experiment was run for three weeks.

Table 2.1 also shows that experimental studies on gravity drainage in non-water-wet porous media are sparse. To date only Dullien et al. (1991), Catalan et al. (1994), Skurdal et al. (1995), Vizika and Lombard (1996), and Paidin and Rao (2007) (not tabulated because S_{org} data was absent) have moved in this direction. Using sand pack and positive spreading oil (Soltrol), Catalan et al. (1994) found that oil-wet system recovered less residual oil than water-wet system. Vizika and Lombard (1996) observed that the residual oil saturation in oil-wet system is similar regardless the sign of the spreading coefficient. Prior study by Skurdal et al. (1995) exhibited contrary trend to that of Vizika and Lombard (1996) in which residual oil saturation is lower for non-spreading oil than spreading oil in oil-wet system. Paidin and Rao (2007) found that oil-wet system with negative spreading oil recovered more oil than water-wet system. From these studies it is evident that more systematic study is needed to investigate this aspect of gravity drainage.

2.2.2 Experimental studies at pore scale

Kantzas et al. (1988b) conducted gravity drainage experiment in a vertical micro-model to visualize the pore-level mechanisms. They observed in a typical water-wet gravity drainage experiment when the gas-oil front was advancing the oil blobs downstream could behave in several ways. The blobs either coalesced into an oil bank which then drained to the outlet or pushed into smaller pores which were then bypassed. If there were no oil blobs downstream the advancing front would thin out with oil film being formed along the pathway. Their work shows the importance of oil film mechanism in water-wet media for oil recovery with gas-assisted gravity drainage.

Further investigations at the pore level were conducted by Øren and Pinczewski (1991), Oren et al. (1992) and Oren and Pinczewski (1994). They were motivated to investigate the three-phase flow mechanism during immiscible gas injection from micromodel experiments.

Their work revealed that three-phase flow process such as that occurring in gravity drainage could be very complex. This is because spreading behavior and wettability affect the fluids pore occupancy and their subsequent mobility. Compared to two-phase system where one phase is wetting and the other non-wetting, in three-phase there is a third phase which is the intermediate phase. The presence of the intermediate phase complicates the fluid configuration at the pore scale and affects the displacement mechanism. In their micromodel experiments they have identified three mechanisms for fluid transport namely direct drainage, double drainage and imbibition-drainage. Direct drainage is a mechanism where a non-wetting or intermediate phase displaces a wetting phase. Double drainage involves two adjacent direct drainage events happening one after another with a non-wetting phase displacing an intermediate phase followed by the intermediate phase displacing a wetting phase. In imbibition-drainage an intermediate phase displaces a non-wetting phase (imbibition event) followed by the non-wetting phase displaces the wetting phase (drainage event).

Øren and Pinczewski (1991) calculated the film thickness for wetting film (water) and spreading film (oil) using augmented Young-Laplace equation. The stability of the film was due to positive disjoining pressure. The calculated film thickness matched measured film thickness from micromodel. They also calculated the velocity field from the film thickness which was then used to estimate the conductivity of the film. The velocity field was integrated over the film cross-section in order to get the average phase velocity. Their calculations showed that average phase velocity increased rapidly when the oil viscosity was low. Their work quantified film thickness for wetting and spreading phase and showed realistic estimate of the film conductivity in a micromodel experiment.

The implication of this phenomenon on oil recovery is further studied by Oren et al. (1992) using micromodel. Oren et al. (1992) investigated the pore-level physics of thin film flow in immiscible tertiary gas displacement and introduced the "double displacement drainage" mechanism as responsible in propagating the gas-oil and oil-water front for a

spreading, water-wet system. The mechanism is possible when spreading oil film exists between water phase and gas phase. Oren et al. (1992) explained that in order to mobilize the stranded residual oil blobs, they need to be reconnected to form larger oil bank through hydraulic path established by the spreading film. Oren et al. (1992) further observed that early in the flow, as gas invaded the pores, the oil-water interfaces propagated easily to outlet through low resistance path provided by the water-wetting film. Later, as the water drained out, the oil-water interfaces had to go through high resistance path provided by the spreading film, which slowed down their propagation. Comparison with non-spreading system using the same micromodel showed the spreading system yields 40% of the residual oil while only 18% for the non-spreading system.

The reason non-spreading system yields lower tertiary recovery is further explained by Oren (1994). In negative spreading water-wet system, oil does not spread in thin film in the presence of gas and water. Instead there exist three phase contact line between gas-oil and oil-water interfaces to minimize the free energy of the system. Additional three phase contact lines are formed when gas invades pores containing oil. This causes the displaced oil to be broken into smaller blobs and trapped in the surrounding pore throats. Film flow occurs mostly in pore throat connecting the pore bodies. When gas-oil front advances from pore throat to pore body, there exists a pressure gradient for oil flow. The pressure gradient causes the oil displaced in the pore body to flow counter current through the film along the pore throat.

Experimental results from Oren et al. (1992) were further analyzed and simulated using invasion percolation network model by Oren (1994). The simulation results were shown to be generally agreed with experiments. Negative spreading system showed lower oil recovery because there was less gas saturation distributed across the network model. This was because little bypassed oil was reconnected due to lack of double drainage displacement taking place. Even when double drainage displacement occurred, the displaced oil broke down into isolated oil blobs. Since there was absence of spreading film, the oil had no

path to reconnect with oil behind the gas front and consequently was trapped in pore throats. Capillary fingering of gas continued throughout the system, which resulted in early gas breakthrough and higher residual oil saturation. When gas invasion occurred in an oil filled-pore for a positive spreading system, the presence of oil film provided a path for the displaced oil to reconnect with the oil behind the gas front. This process was observed to be repeated across the network, which lead to formation of oil bank and later, lower residual oil saturation when the oil bank was produced.

Interestingly, Oren (1994) also demonstrated that increasing the magnitude of the positive spreading coefficient did not affect oil recovery for an already spreading system. Instead, for a spreading system the recovery was influenced by film flow resistance, which was quantified by film capillary number. Their results showed: i. When film capillary number was low, film conductivity was high, which lead to high oil recovery; ii. When film capillary number was high, film conductivity was low, which resulted in low oil recovery; iii. When film capillary number intermediate, the oil recovery was controlled by capillary pressure and film flow pressure. However, for negative spreading system the more negative the spreading coefficient, the less oil recovery.

Soll et al. (1993) conducted micromodel experiment to study three-phase flow fluid behavior in a capillary driven displacement. In their study they found that film transport played important role in mobilizing wetting (water) and intermediate (oil) phase fluids. This was confirmed from analysis of digital images taken during the experiment. From their observation the film was sufficiently thick to drain the wetting and spreading layer. They also found that in most cases although all three fluids were mobile, interactions at local pore involved only two phases. For example in their water-wet system the injected gas tend to prefer displacing oil either in continuous or isolated blobs before displacing water. Their work demonstrates the role of film flow during drainage and imbibition of three-phase system.

Hayden and Voice (1993) performed scanning-electron microscopy analysis to obtain images of NAPL (non-aqueous phase liquid) in a moist soil sample. The sample was saturated with brine, iodobenzene and air before frozen with liquid nitrogen to facilitate the analysis. They found that iodobenzene, which was used as the NAPL phase and has negative spreading coefficient (-8.7 mN/m) formed continuous phase at high, intermediate and low saturation. Some of the NAPL phase was found in pore wedges or irregular-shaped pore geometry. Their study gives evidence that a non-spreading oil can also form continuous phase in porous media, if the phase is located in crevices or angular features of pore spaces. This challenges the previous understanding that only spreading oil can form continuous phase when it is intermediate wetting.

Oren and Pinczewski (1994) conducted three-phase flow experiment using oil-wet micro-model to investigate the effect of spreading and wettability during immiscible gas injection. They used two sets of fluids, spreading and non-spreading oil to observe the displacement mechanisms. When comparing their results with previous work using water-wet micro-models, they found that oil recovery was higher in the oil-wet case for both spreading and non-spreading oils. They explained that better recovery was achieved in oil-wet case due to transport of the mobilized oil through thicker and more conductive oil film. In their comparison, recovery from spreading oil in water-wet micromodel was second and the lowest recovery came from non-spreading oil in water-wet system. Their work demonstrates the role of oil film, both spreading film in the water-wet case and wetting film in the oil-wet case in transporting the mobilized oil to outlet.

Blunt et al. (1994), Blunt et al. (1995), and Fenwick and Blunt (1995) approached the pore-level study of three-phase flow from geometry and intermolecular forces perspective. According to Blunt et al. (1994), oil recovery was higher for system where spreading coefficient was positive because the film was stable, and this stability determined the thickness of the film layer. The film stability is a function of capillary and intermolecular forces. The film is stable at equilibrium thickness when combination of intermolecular forces per

surface area, the disjoining pressure, is equal to capillary pressure. Components of the intermolecular forces that affect film stability are van der Waals force (vdW), the electrostatic forces and the structural force. In their paper Blunt et al. (1994) showed that structural force helped in forming stable film for the fluid system observed. The authors based their claim by comparing disjoining pressure from vdW and structural forces. vdW contributes to negative disjoining pressure, which makes the film unstable. Structural force, which is oscillatory, has an initial maximum positive disjoining pressure which decrease with time so that it is equal to capillary pressure at equilibrium thickness.

Based on pore geometry calculation, Blunt et al. (1995) and Fenwick and Blunt (1995) claimed that non-spreading system could actually form film under the initial condition that the thick oil layer was thinning, which usually happened behind the gas-oil front as it advanced. Their finding was contrary to what had been observed by Oren et al. (1992). Subsequent experimental study with micromodel by Keller et al. (1997) using decane as non-spreading oil phase seemed to support Blunt et al. (1995) and Fenwick and Blunt (1995) assertion.

Keller et al. (1997) conducted micromodel experiment to investigate whether oil with negative spreading coefficient could form layer of oil between gas-water interface in a water-wet media. Their study was motivated by previous work from Dong et al. (1995). Dong et al. performed theoretical study involving free-energy calculation and demonstrated that depending on the pore geometry, oil with negative spreading coefficient could form stable layer. This was validated by their experimental work using capillary tube with angular cross-section. Keller et al. (1997) extended this result by performing experiment using micromodel etched with pattern extracted from a Berea sandstone. Since the pore geometries contained features such as angularities and crevices, they demonstrated that a stable oil layer with negative spreading coefficient could be supported in such pores when oil-water capillary pressure was greater than gas-oil capillary pressure. Using simple geometry model they showed mathematically that this was controlled by the ratio of oil-water to gas-oil radii

or the ratio of gas-oil to oil-water contact angles with the crevice half-angle. This critical ratio was expressed as:

$$R_c = \left(\frac{r_{ow}}{r_{go}} \right)_c = \left(\frac{\gamma_{ow} P_{c_{go}}}{\gamma_{go} P_{c_{ow}}} \right)_c = \frac{\cos(\theta_{go} + \beta)}{\cos(\theta_{ow} + \beta)} \quad (2.4)$$

where r_{go} and r_{ow} are the gas-oil and oil-water radii, γ_{go} and γ_{ow} are the gas-oil and oil-water interfacial tensions, $P_{c_{ow}}$ and $P_{c_{go}}$ are the oil-water and gas-oil capillary pressures, θ_{ow} and θ_{go} are the oil-water and gas-oil contact angles, and β is the half-angle of crevice respectively. The geometry model is shown in Figure 2.3.

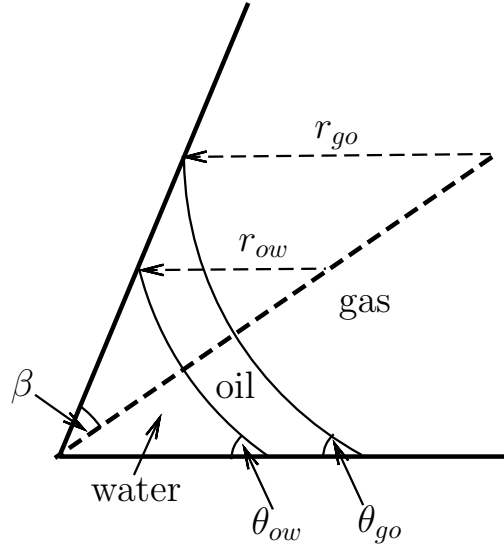


Figure 2.3: Geometry model showing formation of oil layer in wedge-shaped pore

Keller et al. (1997) showed that a stable oil layer could be formed on top of wetting water surfaces in angular crevices even when the equilibrium oil spreading coefficient was negative for value of R less than R_c . However, when the spreading coefficient became more negative, the range of capillary pressures to keep the oil layer stable decreased. Therefore formation of intermediate oil layer is not governed by the magnitude of the spreading coefficient alone but also by other factors such as pore geometries and capillary pressures.

Experimental work by Keller et al. (1997) to validate Blunt et al. (1995) and Fenwick and Blunt (1995) also revealed that for a non-spreading system, besides the double drainage mechanism mentioned earlier by Oren et al. (1992), there were four other mechanisms

involve in fluid transport. The author noted that since these four mechanisms involve gas or water displacement by either phase, they rarely occurs when oil spreads over water in the presence of gas since that will prevent gas from contacting the water directly. Keller et al. (1997) observed that in most cases, double displacement either by drainage or imbibition occurred involving two phases since the third phase usually reside in smaller pores and became immobile due to capillary force.

Keller et al. (1997) observation further explained why non-spreading system in Oren et al. (1992) micromodel did not exhibit spreading layer but Keller et al. (1997) experiment did . The difference was due to the geometry of the pores in the micromodel. In Oren's micromodel, the pore cross-section was circular while the pore space in Keller's model has rectangular cross-section. According to Keller et al. (1997) , rectangular cross-section could support formation of thick oil layer for non-spreading oil based on condition in Equation 2.4. Since $\beta = 90^\circ$ for circular pore, R will be equal to R_c and non-spreading oil will thin out. However in rectangular or angular crevice, $\beta < 90^\circ$ and for water-wet surface, $\theta_{ow} < \theta_{go}$ and R will be less than R_c . This means a thick oil layer with negative spreading coefficient could be formed across the wedge-shaped pore since oil-water capillary pressure was higher than gas-oil capillary pressure.

Vizika et al. (1998) visualized three-phase fluids in rock samples using cryo-scanning electron microscopy. They wanted to study the fluids distribution and the effect of spreading and wettability during three-phase gas injection. The experiment used two sets of fluid samples; spreading and non-spreading oil and two sets of Fontainebleau sandstones; water-wet and oil-wet. Images obtained from the experiments showed existence of oil film for spreading fluid in water-wet sample. In oil-wet sample, their results demonstrated that distribution of residual oil was not influenced by the magnitude of the spreading coefficient. They also found that distribution of water phase differed between spreading and non-spreading condition. In spreading system water was mostly mobilized while in non-spreading system most of the water was stranded.

Sohrabi et al. (2004) reported experiment using high pressure micromodel with live oil and water to investigate three-phase flow during WAG displacement. They built set of micromodels with diverse wettability conditions each (water-wet, oil-wet and mixed-wet) and saturated the micromodel with decane, a non-spreading oil. They found that in water-wet experiment, corner filament flow, through which the wetting phase is transported plays important role in oil displacement. They observed multiple displacement mechanisms taking place in the water-wet experiment; however this was absent in the oil-wet experiment. Their results showed that oil recovery was higher in the oil-wet and mixed-wet experiments. This occurred because given two pores of equal radii, gas would prefer to displace the one filled with oil rather than water since gas-oil IFT was lower.

Studies on pore-level physics above were done primarily using water-wet porous media with spreading or non-spreading oil phase. From the literature, studies on non-spreading system is lacking, possibly because the general assumption that non-spreading system recovers less residual oil than spreading system. However, non-spreading oil phase is more prevalent in actual reservoir, since reservoir crude oil consisted of higher order alkanes homologues. According to Richmond et al. (1973) and Takii and Mori (1993), alkanes series beginning with octane does not spread on water. What if it is possible to enhance the spreading ability of these higher homologues from negative spreading to positive spreading? Studies from Richmond et al. (1973), Thanh-Khac Pham and Hirasaki (1998), and Boinovich and Emelyanenko (2009) have shown that this is possible by changing the salinity of the aqueous phase. However a systematic study of changing spreading coefficient of the oil phase in a gravity drainage experiment has yet to be seen.

Review of experimental work performed above show that even at microscopic level the effect of spreading film improves oil recovery in three-phase flow in water-wet media (Kantzas et al., 1988b; Oren et al., 1992). The thickness and conductivity of the spreading layer has been calculated by Øren and Pinczewski (1991). Pore scale visualization with cryo-scanning electron microscopy (SEM) on actual core sample confirmed the existence of

spreading film Vizika et al. (1998). However, other investigators have also shown that an intermediate oil layer can be formed in wedge-shaped pores for oil with negative spreading coefficient (Dong et al., 1995). This was investigated theoretically (Blunt et al., 1994, 1995) as well as experimentally (Keller et al., 1997). Visualization using cryo-SEM by Hayden and Voice (1993) further confirmed the existence of continuous oil layer for non-spreading oil at high, intermediate and low oil saturation. Although higher oil recovery is often shown for drainage in spreading system with water-wet media, experimental studies by Oren and Pinczewski (1994) and Sohrabi et al. (2004) have proved otherwise. They demonstrated that higher oil recovery was achieved in oil-wet media instead.

Comparison between experimental studies at core and pore levels further underscore the need to investigate gravity drainage mechanism in porous media with wettability condition other than water-wet. This is because the experimental work reviewed so far has not provided a consistent conclusion regarding performance of gravity drainage in such systems. Therefore there exists opportunity to conduct experimental work in gravity drainage not only using water-wet medium, but also oil-wet and fractional-wet media, coupled with spreading and non-spreading fluids system.

2.3 Modeling studies for gravity drainage

In this section we present review of existing modeling studies for gravity drainage. Based on experimental work at core and pore scale it is determined that both spreading and wettability influence gravity drainage recovery. Here in this section we are interested to see whether such mechanisms are captured in the models.

2.3.1 Analytical modeling studies

Analytical model for gravity drainage was first derived by Cardwell and Parsons (1949) using non-linear partial differential equation. Cardwell and Parsons (1949) had to neglect the capillary pressure term in their derivation to make the solution tractable. In explaining their model, Cardwell and Parsons (1949) introduced the “demarcator” concept, which

is the gas/oil front propagation from top to bottom. This model was validated using experimental data from Stahl et al. (1943).

Terwilliger et al. (1951) used Buckley and Leverett (1942) solution to match saturation distribution data over time for their gas/water gravity drainage experiment. Hagoort (1980) also formulated his analytical model based on Buckley and Leverett (1942), but his model is in dimensionless form. Hagoort (1980) introduced an approximate solution by omitting the capillary term.

Dykstra (1978) reformulated Cardwell and Parsons (1949) equations to make it amenable for solution. He also derived a new equation to calculate the oil recovery which was absent in Cardwell and Parsons (1949) model. Similar to Cardwell and Parsons (1949) earlier, he matched the model with experimental data from Stahl et al. (1943).

All the models described so far did not consider the effect of film flow in their derivation except the model from Schechter and Guo (1996). In his derivation, Schechter and Guo (1996) began with volumetric balance and included volume contribution from film flow. Their solution retained the demarcator concept of Cardwell and Parsons (1949) and looked similar, although Schechter and Guo (1996) model was in dimensionless form .

Li and Horne (2008) included capillary pressure term explicitly in their model. By fitting experimental data to their model, one can find the initial oil production rate, the pore distribution index, and the entry capillary pressure index. These parameters were used to predict the oil recovery with their model.

The models described above mostly were designed for FGD system. The models that fall in this category were the ones from Cardwell and Parsons (1949), Dykstra (1978), Schechter and Guo (1996), Zhou and Blunt (1997), Li and Horne (2003) and Li and Horne (2008). The models that work for CGD were mainly based on Buckley and Leverett (1942) model such as Terwilliger et al. (1951) and Hagoort (1980). According to Schechter and Guo (1996), one distinction between FGD and CGD model is that for FGD, the flow rate is not known a priori. In contrast CGD models based on Buckley and Leverett (1942) either

used constant pressure or constant rate in their formulations. However this does not mean that FGD models strictly cannot be used at all for CGD experiments. In the literature there is at least one paper by Kulkarni and Rao (2006a) which attempted to model their CGD experiments using Li and Horne (2003) model.

The experimental data used to validate the models above mostly came from water-wet porous media. However, there was lack of documentation whether the oil phase used was spreading or non-spreading. More over, it was not explicitly mentioned whether the models work for other wettability systems as well. This gap is probably due to lack of experimental data with suitable parameters to test these models. Therefore there exists an opportunity to evaluate spreading or non-spreading experiments from wetting porous media other than water-wet using these models. The insights gained could be used to analyze performance of gravity drainage experiments.

Chapter 3

Experimental Setup, Material, and Procedure

In previous chapter the literature shows that most gravity drainage models do not account for spreading film behavior. Furthermore, it is not known whether the models would work if the oil recovery data comes from non-water-wet rocks. Although we can use experimental data in the literature to evaluate the models, not all reported data contain the parameters required. Moreover, there is few gravity drainage experimental data for systems such as non-spreading fluid and non-water-wet rocks. Therefore, the lack of suitable data limit our ability to evaluate the full range where the models are effective. Consequently, in this research we will conduct gravity drainage experiments to analyze the results with existing literature and evaluate the analytical models with the experimental data.

This chapter will discuss the experimental setup, the materials used and the experimental procedures. The experimental setup covers the apparatus used; the materials section describes the fluid systems and the porous media; and the section on procedures elaborates the steps performed to run the experiments.

3.1 Experimental setup

The experimental setup was designed to be modular. This means the connections and components can be rearranged and interchanged to suit the experiment. Figures 3.1, 3.2, and 3.3 respectively show the experimental setup for water, oil, and gas injection. The components that make up each system can be grouped into the fluid injection system, fluid measurement system, and sand holder.

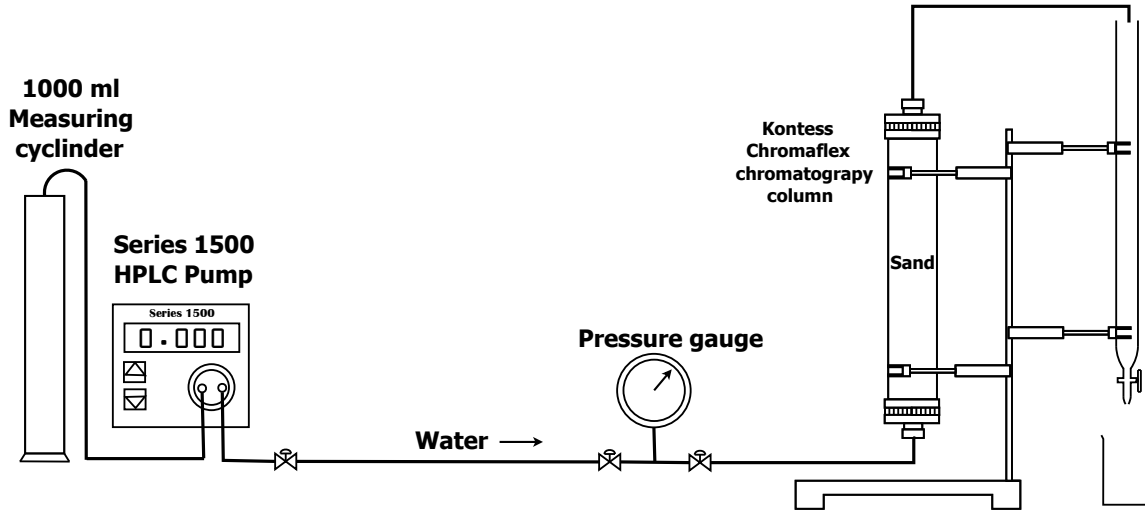


Figure 3.1: Experimental setup for water injection.

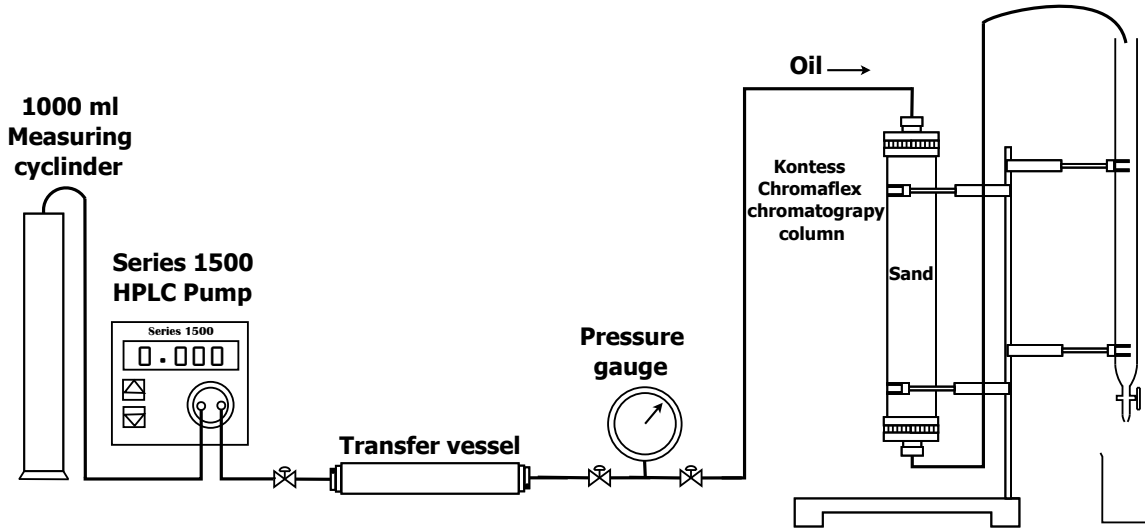


Figure 3.2: Experimental setup for oil injection.

3.1.1 Fluid injection system (oil and water)

In water injection system (Figure 3.1), the components used were HPLC pump and measuring cylinder. For oil injection system (Figure 3.2), the previous two components with the addition of transfer vessel were used.

HPLC pump: High performance liquid chromatography (HPLC) pump from Lab Alliance Series 1500 was used to pump water from the measuring cylinder. The pump can be set to operate at injection rate up to $12 \text{ cm}^3/\text{minute}$. The pumped water was

used to saturate the sand pack to get the pore volume and porosity. In addition, the pump was also used during waterflooding.

Measuring cylinder: The cylinder is graduated at 5 ml interval and can hold 1000 ml of liquid. In our experiments, the measuring cylinder was used as a water reservoir for the pump.

Transfer vessel: The vessel contains a piston which separates the inner chamber into two parts. It can hold 500 ml of liquid. The transfer vessel was used to hold the oil. During oil injection, pumped water came through the inlet port at the bottom of the transfer vessel and pushed the piston upward, which then displaced the oil through the outlet port to saturate the sand pack. The reason we used transfer vessel during oil injection is because the wetted parts inside the HPLC pump will deteriorate if the pump is used directly to pump oil.

3.1.2 Fluid injection system (gas)

For gas injection system (Figure 3.3), the components used were gas cylinder, pressure regulator, mass flow controller and master control unit (MCU).

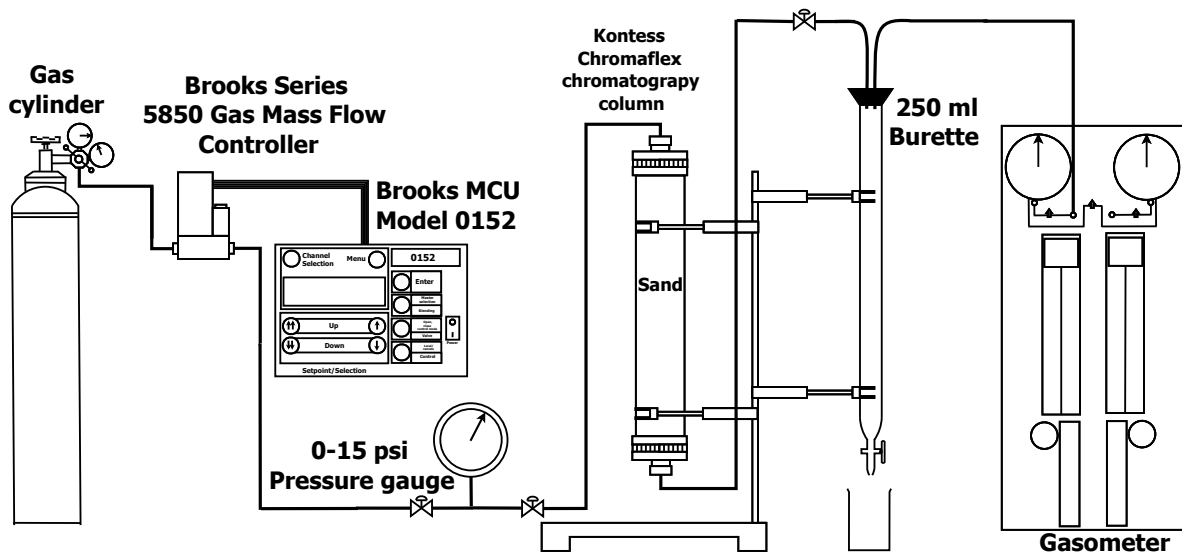


Figure 3.3: Experimental setup for gas injection.

Gas cylinder: The cylinder contained pressurized nitrogen (N_2) for use in gas injection.

The cylinder was secured firmly to the work bench using a stretch band wrapped around its body and a clamp.

Pressure regulator: The regulator was attached to the gas cylinder to set the outlet gas pressure. It was used to maintain a constant pressure during gas injection. In a typical experiment, the outlet pressure was set to 1 - 3 psi. This low pressure range was desired for gas injection experiments to achieve gravity-stabilized flow.

Mass flow controller and MCU: We used Brooks 5850i Mass Flow Controller to set the gas flow rate by adjusting the valve opening through the master control unit (MCU). These two components work together to deliver a constant rate injection. Note that in most experiments, unless otherwise noted, the gas injection was performed in constant pressure mode. This means the control valve was set to 100% open by the MCU to allow the rate to vary while the pressure was set to a constant value by the regulator.

3.1.3 Fluid measurement system

The fluid measurement system in Figures 3.1, 3.2, and 3.3 consisted of the pressure gauge, burette and gasometer. The parameters they measure are pressure, liquid volume, and gas volume respectively.

Pressure gauge: A low-pressure analogue gauge was used in the experiments. The gauge can measure pressures within the range 0 - 5 psi. Because the porous media used was unconsolidated sand, a low-pressure gauge would help to give accurate readings. This is particularly useful, for example in calculating the permeability from Darcy's law.

Burette: The burette functioned as separator for the effluent. The cylinder is graduated at 1 ml interval and can hold up to 250 ml of liquid. At the bottom of the burette, water was filled up to the first graduated line to mark as the base of the volume measurement.

Gasometer: The gasometer was used for volumetric measurement of breakthrough gas. It was connected to the top of the burette with a tube and a steel port attached to the tube's end. The steel port was inserted into an opening on a rubber stopper on top of the burette. Although the volume of gas that broke through was not used in calculation, we used the volumetric measurement by the gasometer to indicate gas breakthrough.

3.1.4 Sand holder

We used Kontes chromatography glass column to pack the sand. The glass column has diameter of 4.8 cm and length of 30 cm, which gives a bulk volume of 543 cm³. It can withstand pressure up to 50 psi. Both end caps are fitted with high-density polyethylene (HDPE) bed supports. These bed supports with microporosity filter prevent sand from coming out of the glass column during experiment. The glass column was used to hold the sand because it is easy to replace the sand when necessary to suit the experiment.

3.1.5 Video capture system

All experimental runs were captured on video using Sony HDR CX440 video recorder. This helped us to observe the gas-oil interfaces later after the experiments were completed. Because a typical run would take several hours, the videos were recorded in *Long Play* (LP) mode.

3.2 The material

In the experiments, the fluids used were Soltrol and Decane as the oil phase, deionized water as the aqueous phase, and nitrogen as the gas phase. The sand used for the sand pack was AFS 50/70 sand. Further descriptions of the materials used are given below.

3.2.1 Fluid system

The fluid systems used are shown in Table 3.1 together with their respective interfacial tensions and spreading coefficients. The fluid combinations were chosen to give spreading and non-spreading behavior as indicated by the spreading coefficients, S_{ow} . A positive S_{ow} means the oil spreads over water in the presence of gas. Conversely a negative S_{ow} indicates the oil does not spread over water. We did not measure the parameters. Rather the values were obtained from literature. The oil was dyed red with Sudan IV dye to give better contrast when observing the fluids displacement during the experiment. The densities and viscosities of the fluids used are shown in Table 3.2. Likewise with the parameters before, we used values from literature.

Table 3.1: Fluid systems used in experiments.

	σ_{wg} (dyne cm ⁻¹)	σ_{go} (dyne cm ⁻¹)	σ_{ow} (dyne cm ⁻¹)	S_{ow} (dyne cm ⁻¹)	Reference
N ₂ \Soltrol\ DI water	71.0	24.0	35.0	+12.0	Chatzis and Ayatollahi (1993)
N ₂ \Decane\ DI water	72.1	23.5	52.0	-3.4	Zhou and Blunt (1997)

Table 3.2: Fluid densities and viscosities used in experiments.

	ρ (g/cm ³)	μ (g/cm.s)	Reference
Decane	0.734	0.0084	Sharma and Rao (2008)
Soltrol	0.781	0.0274	Chatzis and Ayatollahi (1993)
Water	0.9982	0.0100	Sharma and Rao (2008)
Nitrogen	0.001165	0.0001755	Sharma and Rao (2008)

3.2.2 Sand

The sand used was AFS 50/70 sand from US Silica. This is fine sand with specific gravity of 2.65 and median particle size (D_{50}) of 0.26 mm. The sand was packed in the glass column before running the experiments. We replaced the sand with a new batch after completing each run. Some batches were treated with chemicals to change their wettability to oil-wet.

3.3 Experimental procedures

The experimental work was carried out according to procedures described in this section. The plan of experimental work is described first, followed by the procedures. These procedures include preparing the sand pack, altering the sand pack wettability, measuring the porosity and absolute permeability; and running the experiments.

3.3.1 Plan of experimental work

The experimental work was designed to cover gravity drainage experiments for spreading and non-spreading oil; in water-wet, oil-wet, and fractional-wet sand. The plan of experimental work is shown in Table 3.3. We followed this plan when conducting the experiments to give us the data which is used to compare to the mathematical models later on.

Table 3.3: Matrix of experimental work showing the combination of fluid and wettability system used in gravity drainage experiments. The numbering is used to identify the experiments.

Wettability \ Fluid	N ₂ \S\DIW	N ₂ \D\DIW
	WW1	WW2
Oil-wet	OW1	OW2
Fractional-wet	FW1	FW2

N₂= nitrogen, S = Soltrol, DIW = deionized water, D = n-decane

3.3.2 Preparing the sand pack

The sand was packed inside the glass column using the dry packing method. In this method the sand was sprinkled from a spoon containing 40 g of the sand. The spoon was always held at a height of 1 cm above the sand mound inside the glass column. After every 1 cm of sand layer is formed, we used a solid object to pack the sand. According to Oliviera et al. (1996), this method achieved a uniform and reproducible packing.

For a fractional-wet experiment, the weight of sand needed to fill up the glass column was measured. Then equal proportion by weigh of water-wet and oil-wet sand were mixed according to the packing procedures described above. In this work the fractional-wet sand was prepared with 50:50 ratio.

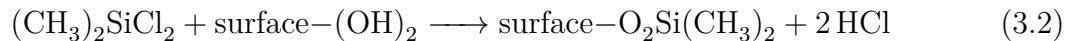
3.3.3 Altering the wettability of the sand pack

To study the effect of wettability we treated the sand with chemicals using a process known as silanization. In this process, dichlorodimethylsilane ($(\text{CH}_3)_2\text{SiCl}_2$ or DCDMS) is used as the silylating agent to make the sand grain water repellent. According to Seed (2001), the surface of the sand grain is water-wet because it contains silanol groups. DCDMS reacts with the surface to form a light oil coating which is chemically bonded to the surface. This oil coating changes the sand wettability to oil-wet.

Specifically, when DCDMS reacts with the silanol groups, it forms siloxane $\text{Si}-\text{O}-\text{Si}$ linkage and releases HCl . From Herzberg and Erwin (1970), the reaction is a chemisorption on the surface which is described by the chemical equations below:



The second chlorine in $(\text{CH}_3)_2\text{SiCl}_2$ further reacts with the hydroxyl group on the sand surface:



The reaction in Equation 3.2 forms more siloxane polymer and gives HCl. In this process the adsorbed water on the sand surface hydrolyzes the silanes and acts as catalyst. The polymeric siloxane that results from these reactions is the silicone oil that coats the grain surface and turns it hydrophobic.

The procedures to change the sand wettability are described as follows: a solution of 5% by volume of DCDMS was prepared by dissolving DCDMS in toluene. Because the reactions produce hazardous HCl, this step and subsequent ones were performed in a fume hood with the operator wearing personal protective equipment. The batch of sand to be processed was soaked in this solution for 15 minutes and then the sand was rinsed with methanol. The sand was then left overnight in the fume hood to dry and evaporate the organic solvent. Finally the sand was cured by baking in an oven at 80 – 100°C for four hours.

The wettability was evaluated qualitatively by placing samples of treated sand on a cellophane strip and pipetting a droplet of water on top. The sand is oil-wet if the water droplet beads up. A low-cost method to measure contact angle was proposed by Ribe et al. (2016). We modified their procedures by using open-source image analysis software, *ImageJ* with the *DropSnake* plugin. Following this new procedure we were able to confirm that the treated sand is oil-wet ($\theta_{gw} > 90^\circ$). This is shown in Figure 3.4. Although silanization treatment changes the grain surface chemically, Vizika and Lombard (1996) observed through microscope that the treatment does not affect the grain size distribution or its morphology.

3.3.4 Measuring the porosity and absolute permeability

The porosity was measured by saturating the sand with water from bottom up. Water was injected at a constant rate of 1 cm³/min. The pore volume was determined first from the amount of water it took to saturate the sand. Then, porosity was calculated from:

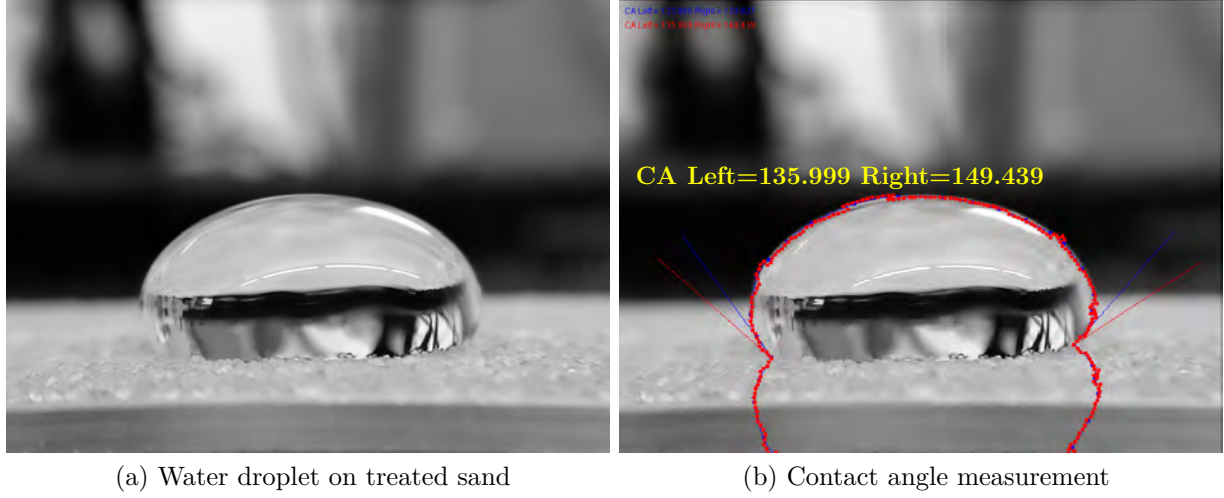


Figure 3.4: Procedures to measure contact angle of oil-wet sand: (a) Droplet of water is pipetted on strip of treated sand taped to a glass slide; (b) Photo of (a) taken and analyzed in *ImageJ* software to calculate the contact angle.

$$Porosity, \phi = \frac{PV}{BV} \quad (3.3)$$

where PV is the pore volume and BV is the bulk volume. In this case, bulk volume is the volume of the sand that is contained in the glass column, which is 543 cm^3 .

The absolute permeability was measured by allowing water to continue saturating the sand pack at the current injection rate ($1 \text{ cm}^3/\text{min}$) and be produced. Then pressure was read from the pressure gauge after five minutes. Pressure reading was recorded for each increment of injection rate until $5 \text{ cm}^3/\text{min}$. Absolute permeability, k_{abs} was calculated from Darcy's law:

$$k_{abs} = \frac{q\mu L}{A\Delta P} \quad (3.4)$$

where k_{abs} is the absolute permeability in *Darcy*, q is the average flow rate in cm^3/s , μ is the viscosity of displaced fluid in *cp*, L and A are the sand pack length and cross-section area in *cm* and cm^2 respectively; and ΔP is the average pressure drop in *atm*. With the

data collected we can use Equation 3.4 by plotting q/A as the y-axis and $\Delta P/L\mu$ as the x-axis. A trendline is fitted to the data and the slope will give us k_{abs} .

According to Holbrook and Bernard (1958), the fluid that first contacted the dry sand affects its initial wettability. Therefore for experiments requiring oil-wet or fractional-wet sand, the silanized sand was initially saturated with oil phase and left overnight for aging and to establish its wettability. Then the above procedures were used by replacing water with oil to find ϕ and k_{abs} .

3.3.5 Running the experiments

The gravity drainage experiments we plan to perform consisted of secondary and tertiary mode. In secondary mode we perform free-fall gravity drainage (FGD) where the top of the glass column is opened to atmosphere; and controlled gravity drainage (sec.CGD) where gas is injected at constant pressure. In tertiary mode (tert. CGD) gravity drainage experiment with constant gas injection is performed after waterflooding. The steps performed during each experiment is shown in Figure 3.5 for water-wet sand and Figure 3.6 for oil-wet and fractional-wet sand.

For a water-wet experiment using either spreading or non-spreading fluid system (Figure 3.5), a typical run would begin by saturating the sand with water bottom-up to get the pore volume, porosity and the absolute permeability. This is followed with oilflooding from top-down to get the original oil in place (OOIP) and end-point oil relative permeability at connate water saturation (K_{ro}^*). Free-fall gravity drainage (FGD) commences after establishing the saturation history. After FGD, the sand pack is resaturated with oil top-down before starting the secondary controlled gravity drainage experiment. For the tertiary controlled gravity drainage, we resaturate the sand pack again with oil followed by 0.35 pore volume of water injection at 1 cm³/min from bottom-up. In both secondary and tertiary CGD the gas injection was controlled by setting the pressure constant at 1 psig. The procedures for running FGD and both secondary and tertiary CGD remain the same for oil-wet and fractional-wet sand (Figure 3.6). However, the saturation history was first

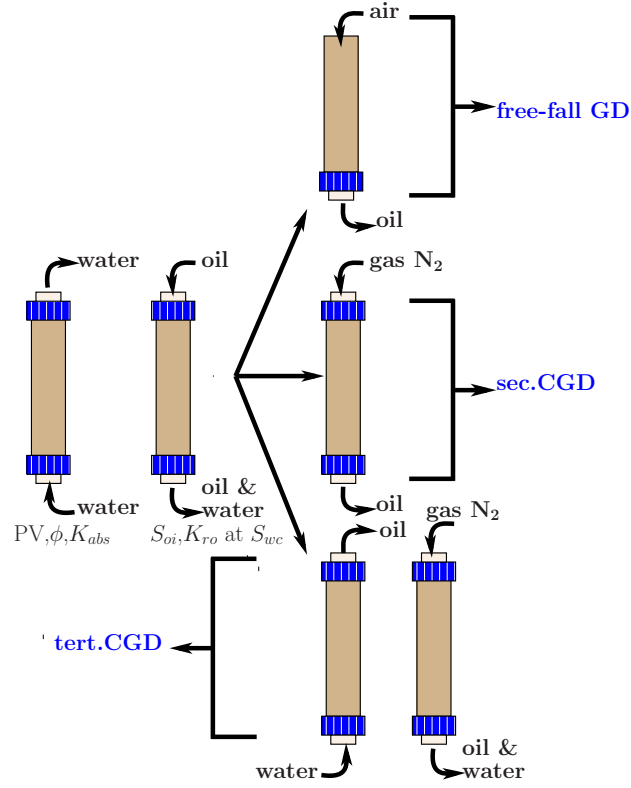


Figure 3.5: The steps performed during each experiment with water-wet sand.

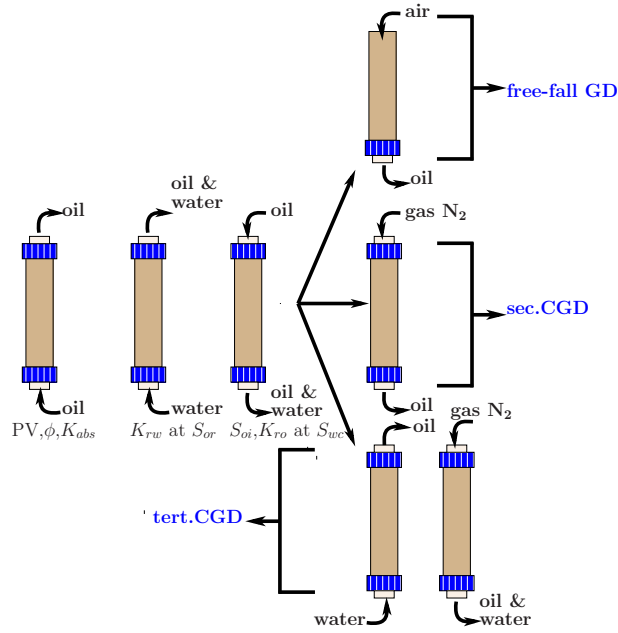


Figure 3.6: The steps performed during each experiment with oil-wet sand.

established by saturating the sand with oil to get the pore volume, porosity and absolute permeability; followed by water flooding to get end-point water relative permeability at residual oil saturation; and lastly oil flooding to get OOIP and K_{ro}^* . The procedures to carry out these experiments are further explained below.

3.3.5.1 Free-fall gravity drainage (FGD)

Before FGD experiment was run, we displaced the water initially present by injecting oil from the top down to establish connate water saturation, S_{wc} . The S_{wc} was calculated below:

$$S_{wc} = \frac{PV - OOIP}{PV} \quad (3.5)$$

where $OOIP$, the original oil in place, was the oil volume it took to displace the water until breakthrough. The initial oil saturation was calculated as $S_{oi} = 1 - S_{wc}$. The oil was allowed to continue saturating the sand pack. The oil effective permeability, k_{eo} , was calculated using the procedures described in subsection 3.3.4. Then we calculated the end-point oil relative permeability, K_{ro}^* at S_{wc} :

$$K_{ro}^* = \frac{k_{eo}}{k_{abs}} \quad (3.6)$$

The FGD experiment began by opening the top lid of the glass column to allow atmospheric pressure to displace the oil. The experiment was run for twelve hours. During the course of the experiment, the volume of oil recovered and the pressure were recorded.

3.3.5.2 Secondary controlled gravity drainage (sec. CGD)

Before running this experiment, the sand pack was resaturated with oil. We assumed that S_{wc} , S_{oi} , and K_{ro}^* were the same with the ones from FGD experiment. In secondary CGD, the top lid was closed and the fluid injection system for gas was set up according to Figure 3.3. In this experiment, the gas was injected from the top and injection was set

at constant pressure. The experiment began as soon as the gas valve was opened. Similar to FGD experiment, we ran it for twelve hours and recorded the oil recovery and pressure drop.

3.3.5.3 Secondary waterflooding

Secondary water flooding was performed prior to running tertiary CGD. The purpose was to establish water flood residual oil saturation, S_{orw} . The water injection system was set up according to Figure 3.1. To ensure sufficient oil remained for tertiary CGD, waterflooding was carried out by injecting 0.35 PV of water at 1 cm³/minute. During the course of this experiment, we recorded the oil recovery and the pressure drop.

3.3.5.4 Tertiary controlled gravity drainage (tert. CGD)

Tertiary CGD was run after secondary waterflooding. The experiment was set up according to Figure 3.3. The gas was injected at constant pressure of 1 psig from the top for twelve hours. Similar to previous experiments, we recorded the oil recovery and pressure drop.

Chapter 4

Gravity Drainage Experiments for Spreading and Non-Spreading Systems

In this chapter we present the results from gravity drainage experiments performed in secondary and tertiary mode. Free-fall gravity drainage (FGD) and secondary controlled gravity drainage (sec.CGD) are categorized under the secondary mode and tertiary controlled gravity drainage (tert.CGD) is in tertiary mode. Our experiments consisted of gravity drainage in glass columns with water-wet, oil-wet and fractional-wet sand. We used Soltrol as spreading oil and Decane as non-spreading. The results were compared with those from literature and we found cases where our experimental data contradict available reports. We explained the underlying mechanisms at pore level and analyzed the results with dimensionless numbers.

4.1 Experimental results

The experimental results are summarized in Table 4.1. We arranged the results according to wettability and its corresponding fluid system to observe the effect of spreading on oil recovery. The results presented here came from gravity drainage experiments that were run for twelve hours. The same duration for all experiments provided consistent basis for comparison. The oil recoveries tabulated represent the terminal point at the conclusion of each experiment.

From Table 4.1 it is shown that gravity drainage experiments in water-wet sand produced more oil in secondary and tertiary mode when the fluid system is spreading. In oil-wet sand the higher oil recovery came from experiments using non-spreading fluid. Higher recovery from non-spreading fluid system is also observed from fractional-wet experiments. We discuss these observations in the following sections.

Table 4.1: Summary of experimental results for free-fall gravity drainage, secondary controlled gravity drainage and tertiary controlled gravity drainage

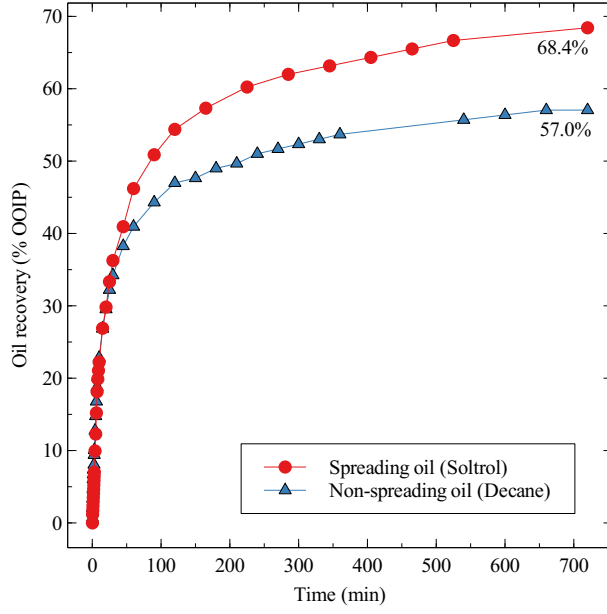
Wettability	Fluid system	ϕ	k (Darcy)	S_{wc}	$S_{org,fgd}$	$S_{org,cgd2}$	S_{orw}	$S_{org,cgd3}$	RF_{fgd}	RF_{cgd2}	RF_{cgd3}
w-w	sp	0.346	3.8	0.09	0.287	0.229	0.559	0.330	68.4	74.9	41.0
w-w	non-sp	0.363	3.8	0.244	0.325	0.284	0.442	0.299	57.0	62.4	32.2
o-w	sp	0.413	6.6	0.134	0.393	0.379	0.594	0.379	54.6	56.2	36.1
o-w	non-sp	0.346	3.2	0.144	0.271	0.213	0.537	0.223	68.3	75.2	58.4
f-w	sp	0.365	8.9	0.172	0.424	0.384	0.556	0.369	48.8	53.7	33.6
f-w	non-sp	0.355	5.5	0.181	0.269	0.241	0.534	0.249	67.1	70.3	54.4

ϕ :	Porosity (dimensionless)	RF_{cgd2} :	Recovery factor for secondary controlled gravity drainage (% OOIP)
k:	Absolute permeability (Darcy)	RF_{cgd3} :	Recovery factor for tertiary controlled gravity drainage (% ROIP)
S_{wc} :	Connate water saturation (dimensionless)	sp:	Spreading fluid (N ₂ \Soltrol\Deionized Water (DIW))
$S_{org,fgd}$:	Residual oil saturation after free-fall gravity drainage (dimensionless)	non-sp:	non-spreading fluid (N ₂ \Decane\DIW)
$S_{org,cgd2}$:	Residual oil saturation after secondary controlled gravity drainage (dimensionless)	w-w:	Water-wet sand
S_{orw} :	Residual oil saturation after waterflooding (dimensionless)	o-w:	Oil-wet sand
$S_{org,cgd3}$:	Reduced residual oil saturation after tertiary controlled gravity drainage (dimensionless)	f-w:	Fractional-wet sand
RF_{fgd} :	Recovery factor for free-fall gravity drainage (%OOIP)		

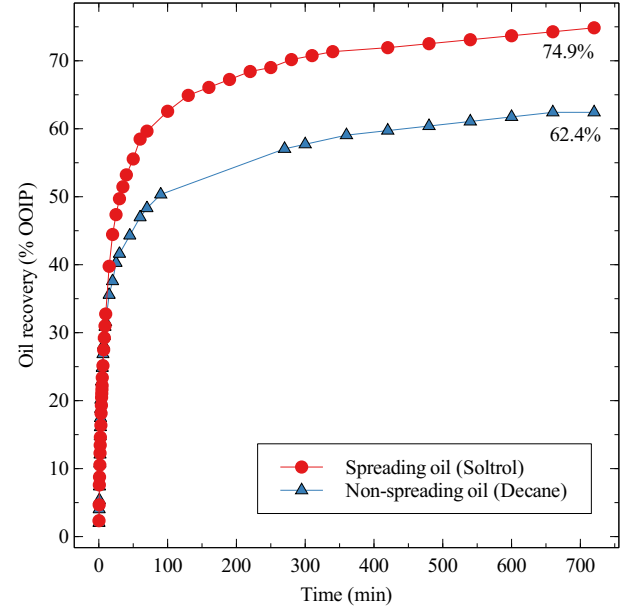
4.1.1 Gravity drainage in water-wet sand

From Figure 4.1 it is observed that GAGD in water-wet sand with spreading fluid system typically recovers more oil than the corresponding non-spreading fluid. Free-fall gravity drainage with Soltrol for example, recovered 68.4% OOIP compared to decane with only 57% OOIP. High oil recovery trends were observed for all GAGD injection modes performed in water-wet sand. From Table 4.1 the average recovery of all injection modes (secondary and tertiary) for the spreading group in water-wet sand is 61.4% while the average for non-spreading group is 50.5%.

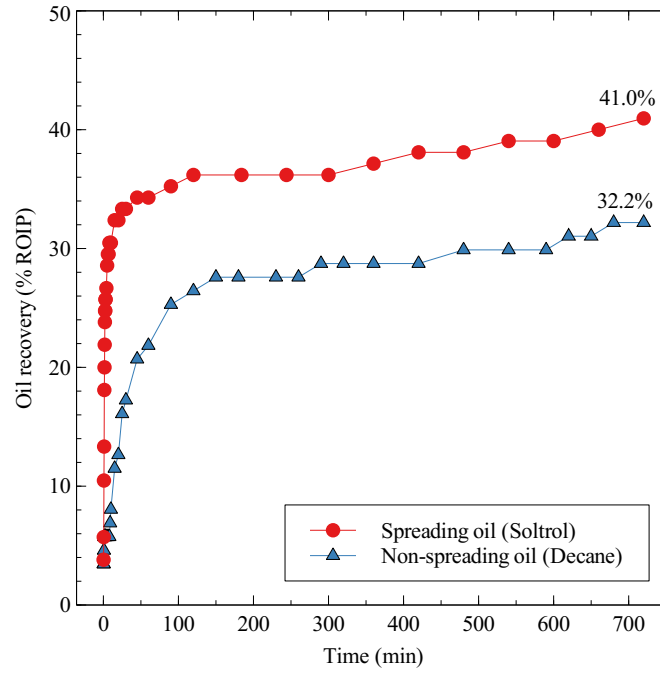
Our results confirm similar findings from other workers (Kantzas et al. (1988a), Vizika (1993), Kalaydjian et al. (1995), and Maeda and Okatsu (2008)). In their work they also reported higher recovery for gravity drainage performed in water-wet sand with spreading oil. According to Kantzas et al. (1988b) and Oren et al. (1992), the higher oil recovery observed in these experiments can be explained by the spreading film phenomenon. In



(a) FGD in water-wet sand



(b) Secondary CGD in water-wet sand



(c) Tertiary CGD in water-wet sand

Figure 4.1: Recovery profile of secondary CGD and tertiary CGD in water-wet sand. The annotation shows the terminal oil recovery. Oil recovery in spreading fluid system is greater than the non-spreading system.

water-wet media, oil phase is the intermediate phase. When the sign of the oil spreading coefficient is positive, the oil spreads and forms thin film spontaneously in the presence of water and air. This film maintains hydraulic conductivity even at low saturation, as reported in a three-phase relative permeability study by DiCarlo et al. (2000). In their experimental work DiCarlo et al. (2000) observed that oil relative permeability for the spreading oil (hexane and octane) remained finite, spanning six orders of magnitude at low saturation while oil relative permeability for non-spreading oil (decane) dropped off to zero. This means the film formed by the spreading oil provides a continuous path so that bypassed oil blobs behind the advancing gas front in the sand column can be reconnected and effectively drained. In a non-spreading system, since the spreading coefficient is negative (c.f. Table 3.1 on page 33), the oil did not spread and the conductivity layer for residual oil flow was not established.

We have recorded continuous video for each experimental runs. Since the file sizes were large, the videos were processed using the open-source software package *ffmpeg*. The time-lapsed photos captured from the videos are presented in Figures 4.2, 4.3, and 4.4 for FGD, secondary CGD and tertiary CGD respectively.

Figure 4.2 shows the sequence of displacements taking place over time in free-fall gravity drainage (FGD). In this experiment oil production is allowed to proceed by the action of gravity forces after we opened the top and bottom valves of the column to atmosphere. We can see the progression of the gas-oil interface for both spreading (4.2a) and non-spreading (4.2b) as it advanced through the sand column. At $t = 60$ seconds, the beginning of the gas front was observed. At this stage, gas as the non-wetting phase occupied the larger pores and simultaneously displaced oil, which is the intermediate phase. From $t = 10$ minutes until $t = 2$ hours the front propagated and displaced the bulk of the oil to the outlet. Under free-fall mode we observed the gas front advanced at a faster rate for both spreading and non-spreading systems. Consequently there was no instance of a stable oil bank being formed ahead of the gas front. According to Chatzis and Ayatollahi (1993) in free-fall mode

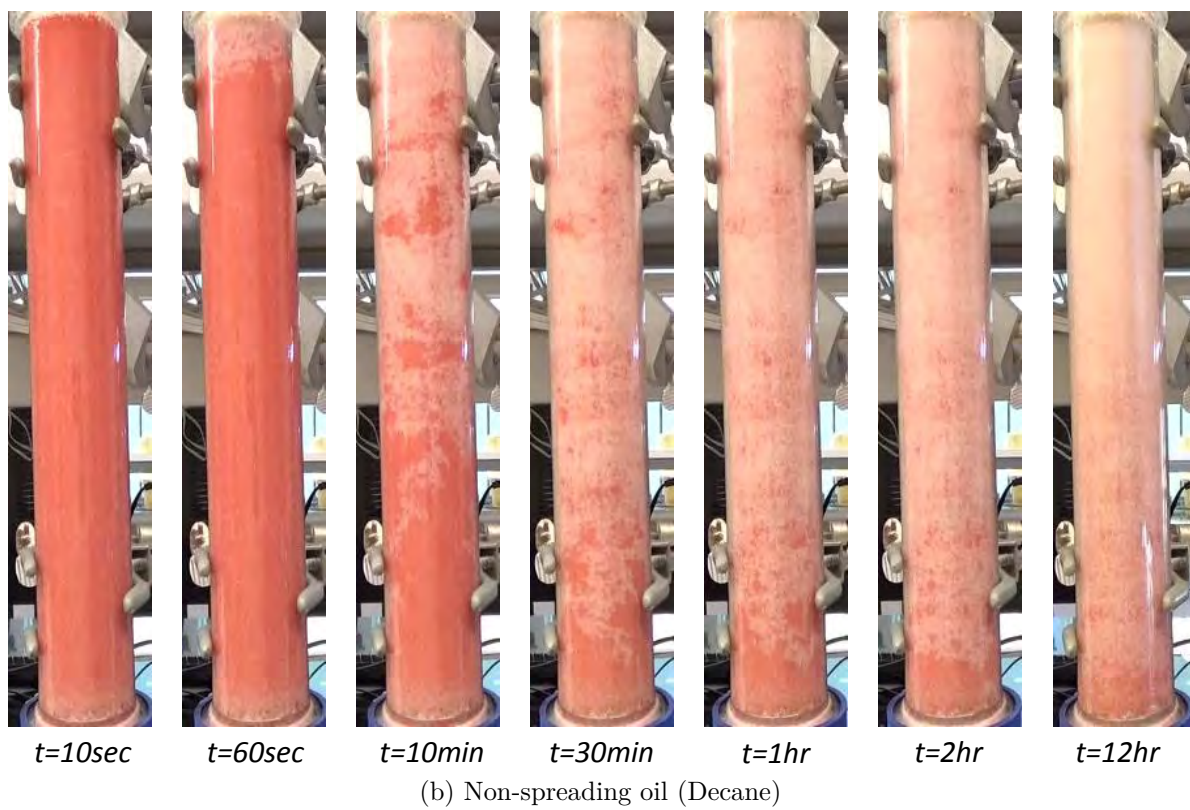
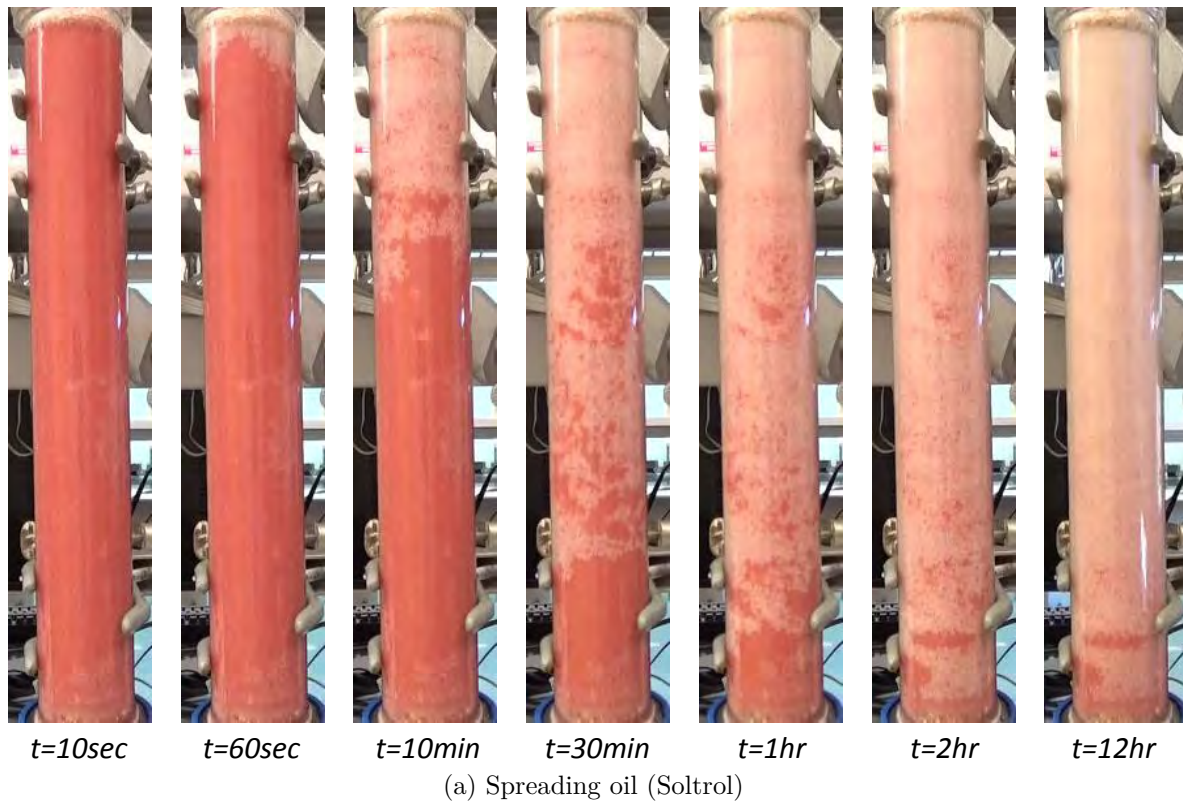


Figure 4.2: Time-lapsed photos of water-wet GAGD in FGD mode

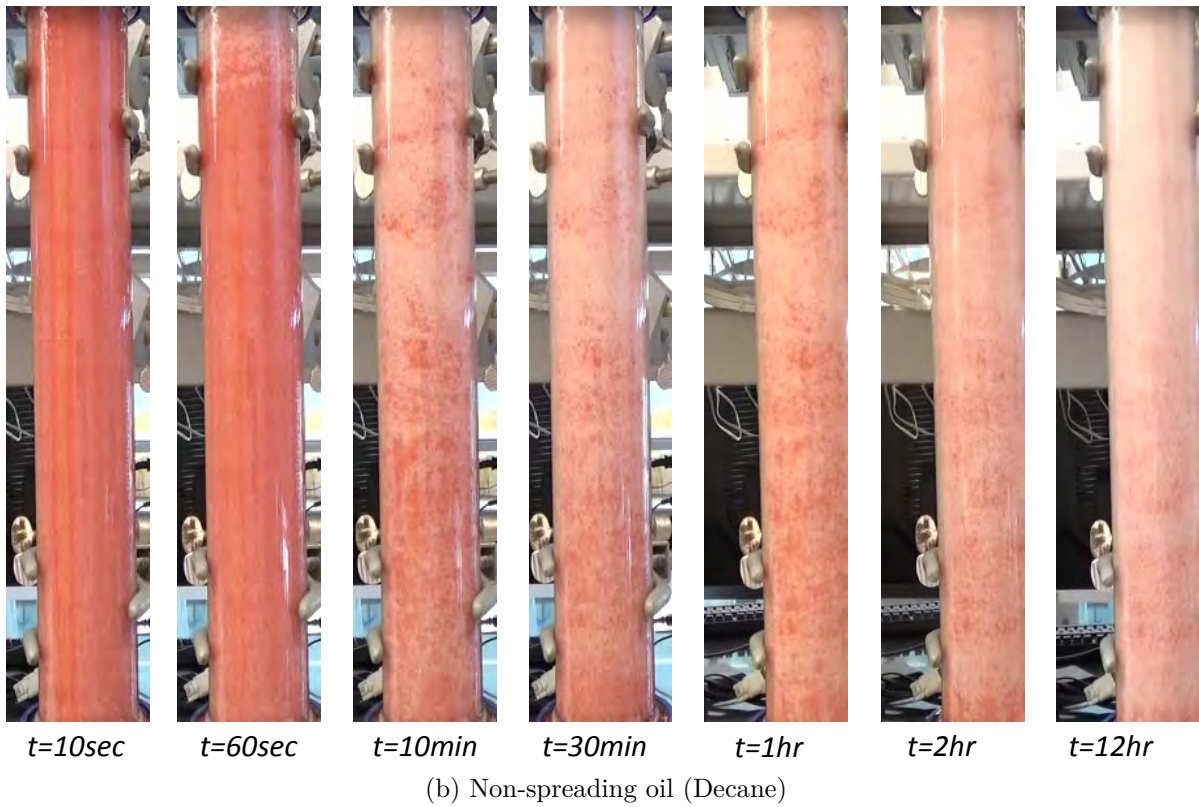
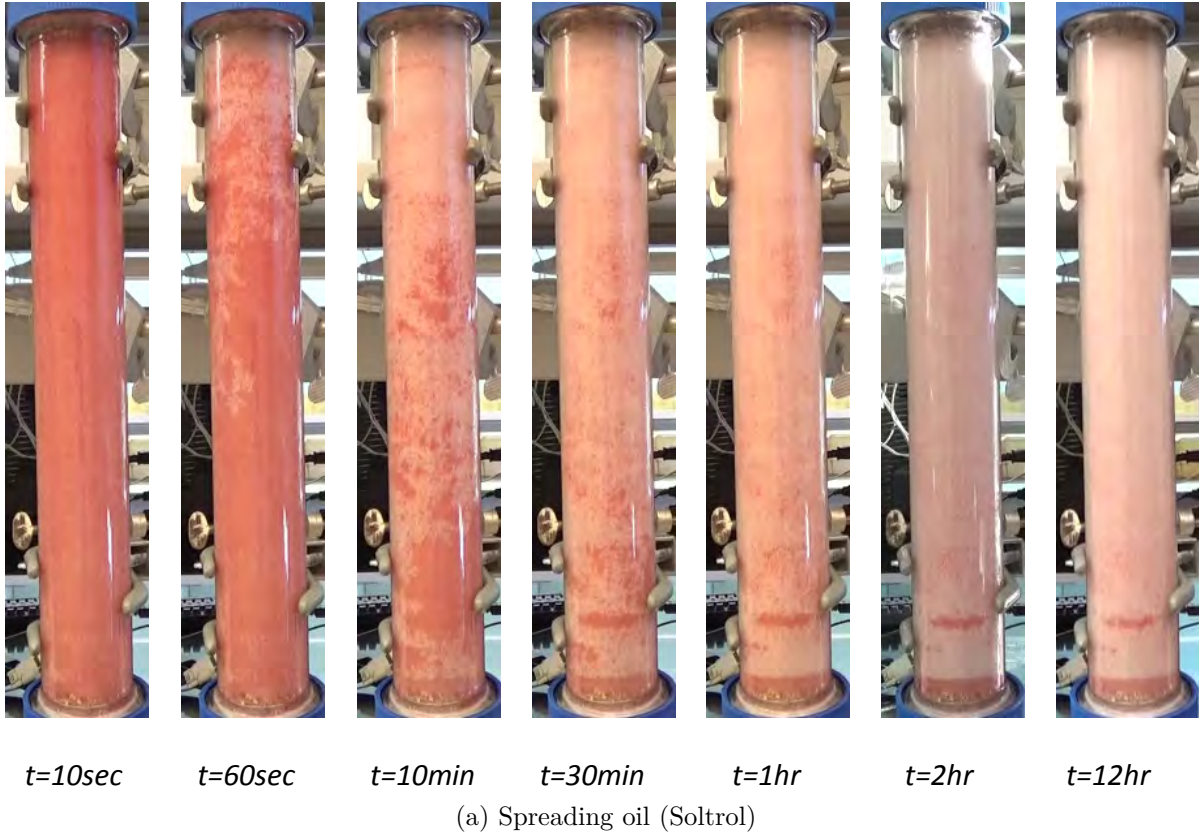


Figure 4.3: Time-lapsed photos of water-wet GAGD in secondary CGD mode

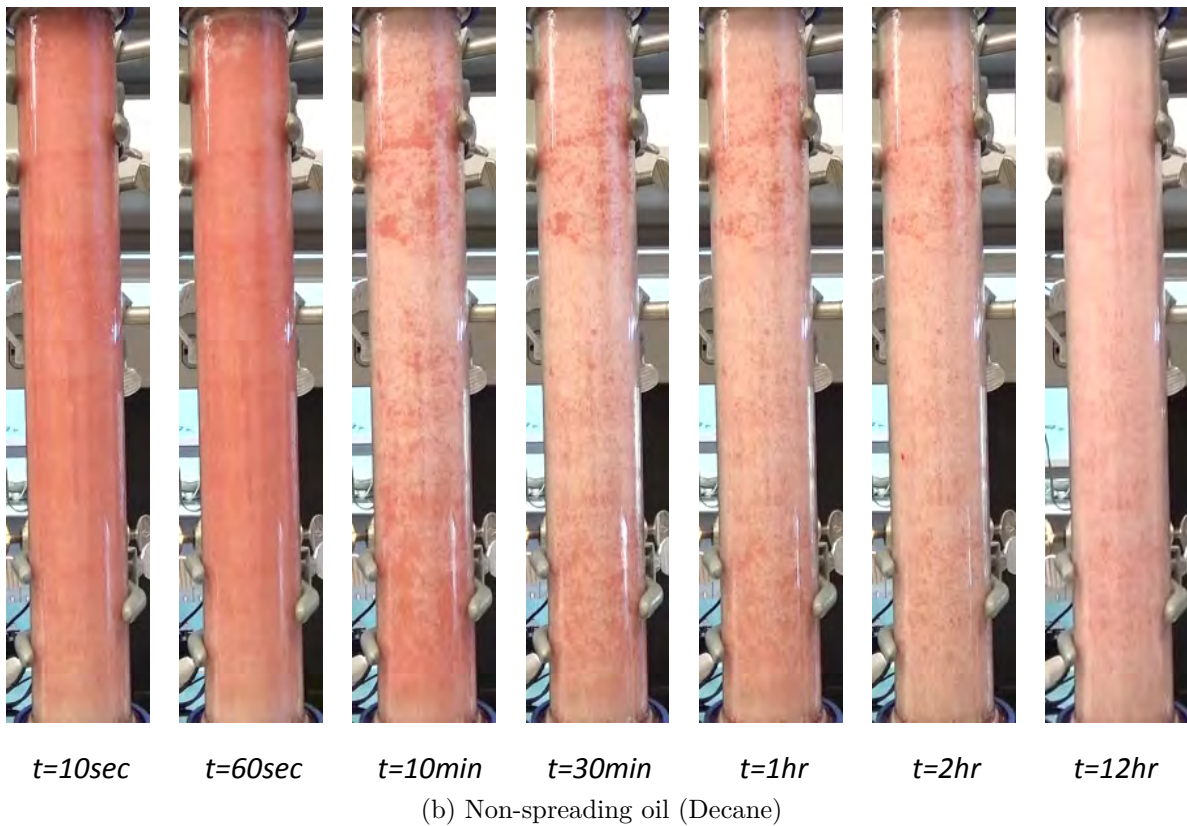
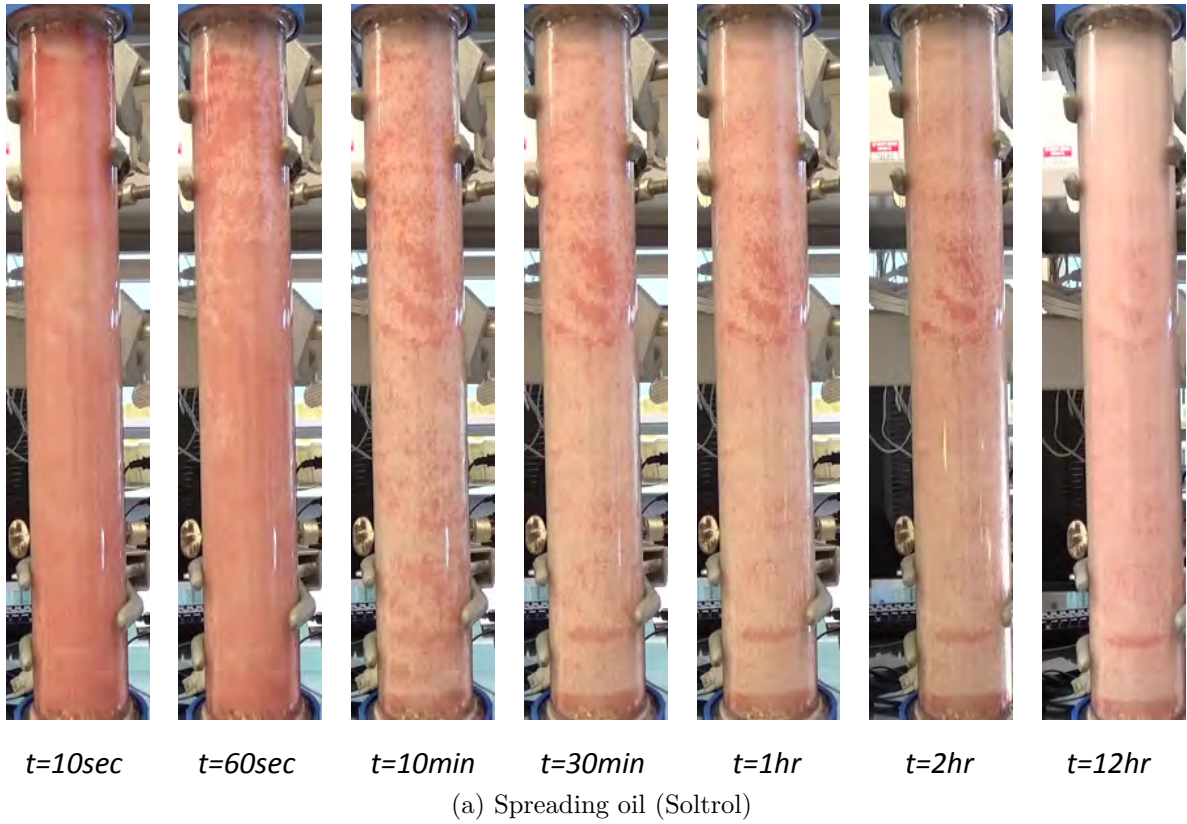


Figure 4.4: Time-lapsed photos of water-wet GAGD in tertiary CGD mode

the rate of oil drainage from film flow is much smaller than the advancing rate of the gas front. This makes it impossible for the bypassed oil to accumulate in sufficient amount to form oil bank ahead of the gas-oil front. Although significant volume of sand was contacted by the invading air, we could still see residual oil blobs left behind by the gas front. These oil blobs were initially disconnected from the bulk oil. However, through the mechanism of spreading oil, the thin film reconnected the isolated blobs and slowly drained the oil. Since the sand was water-wet, it can be thought that the wetting layer acts as a “lubricant” for the oil film to slide through. However because oil drainage through film flow is a slow process, it was not until the end of the experiment that we see most of the residual oil blobs in the transition zone were eventually produced.

Displacement sequences for secondary and tertiary CGD are shown in Figures 4.3 and 4.4 respectively. In both experiments nitrogen was injected at a constant pressure of 1psig and the valve at the bottom of the column was opened to atmosphere. For the tertiary case, residual oil saturation was established first by waterflooding the column bottom up before injecting gas. In Figure 4.3 for the secondary CGD, both spreading (4.3a) and non-spreading 4.3b systems show no formation of oil bank ahead of the gas front. This is also observed for the tertiary case in spreading (4.4a) and non-spreading (4.4b) systems. Based on the visualization, it is suspected that gas propagated too fast, and perhaps due to local heterogeneities patches of oil blobs were left behind. The residual oil blobs were reconnected and eventually found their way to the outlet through the continuous, albeit slow path provided by the spreading film.

From the visualizations of the displacement sequences we have seen so far (Figures 4.2, 4.3, and 4.4) it is observed that patches of bypassed oil blobs can also be found in the sand columns during gravity drainage of non-spreading oil (4.2b, 4.3b, and 4.4b). Although there was no spreading layer formed, due to the fact that spreading coefficient is negative for decane, we noted that the oil blobs were also drained to the outlet. This was because the oil patches slowly disappeared over the course of the experiments. Even though there

was no continuous path established by the spreading layer, it is assumed that the oil was drained through interconnected path across pores and throats filled with oil. Keller et al. (1997) explained that an intermediate oil layer could be formed, even when the oil is non-spreading given a range of pore geometries and ratio of gas-oil and oil-water capillary pressures. However, this path did not remain continuous to the outlet. This was because over time, as the network of oil-filled pores at the bottom of the column were drained the available paths for drainage were cut off from the outlet, leaving the oil blobs stranded. Furthermore according to Oren et al. (1992), the invading gas has tendency to contact water directly because there is no oil film between the gas-water interface. As more and more gas-water interfaces are formed, reconnection of oil blobs become arduous as each gas-displacement events does not necessarily lead to oil mobilization.

Although residual oil recovery during gravity drainage in water-wet sand benefits from the spreading film mechanism, this process requires a longer time to achieve ultimate recovery. In Figure 4.5, we correlate the oil recovery with visualization of time-lapsed photos in Figure 4.3a for secondary CGD with Soltrol. From Figure 4.5 it took two hours to drain 63% of original oil in place. During this period the bulk of the oil was produced to the outlet, as seen by tracking the time in the time-lapsed photos in Figure 4.3a. Between $2 < t < 12$ hours layer flow became the dominant mechanism draining the residual oil. We define layer flow here to encompass both film flow from the spreading oil and intermediate oil layer formed in the pore wedges for the non-spreading oil. By making this distinction between bulk flow and layer flow we can generalize the trend to non-spreading experiments. Therefore based on our observations in Figures 4.2, 4.3 and 4.4 the recovery profile for gravity drainage experiments can be characterized as having initial rise marked by a short duration and recovery of the bulk of the oil reaching almost 50-60 %OOIP; followed by tapering off of the profile, due to slow drainage from layer flow reaching an asymptote over a longer time span. This observation is similar to that reported by Vizika and Lombard (1996) in their experimental study.

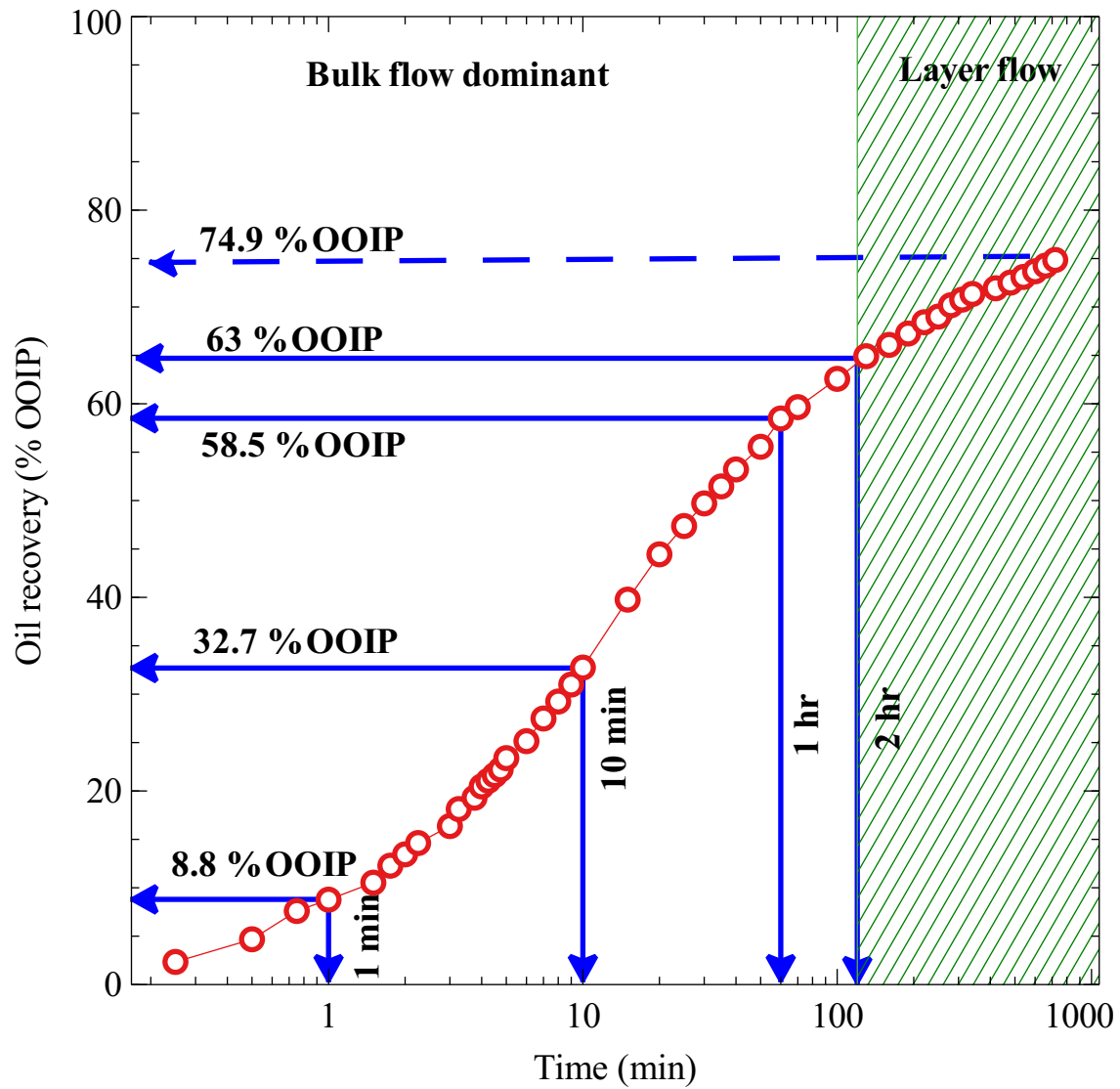


Figure 4.5: Recovery profile for secondary CGD in water-wet sand with spreading oil (Soltrol), showing regions of bulk flow and layer flow

In the literature Parsaei and Chatzis (2011) has shown that the reconnected oil through the spreading film eventually forms oil bank; and the oil bank further reconnects more isolated blobs as it is displaced to the outlet. It is believed that the formation of oil bank during gravity drainage is possible when gravity forces overcome the viscous forces at a velocity lower than the critical gravity drainage velocity (Rostami et al., 2010). The critical gravity drainage velocity concept comes from the work of Dumore (1964) and the equation is given as:

$$v_c = \frac{k}{\mu_o} (\Delta\rho g) \quad (4.1)$$

where k is the absolute permeability, μ_o is the oil viscosity, $\Delta\rho$ is the gas-oil density difference and g is the gravity acceleration constant. Using the fluid properties from Table 3.2 and the permeabilities from Table 4.1 on page 43 we calculated the critical velocity to be 0.00103 cm/s or 0.89 m/day for the spreading case and 0.0032 cm/s or 2.76 m/day for the non-spreading case. This can be achieved in the laboratory setup by producing the oil at a constant rate of 0.13 cm³/min for the spreading case and 0.42 cm³/min for the non-spreading case. However this was not attempted in our case due to limitation of the equipment.

Using production data and the method introduced by Grattoni et al. (2001), we calculated the gas velocity profiles for the spreading and non-spreading system in water-wet media for all injection modes. Our calculation in Figure 4.6 shows that the initial velocities exceeded the critical gas velocity with the maximum over 0.05 cm/s. Only later in the displacement, when $t > 100$ minutes we see the velocities decreasing to values close to the critical velocity. However at this point the bulk of the oil has already been produced, which left little oil in sufficient quantity to form a visible oil bank. This coincides with the visual observation when $t = 2$ hours in Figures 4.2, 4.3 and 4.4.

From the experimental results and the calculations, we see that GAGD recovery delivers higher recovery when performed in a water-wet sand and the fluid system has a positive

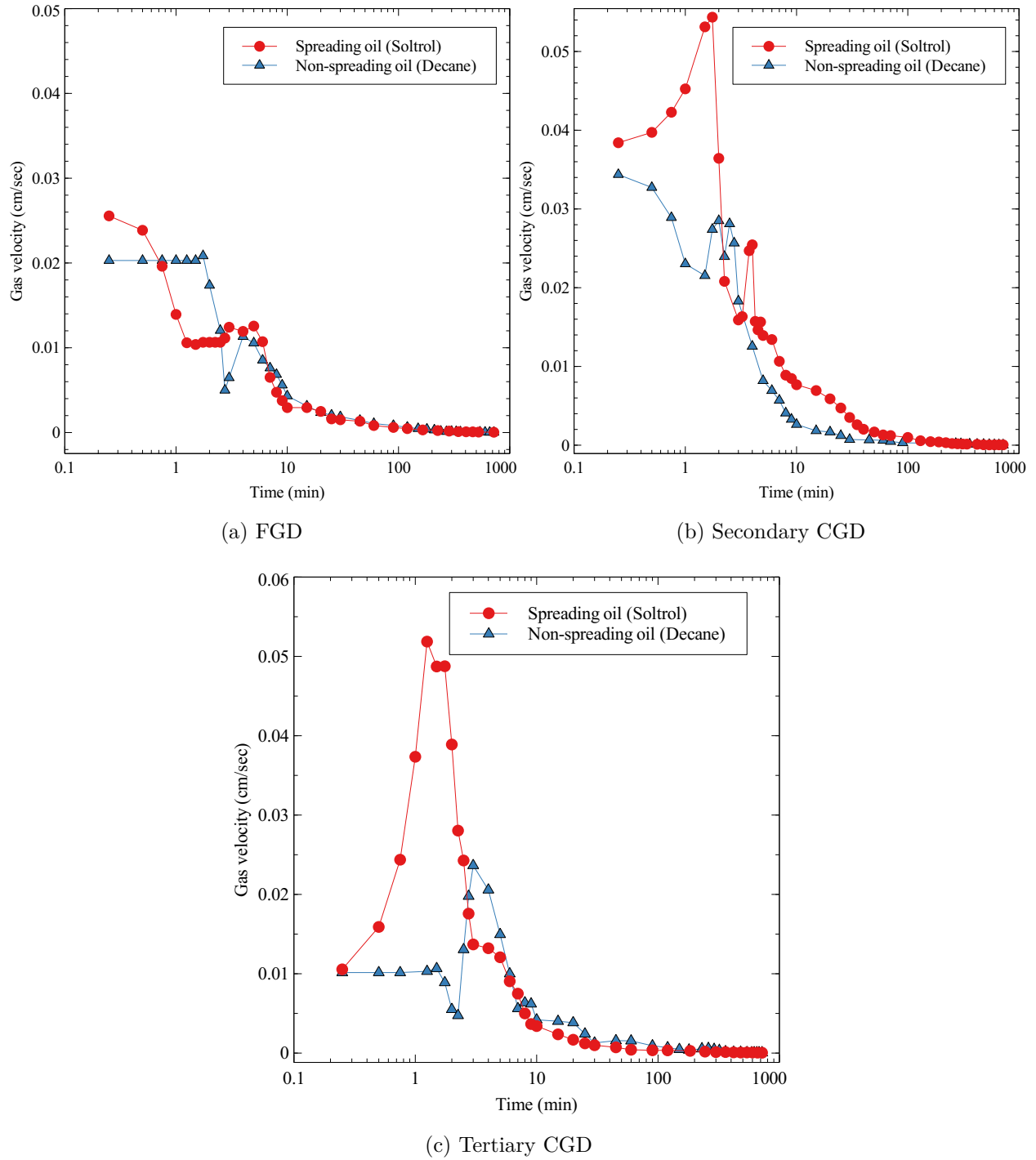


Figure 4.6: Gas velocity profiles for all injection modes of GAGD in water-wet sand.

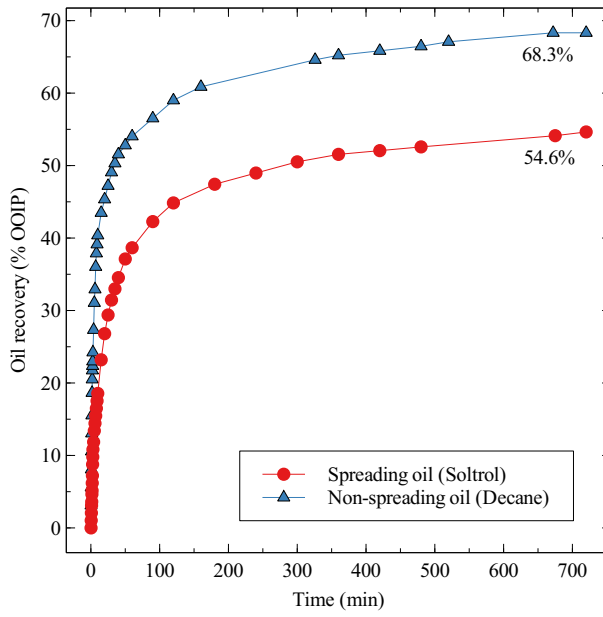
spreading coefficient. The reason for higher recovery is explained based on literature and the recovery profile is characterized and generalized for both spreading and non-spreading fluid system. Although we did not observe formation of oil bank the reason is explained based on gas velocity calculation. In the next section we will see how the recovery profiles change when GAGD is conducted in oil-wet media.

4.1.2 Gravity drainage in oil-wet sand

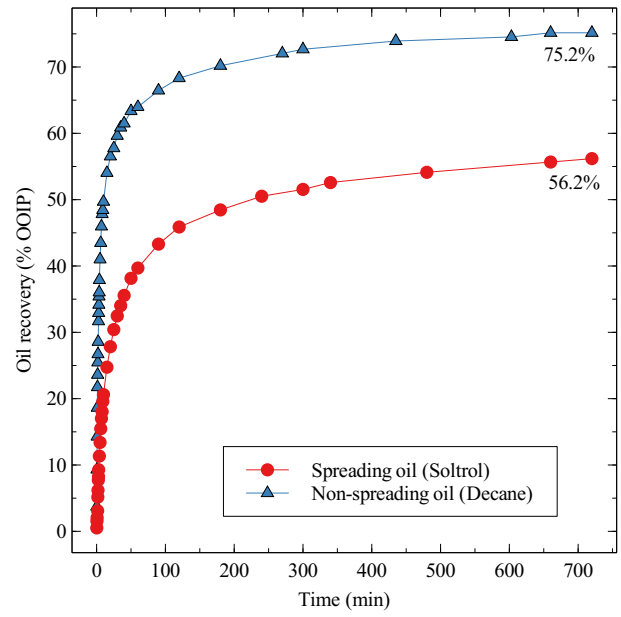
For oil-wet experiments, Figure 4.7 shows that gravity drainage with non-spreading fluid system produced more oil compared to spreading fluid system. For example in free-fall mode (FGD) oil recovery from non-spreading decane was 68.3% OOIP compared to 54.6% OOIP for spreading Soltrol. This trend is consistent for all injection modes. From Table 4.1 on average the oil recovery in oil-wet sand for all three modes for non-spreading system is 67.3% while the spreading system is 49%. In the literature we found two conflicting reports about oil recovery in three-phase oil-wet porous media.

Oren and Pinczewski (1994) reported that highest oil recovery was achieved in oil-wet media for both spreading and non-spreading oil. The result came from three-phase flow experiment with micromodel. When the recoveries were ranked, the highest oil recovery went to oil-wet media, followed by water-wet media with spreading fluid and the last was water-wet media with non-spreading fluid. They explained that in oil-wet media the sign of the spreading coefficient was not important because oil was drained through the continuous wetting phase. The drainage rate which also corresponds to oil recovery, was faster because the wetting film was thicker which lead to higher conductivity flow path.

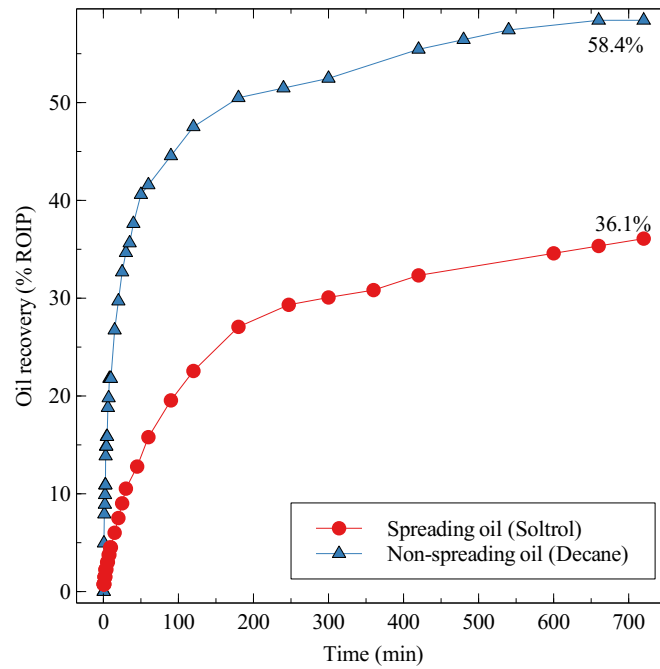
Vizika and Lombard (1996) presented their results and observed that oil recovery in oil-wet media was the lowest overall when compared to oil recovery from water-wet and fractional-wet sand. Both spreading and non-spreading oil have similar recovery in oil-wet media, which suggested that the spreading behavior was not important in oil-wet system.



(a) FGD in oil-wet sand



(b) Secondary CGD in oil-wet sand



(c) Tertiary CGD in oil-wet sand

Figure 4.7: Recovery profile of FGD, secondary CGD and tertiary CGD in oil-wet sand. In all injection modes, non-spreading system shows greater oil recovery than spreading system.

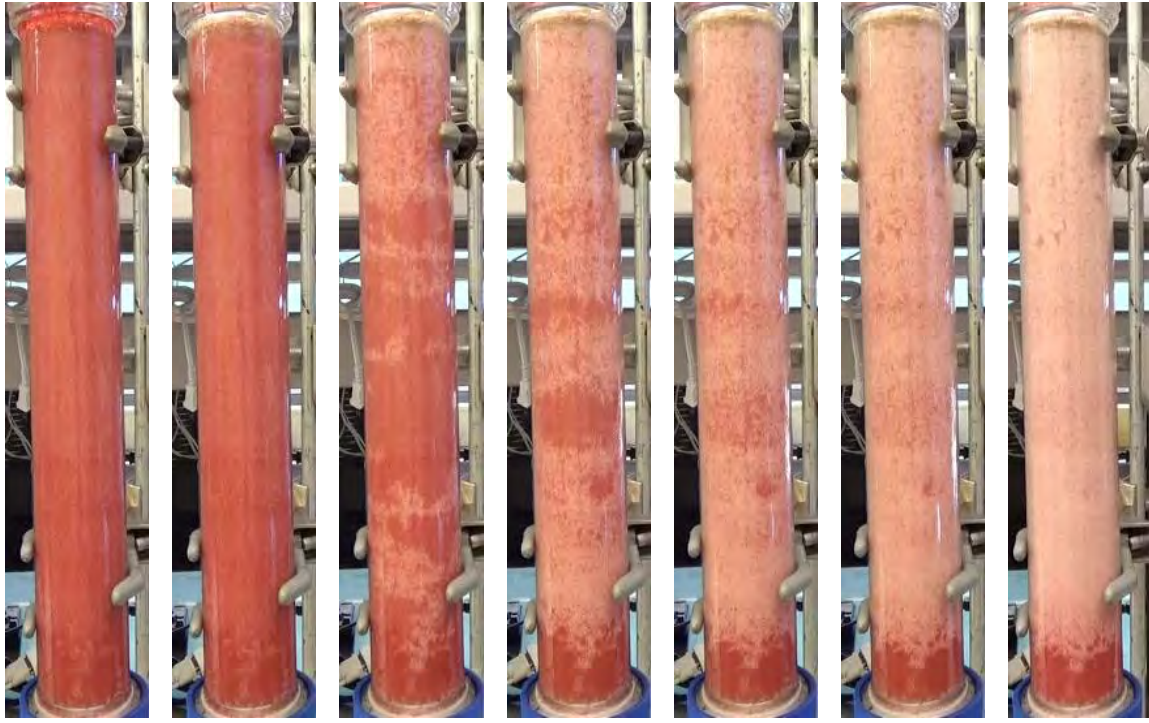
They explained that the presence of water as the non-wetting phase in the larger pores blocked the passage of gas invasion to displace oil which eventually resulted in low recovery.

It must be noted that Oren and Pinczewski and Vizika and Lombard studies were performed at different scale, with Oren and Pinczewski at pore scale and Vizika and Lombard at core scale. Another notable difference was the saturation history prior to the start of the experiment: Oren and Pinczewski experiment was conducted at residual oil saturation while Vizika and Lombard at residual water saturation. Clearly a direct comparison between the two must be approached with caution.

Our results for tertiary experiments in oil-wet sand generally agree with observation from Oren and Pinczewski (1994). For example looking at experimental data from water-wet and oil-wet sand in Table 4.1, tertiary oil recovery was highest for non-spreading oil-wet system (58.4%) followed by spreading water-wet system (41%) and lowest for non-spreading water-wet system (32.2%). Similar observation can also be made for recoveries in secondary mode.

Although Vizika and Lombard showed in their experimental results that oil recoveries from oil-wet sand were similar and not affected by the sign of the spreading coefficient, we found our results to be different. Comparison of recoveries in oil-wet sand between spreading and non-spreading system showed that they were not similar; in fact recovery was higher in non-spreading system for all injection modes. We will discuss this further by looking at the pore-scale mechanism later in Section 4.2.

We present time-lapsed photos of FGD experiments in oil-wet sand for both spreading and non-spreading fluid systems in Figure 4.8a and 4.8b respectively. It is observed in both figures that for the same time sequence, the gas front in the non-spreading system propagated faster than the non-spreading system. At $t = 60$ seconds, the gas front had traveled halfway through the length of the glass tube (Figure 4.8b) while most of the oil still remained in the sand for the same time in Figure 4.8a. When gas started invading the pores and displacing oil, significant amount of oil blobs were left behind in the spreading



$t=10\text{sec}$

$t=60\text{sec}$

$t=10\text{min}$

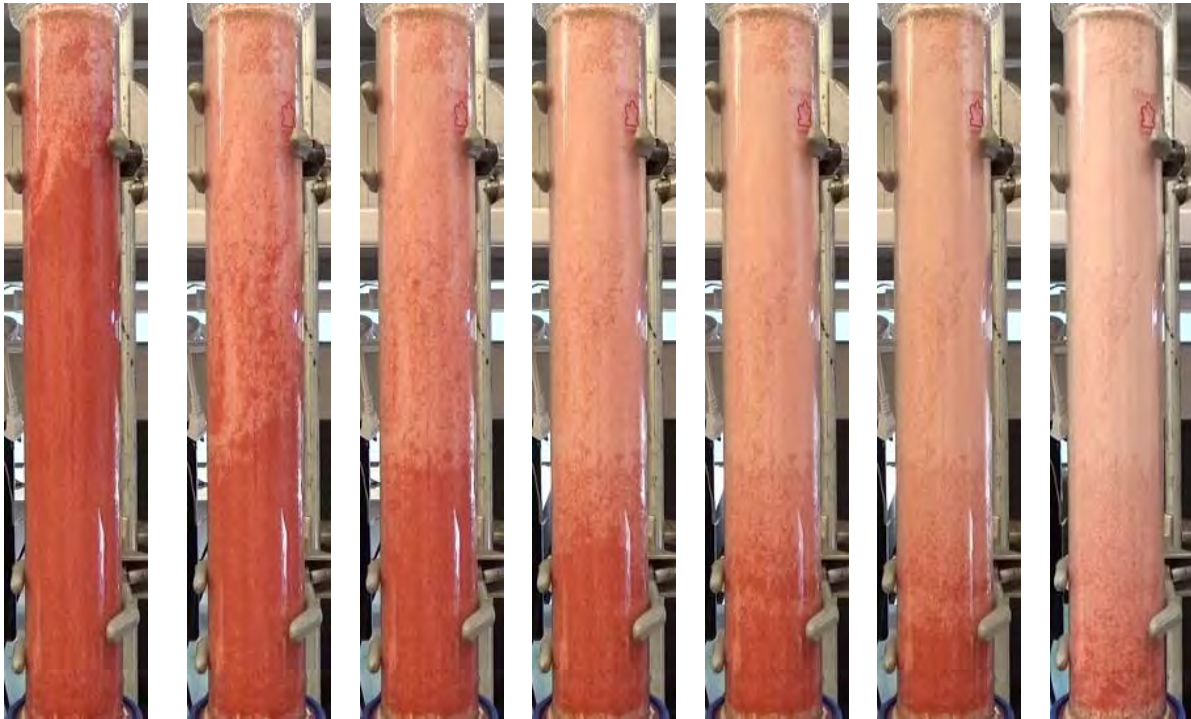
$t=30\text{min}$

$t=60\text{min}$

$t=2\text{hr}$

$t=12\text{hr}$

(a) Spreading oil (Soltrol)



$t=10\text{sec}$

$t=60\text{sec}$

$t=10\text{min}$

$t=30\text{min}$

$t=1\text{hr}$

$t=2\text{hr}$

$t=12\text{hr}$

(b) Non-spreading oil (Decane)

Figure 4.8: Time-lapsed photos of FGD in oil-wet sand.

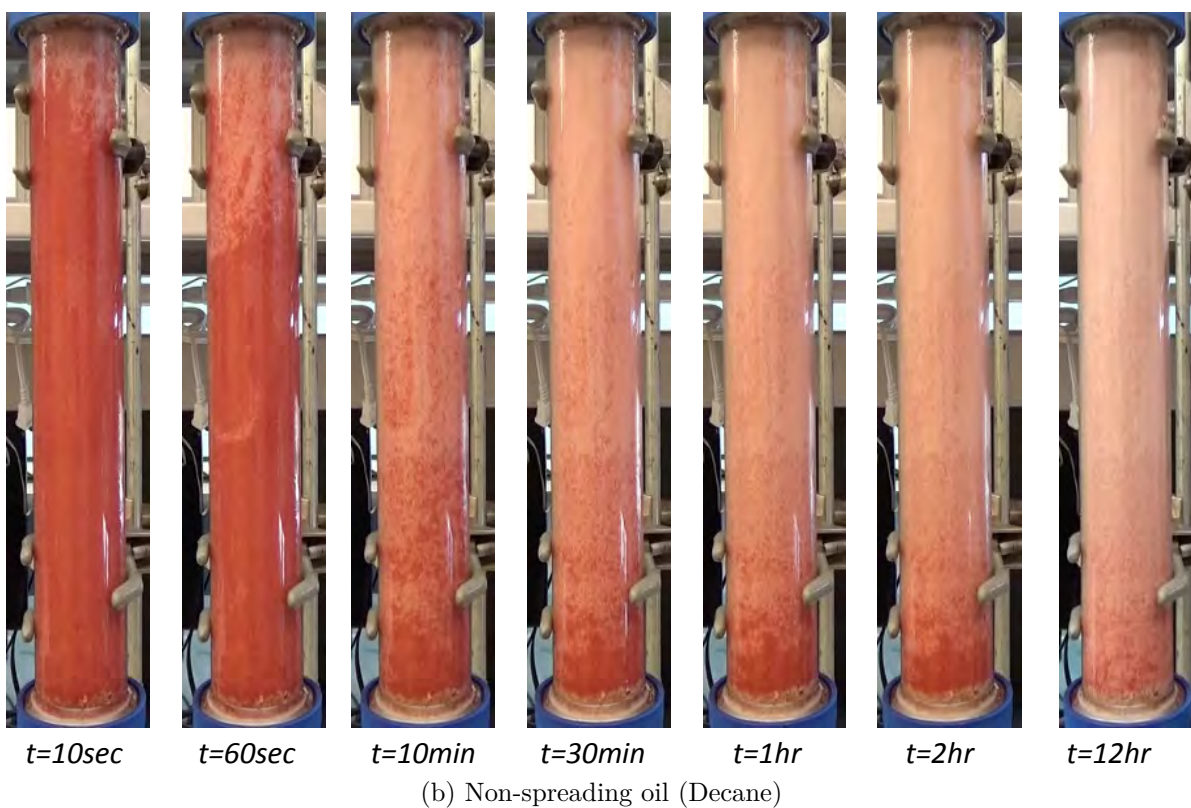
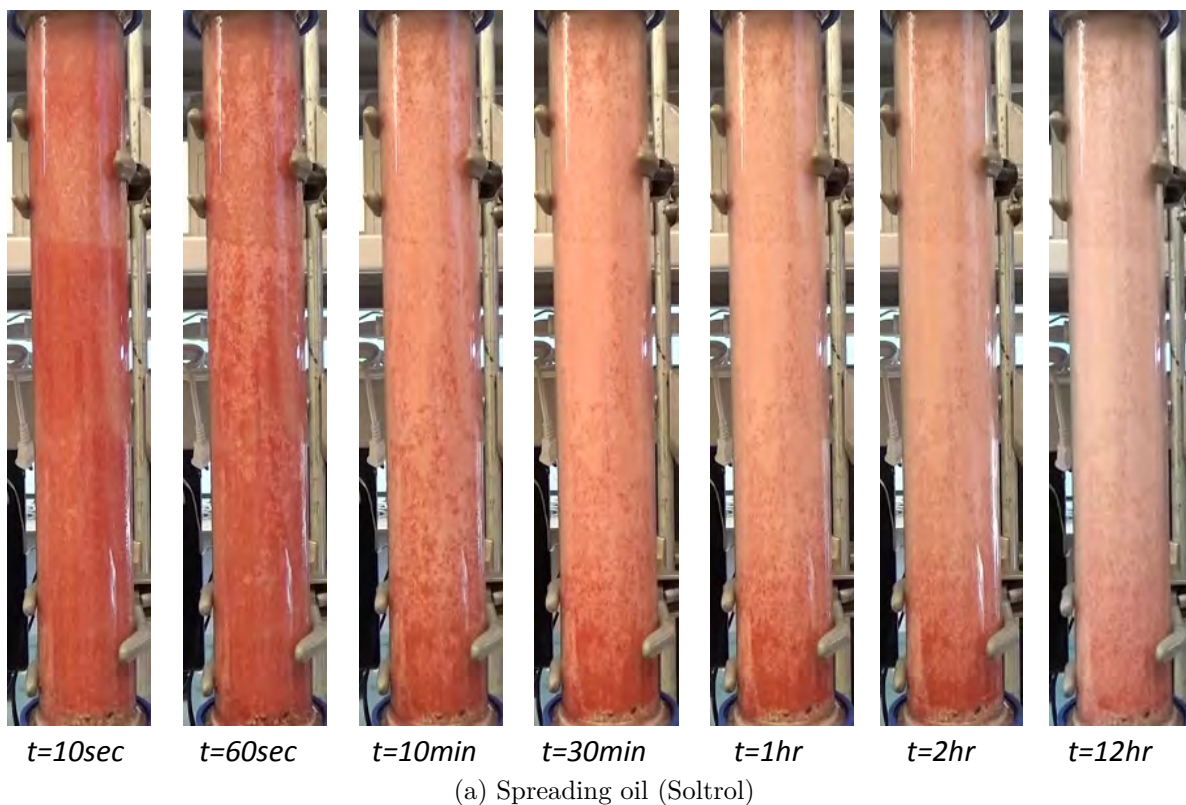


Figure 4.9: Time-lapsed photos of secondary CGD in oil-wet sand.

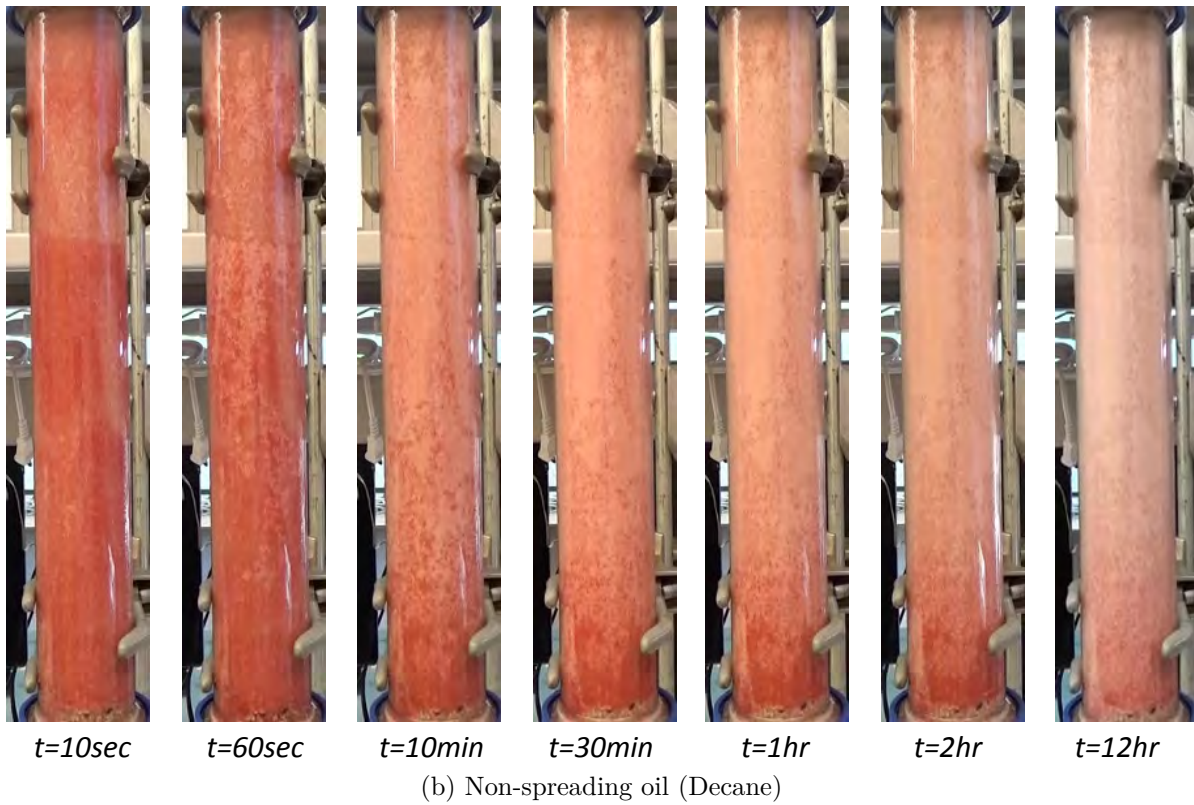
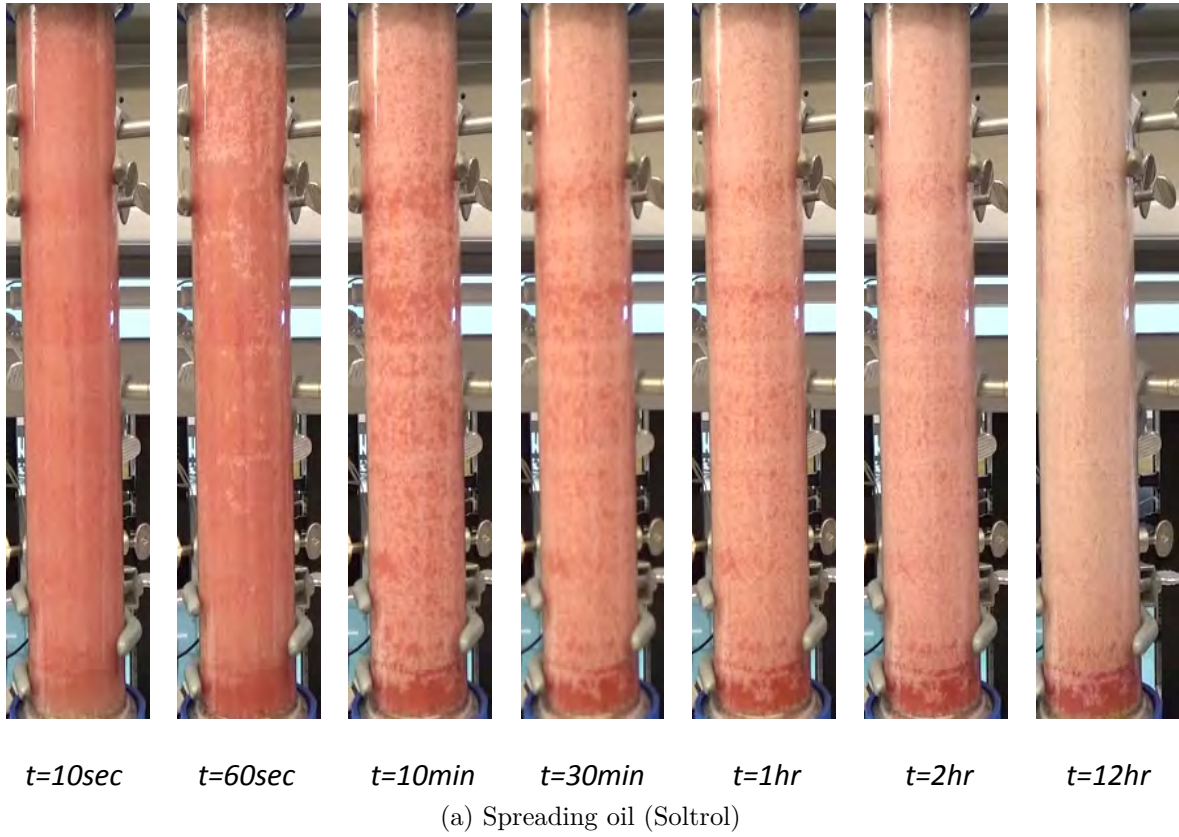


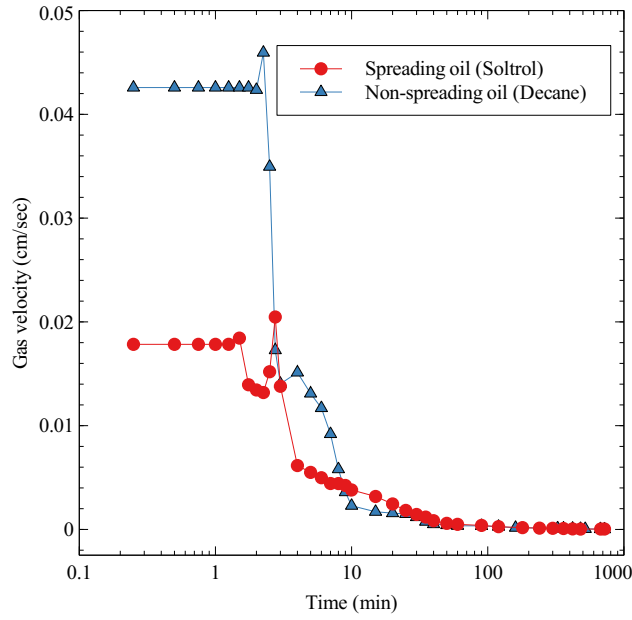
Figure 4.10: Time-lapsed photos of tertiary CGD in oil-wet sand.

case (4.8a). This was evident from the oil patches left behind along the length of the sand column. This continued for the remainder of the experiment. It took almost twelve hours to drain most of the residual oil, and yet a short column of oil can still be seen at the bottom after the experiment was stopped. This contrasts with drainage sequences in the non-spreading, oil-wet sand. At early time, the recovery was contributed mostly from bulk oil drainage. There were few oil patches visible as the gas front migrated downward. At later time, most of the residual oil was drained through the wetting film.

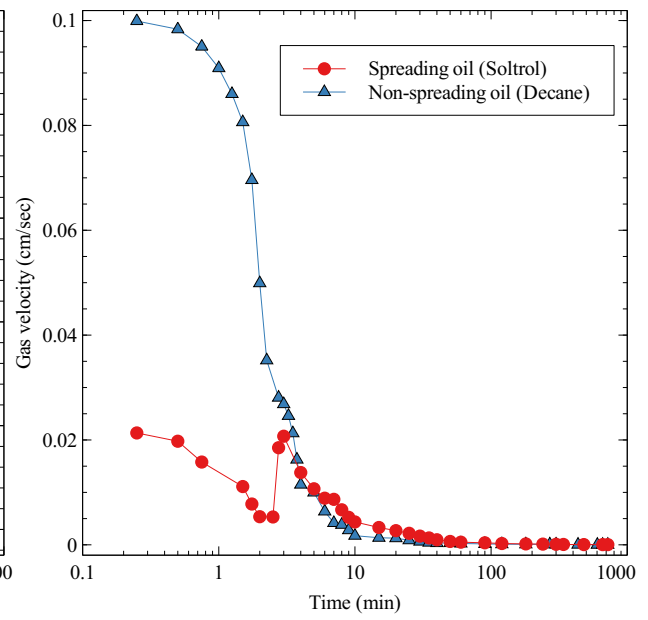
It must be pointed out here that in both cases (4.8a and 4.8b) a clear demarcator separating gas-oil front with oil bank was not seen. Using the critical velocity Equation 4.1 on page 52 the calculated velocity was 0.00179 cm/s for spreading case and 0.00270 cm/s for the non-spreading case. This corresponds to withdrawal rate of 0.266 cm³/min and 0.337 cm³/min for spreading and non-spreading respectively. This means a stabilized drainage where oil bank can be formed ahead of the gas-oil front can be achieved by producing the oil below the calculated withdrawal rate.

The time-lapsed photos for secondary CGD in Figure 4.9 look almost similar between the spreading (4.9a) and non-spreading case (4.9b) when compared at each time steps. This was despite the fact that oil recovery for the non-spreading case was higher (75.2 %OOIP) compared to spreading case (cf. Figure 4.7). One notable difference was that oil drainage started earlier in non-spreading case. At $10 < t < 60$ seconds gas had already displaced oil in the top quarter of the column in Figure 4.9b compared to the spreading case for the same period. Earlier onset of bulk flow regime could be a possible reason for higher oil production in the non-spreading case.

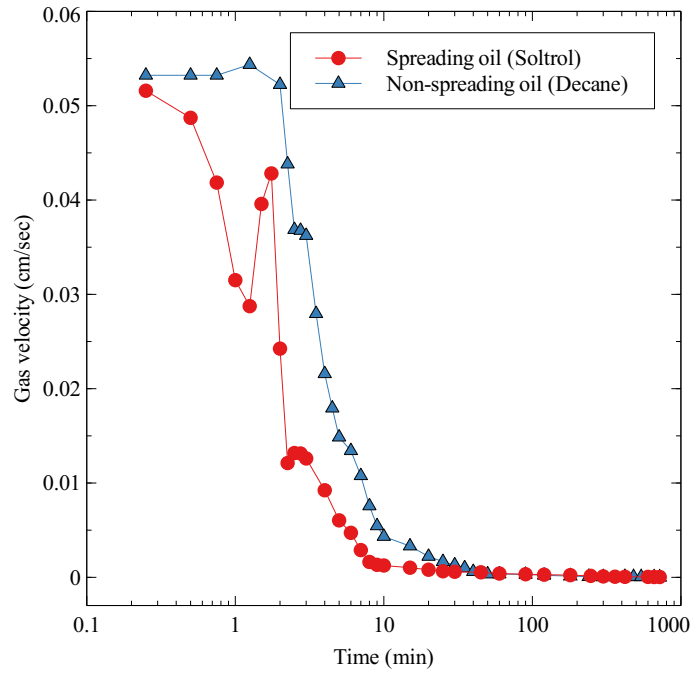
In tertiary CGD it appears that drainage rate is faster for non-spreading system. Comparing the time-lapsed photos from $t = 10$ minutes onward we see that patches of residual oil were left behind in the top half of the column in the spreading case (4.10a). The residual oil was eventually drained at $t = 12$ hours but there was still a small accumulation of oil at the bottom. In the same duration it is noted that there was also oil patches for the



(a) FGD



(b) Secondary CGD



(c) Tertiary CGD

Figure 4.11: Gas velocity profiles for all injection modes of GAGD in oil-wet sand.

non-spreading case (4.10b) but they were located mostly in the bottom half of the column and their density was much less than that of the spreading case.

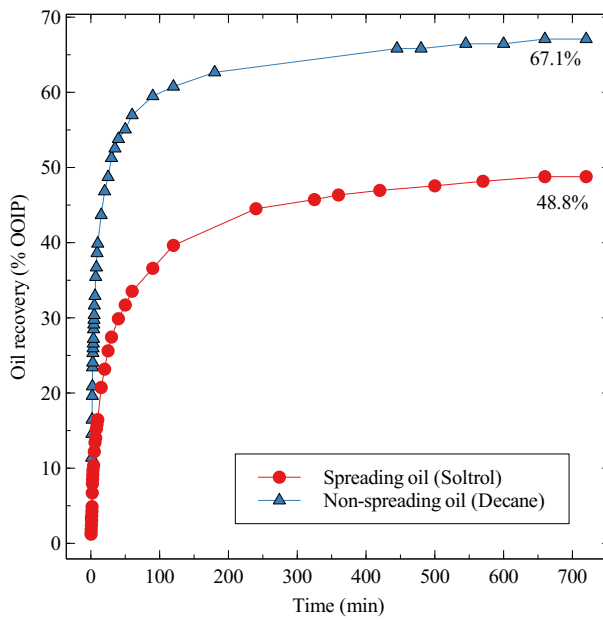
When analyzing the displacement sequences from the time-lapsed photos, particularly for the secondary and tertiary experiments we admit that some of our observations were qualitative in nature. Therefore we calculated the gas velocity profile to correlate with our visual observations.

The gas velocity profiles were plotted in Figure 4.11 to better understand these observations. The procedure to obtain the plot was explained in Grattoni et al. (2001). In the FGD (4.11a) and secondary CGD (4.11b) experiments the gas velocity for the non-spreading system was higher initially, which coincided with the beginning of bulk flow regime. Flow through the wetting film became dominant at a later time ($t > 100$ minutes) when the gas was slowing down. In oil-wet sand with spreading oil the gas velocity was lower initially, which accounted for the oil remaining in the sand when $t < 60$ seconds (cf. 4.8a and 4.9a). The recovery from bulk flow regime also happened gradually, which matched the gas velocity profile for $10 < t < 100$ minutes. It was only at a later time ($t > 100$ minutes) that drainage from wetting film became dominant.

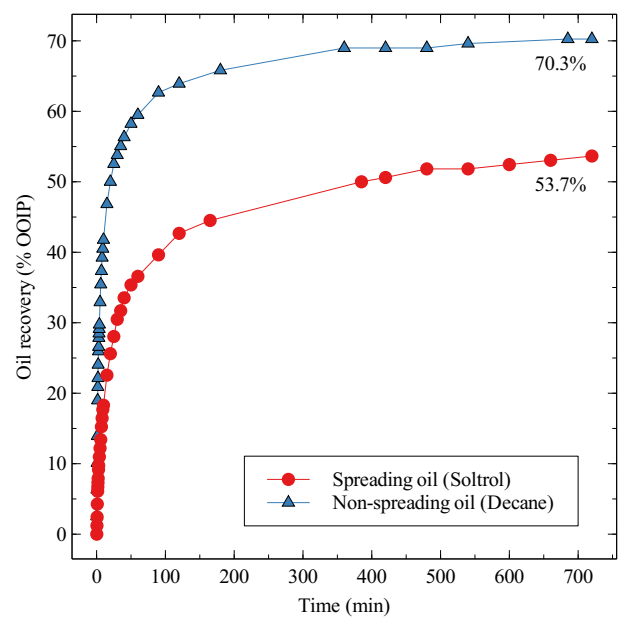
In Figure 4.11c for tertiary CGD the gas velocities for the spreading and non-spreading system almost tracked each other. However the velocity for the non-spreading case was consistently higher than the spreading case for duration $t < 100$ minutes. This resulted in more oil being drained overall, which lead to oil recovery of 58.4% ROIP compared to only 36.1% ROIP for the non-spreading system.

4.1.3 Gravity drainage in fractional-wet sand

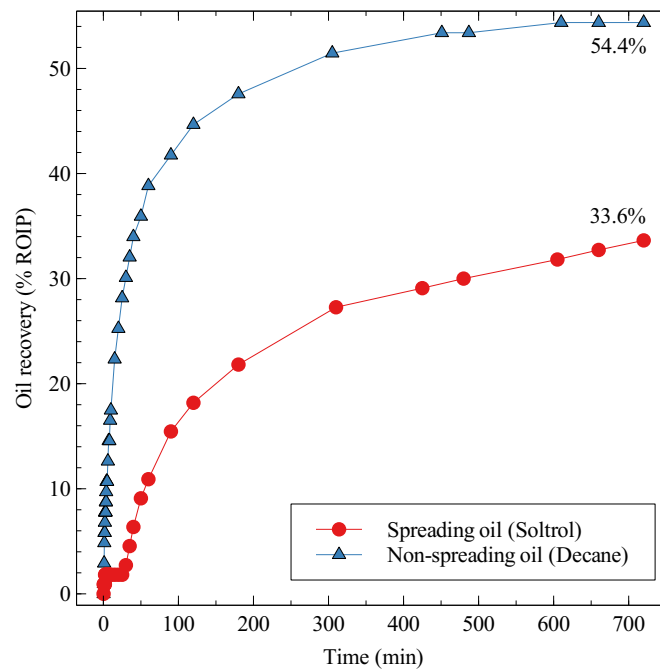
In Figure 4.12 we observed higher recovery for the non-spreading oil in fractional-wet sand compared to the spreading oil in all injection modes. This observation is similar to that observed in the previous section for oil-wet sand.



(a) FGD in fractional-wet sand



(b) Secondary CGD in fractional-wet sand



(c) Tertiary CGD in fractional-wet sand

Figure 4.12: Recovery profile of FGD, secondary CGD and tertiary CGD in fractional-wet sand.

The oil recovery was 67.1% OOIP in FGD experiment and 70.3% OOIP in secondary CGD for the non-spreading system. The recovery under tertiary mode was notable because it is almost 20% higher than the spreading system.

Experimental work by Vizika and Lombard (1996) on fractional-wet sand showed that the oil recovery was higher in spreading fluid system. When compared with their other results the oil recoveries for spreading fluid system in both water-wet and fractional-wet sand were similar and higher than that of oil-wet sand. The higher recovery was attributed to the internal construction of the sand pack. Since in the fractional-wet system the water-wet sand and oil-wet sand were mixed uniformly, the mobilization of residual oil benefits from the hydraulic conductivity path provided by the wetting film on the oil-wet sand and spreading film on the water-wet sand.

Our results indicate that higher recovery was obtained in non-spreading system. Analysis of the time-lapsed photos revealed that the displacement history for both systems were different. Figures 4.13, 4.14, and 4.15 show the displacement history as revealed from time-lapsed photos for fractional-wet experiments in FGD, secondary CGD and tertiary CGD respectively.

In Figure 4.13a for the spreading oil, the gas took longer time in the beginning of the experiment to invade the larger pores and subsequently displace oil in the smaller pores of oil-wet grains or water in the water-wet grains. This could be due to capillary pressure buildup to overcome the pore-throat threshold pressure. When the experiment were progressing at a later time, there were regions where oil was bypassed by the advancing gas front. The residual oil was eventually drained either through spreading or wetting film. At the end of the run there was significant amount of oil left at the bottom, possibly due to capillary retention.

In Figure 4.13b for the non-spreading oil, it is observed that gas invasion occurred much earlier. The gas front displaced the bulk of the oil within the first ten minutes after the experiment started. Since most of the oil was displaced in the bulk flow regime, the

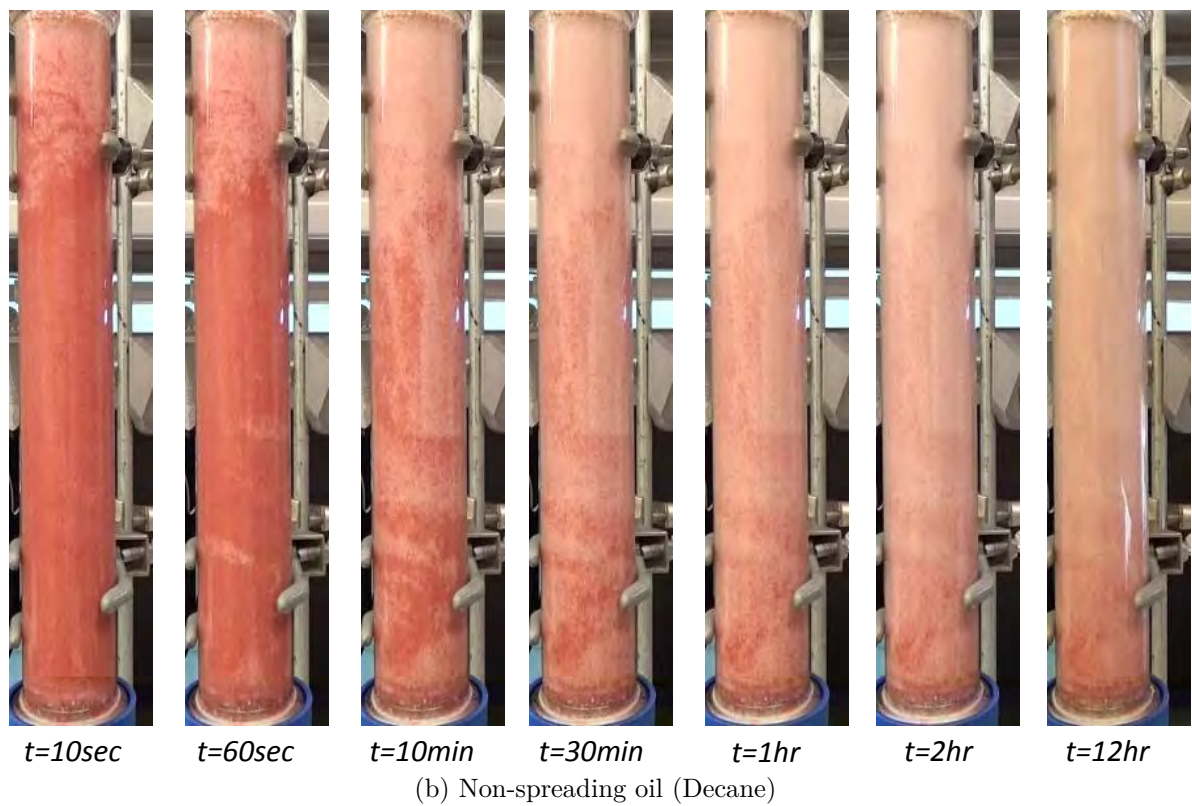
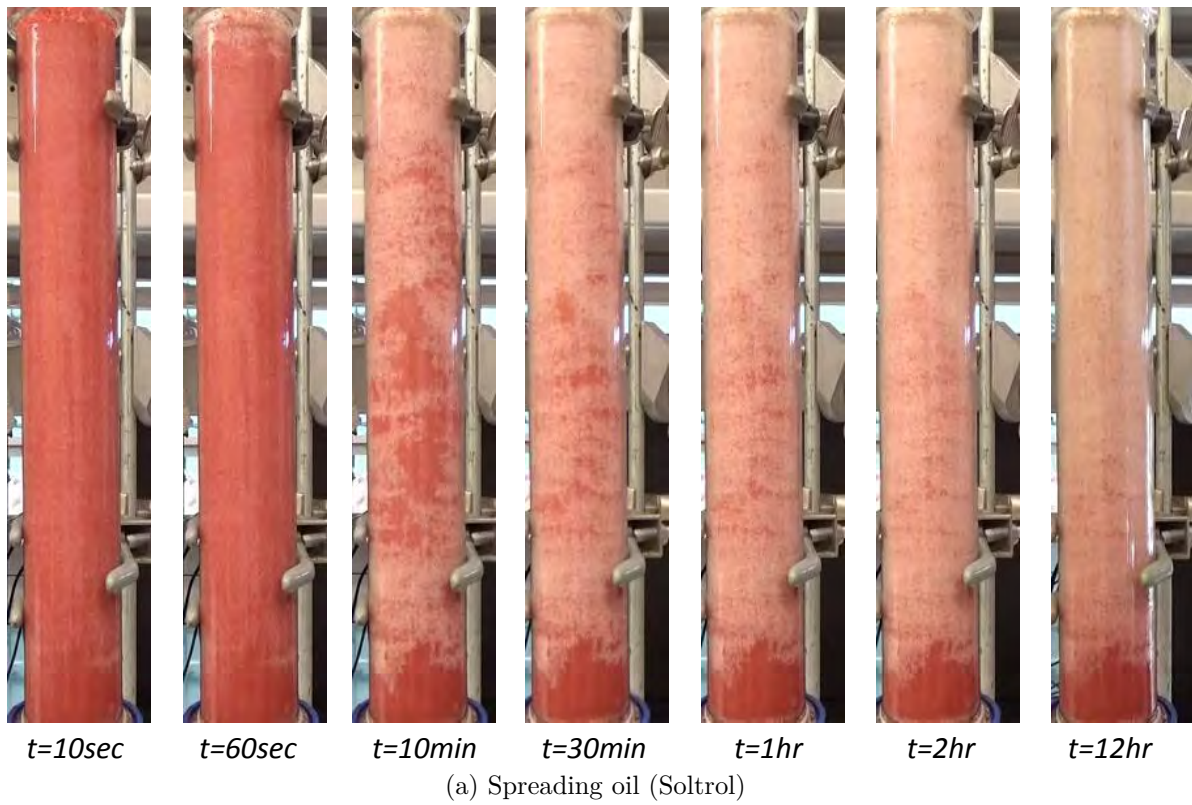


Figure 4.13: Time-lapsed photos of FGD in fractional-wet sand.

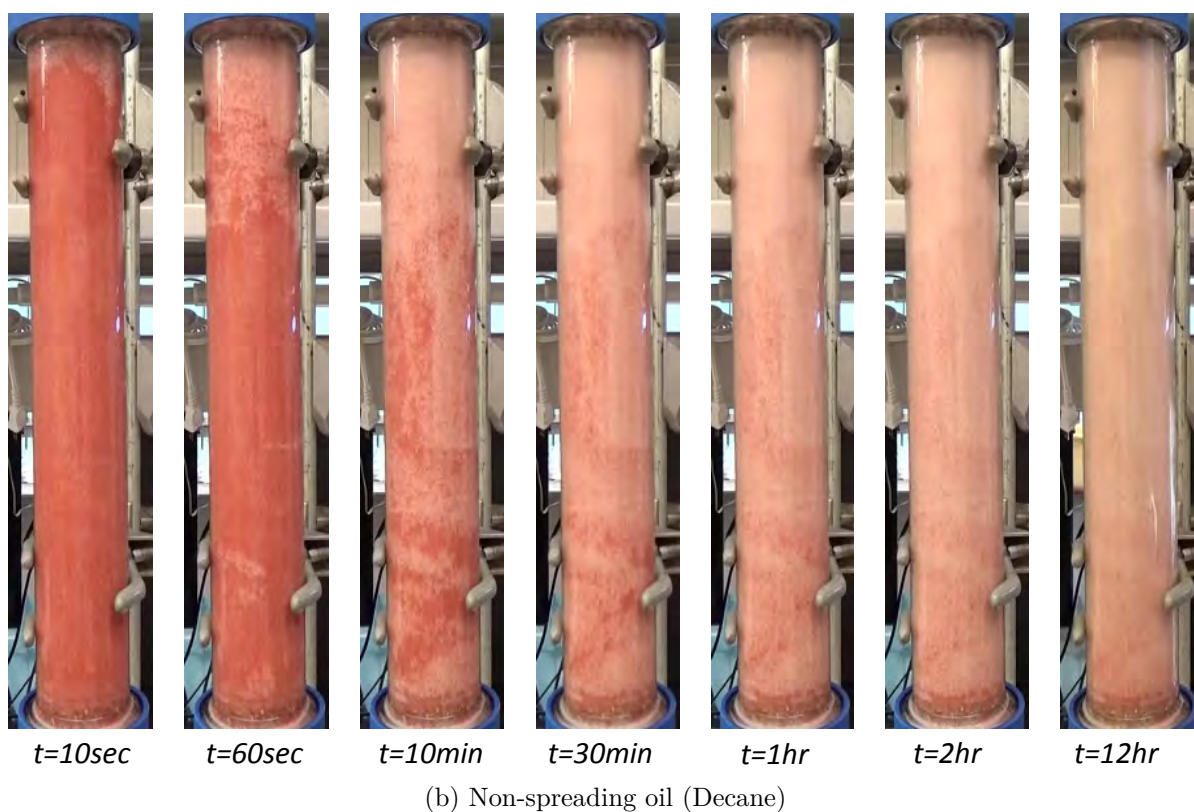
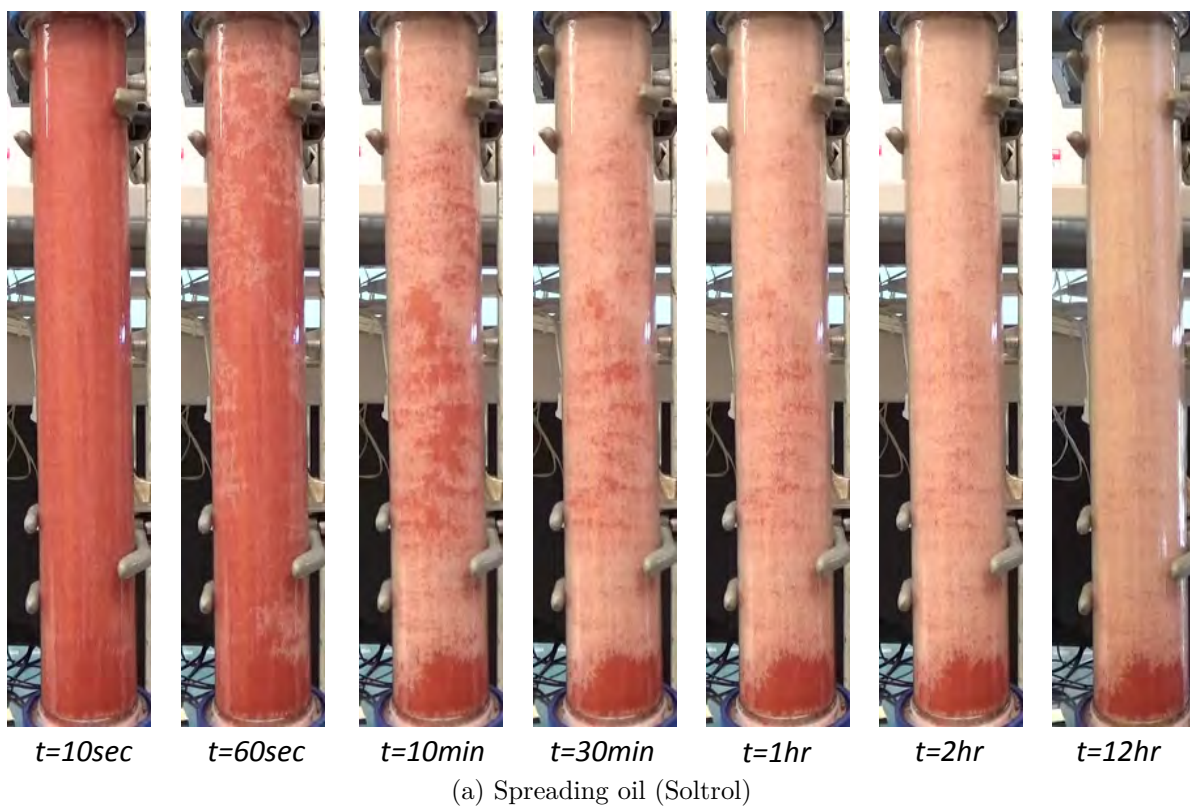


Figure 4.14: Time-lapsed photos of secondary CGD in fractional-wet sand.

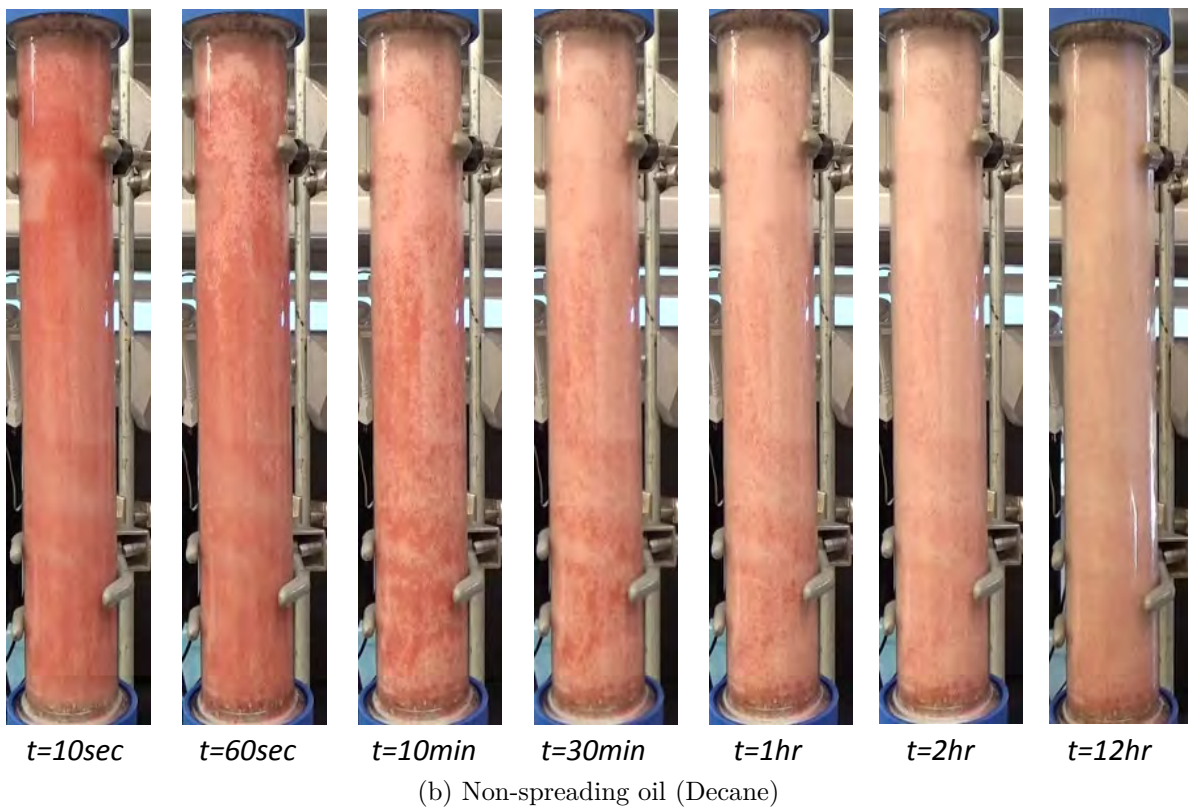
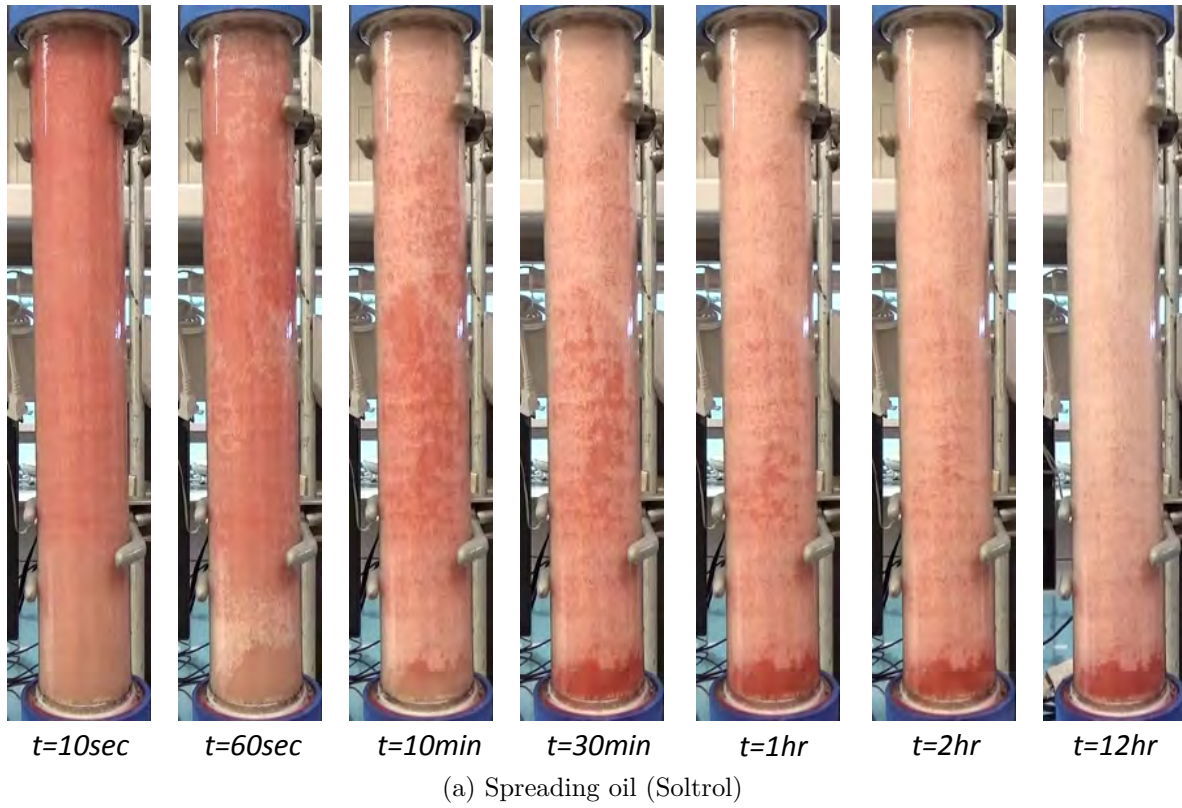


Figure 4.15: Time-lapsed photos of tertiary CGD in fractional-wet sand.

remaining oil was displaced at later time through wetting film. Rapid production through bulk flow at early time followed by drainage through wetting film at later time could possibly explain the higher oil recovery observed for this system.

For secondary CGD the same behavior is observed for the spreading system (4.14a). Oil drainage was delayed in the first 60 seconds with oil patches were seen in the middle of the sand column during the course of the experiment. Although the residual oil was eventually drained, there was still a small accumulation of oil at the bottom of the column when the experiment finished. In the non-spreading system (4.14b) oil drainage occurred immediately after the experiment started. The bulk of the oil was displaced within the first hour and the remaining oil was drained through wetting film for the remainder of the experiment. One notable difference was that there was no visible oil accumulation at the bottom of the column when the experiment was stopped.

In tertiary CGD for the spreading system (4.15a) oil recovery was initially preceded by water production, as can be seen at the bottom of the column in the first 60 seconds. From 60 seconds onward the oil was produced alongside water. This continued for some time, approximately within the first 30 minutes after which the outlet started producing only oil in diminishing amount. During the course of the experiment oil patches were seen, similar to that observed in the previous two experiments. Eventually the residual oil in the patches was drained, but there was still a visible oil accumulation at the bottom when the experiment terminated.

In non-spreading system under tertiary CGD (4.15b) oil and water was produced simultaneously since the beginning of the experiment. There were few oil patches, with most of them observed to be moving downward toward the outlet beginning at $t = 10$ minutes. The concentration of oil patches eventually became more dispersed and sparse as the experiment progressed.

We plot the gas velocity profiles and correlate with the time-lapsed photos of the FGD experiments in Figure 4.16a for spreading oil and Figure 4.16b for non-spreading oil. For

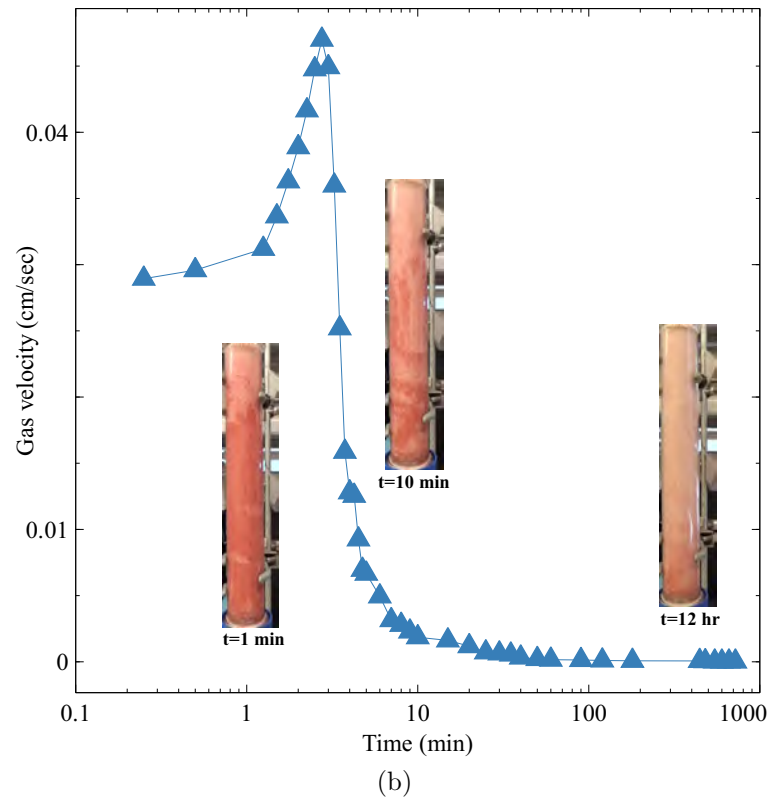
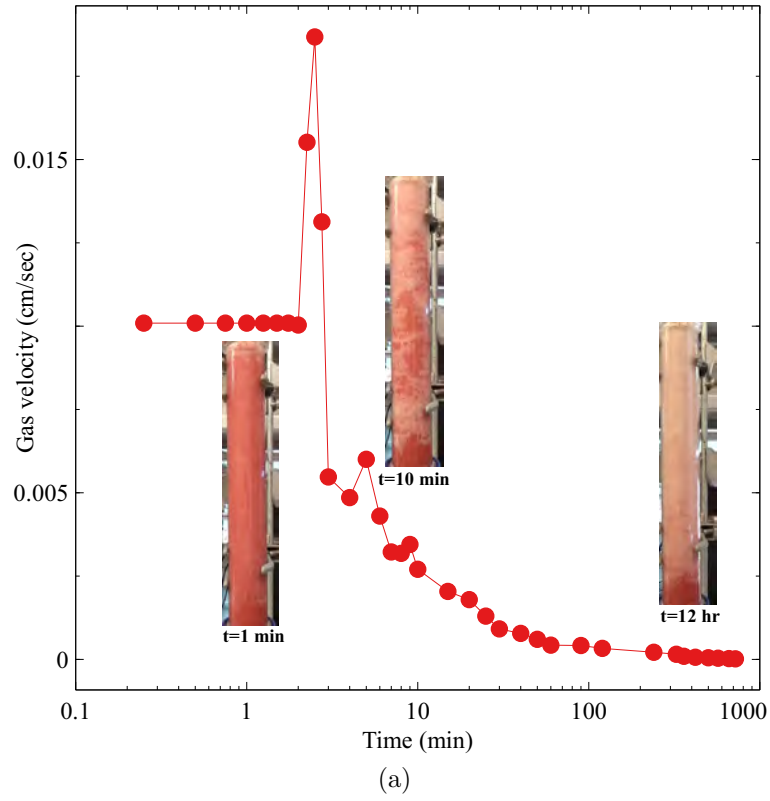


Figure 4.16: Gas velocity profile for FGD experiments in fractional-wet sand correlated with time-lapsed photos of (a) spreading fluid system (Soltrol) (b) non-spreading fluid system (Decane).

the spreading oil the initial velocity profile in Figure 4.16a remained constant until $t = 2$ minutes when the velocity increased for a short time before decreasing gradually until the end of the experiment. The initial flat profile corresponds to the visual observation where capillary pressure was building up to overcome capillary threshold for subsequent invasion. The peak after the flat profile was the maximum velocity attained in the spreading oil system. This also marked the point where sufficient pressure had been generated for successive gas invasion into smaller pores. Since the peak for spreading system was lower than non-spreading system, the average viscous force operating to displace the oil during bulk flow regime was smaller. At later time gas velocity decreased significantly and capillary retention trapped the oil at the bottom.

In non-spreading system, Figure 4.16b showed rapid increase of the gas velocity toward maximum after the experiment started. Capillary pressure build-up occurred much sooner, and consequently most of the pores in the top column were invaded by the gas phase. The maximum velocity was higher, meaning there was greater average viscous force available to the gas front to mobilize the bulk of the oil. This coincided with the rapid oil displacement as seen in the time-lapsed photo for $t = 10$ minutes. Eventually the velocity decreased since most of the pore spaces in the sand have been invaded by gas, and further invasion into even smaller pores would require higher capillary pressure to overcome even greater capillary threshold. At this later stage the oil was drained mostly through the wetting film.

The gas velocity profile for secondary CGD in Figure 4.17 also shows similar trend with the profile for FGD experiment in Figure 4.16. This is not surprising because the displacement sequences as visualized in the time-lapsed photos are similar (cf. Figures 4.13 and 4.14).

In Figure 4.18 the gas velocity profile for tertiary CGD exhibits different behavior from the previous two experiments. Although the velocity was higher initially for the spreading system, it gradually decreased before it jumped to the peak followed by steep decline to very low value. After 10 minutes the gas velocity remained at low value until the end. In

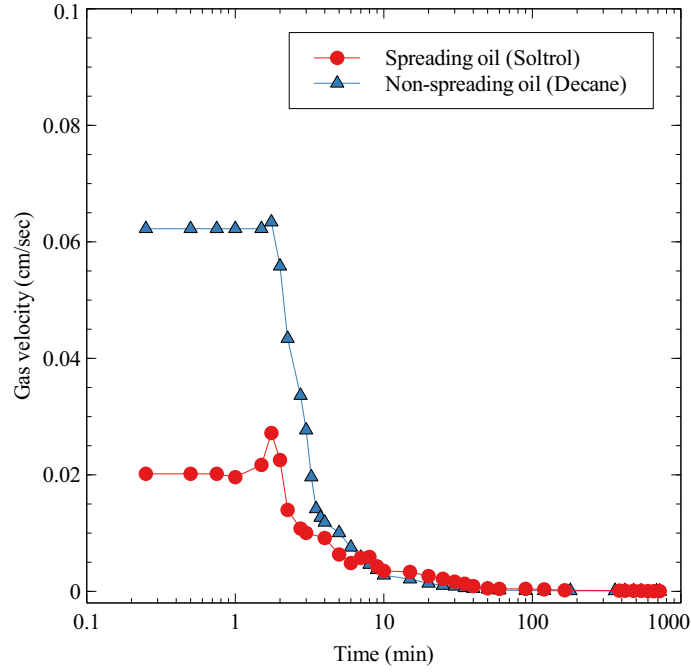


Figure 4.17: Gas velocity profiles for secondary CGD in fractional-wet sand.

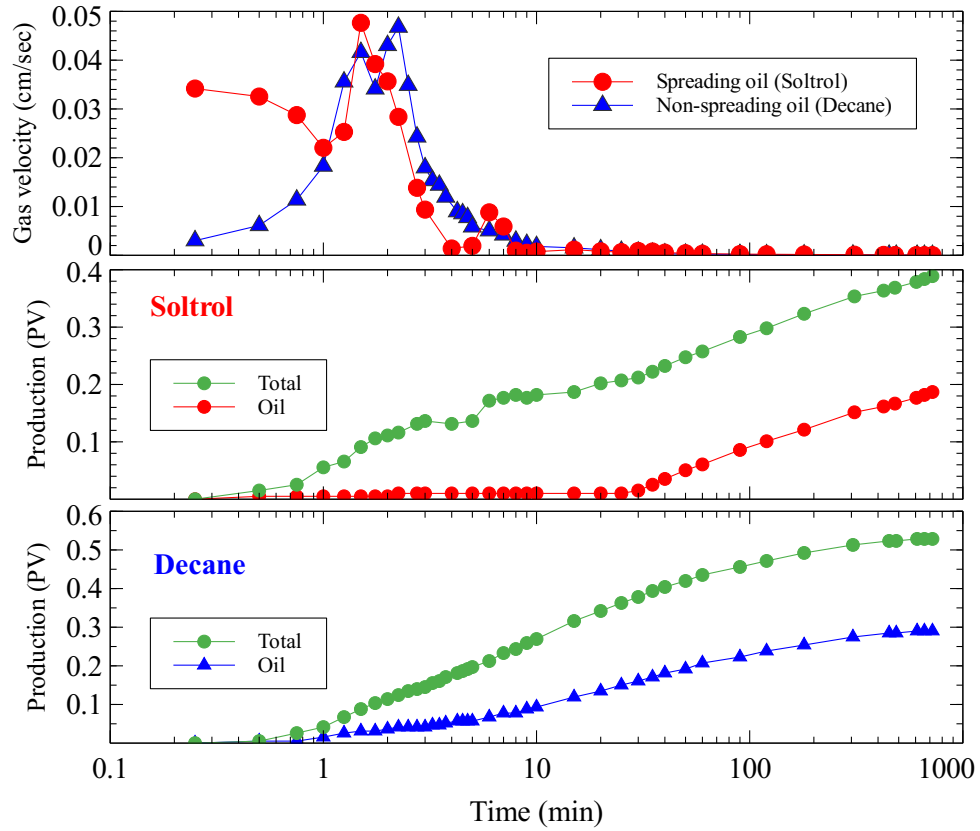


Figure 4.18: Gas velocity and liquid production profile for tertiary CGD in fractional-wet sand.

the non-spreading system the gas velocity increased gradually until $t = 1$ minutes where it jumped to the peak and remained there slightly longer than the spreading case before a steep decline to a very low value. It is observed that during the decline the profile for the non-spreading system was consistently higher than the spreading system.

To understand this behavior further we plot the liquid production profile for both Soltrol and Decane system in Figure 4.18. In the Soltrol case water was produced initially for the first 30 minutes before oil production picked up. This coincided with our observation previously in the time-lapsed photos (4.15a). In the Decane case both water and oil was produced together since the start of the experiment until the end. This is also consistent with the displacement observed in the time-lapsed photos (4.15b).

Therefore we could infer that during tertiary CGD the gas in the spreading system occupied the larger pores since it is non-wetting phase. The gas entered the larger pores in the oil-wet regions where water, also a non-wetting phase, and displaced the water there. This could explain the gradual decrease in velocity initially in the velocity profile. The velocity profile increased afterward because gas was entering the smaller pores in the oil-wet regions to displace the oil there and at the same time displacing oil in the larger pores in the water-wet regions in the sand pack.

In the non-spreading system gas is also the non-wetting phase. The gas velocity gradually increased because early on gas was displacing water in the larger pores in the oil-wet regions and oil in the larger pores in the water-wet regions. Later the velocity peaked to maximum because gas was entering the smaller pores to displace oil in the oil-wet regions and water in the water-wet regions. This explains the simultaneous production of both oil and water in the first 10 minutes into the experiment. Later in the experiment gas velocity both decreased to very low value and remained there until the end for both spreading and non-spreading system. It was during this time that oil drainage was mainly controlled by wetting and spreading film flow.

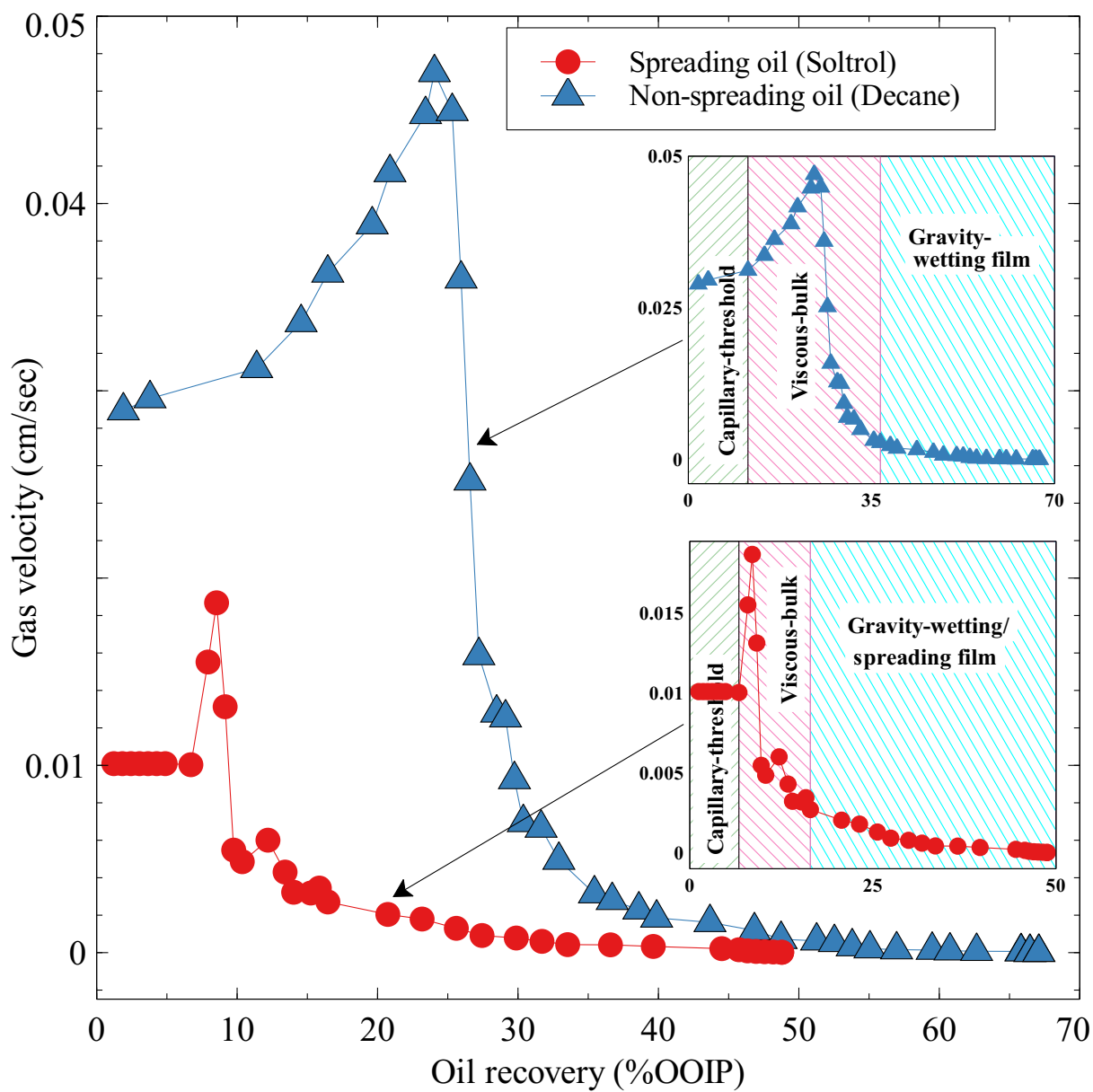


Figure 4.19: Flow-regime for FGD experiments in fractional-wet sand.

Based on visual observation of the displacement process and analysis of the gas profiles, we propose a flow regime map for the particular case of FGD experiment in fractional-wet sand. Figure 4.19 shows the gas velocity profiles plotted against the oil recovery. The top right inset shows the flow regime for the non-spreading fluid system and the bottom right inset for the spreading fluid system. Although the demarcation line separating the boundary between each flow regimes is placed arbitrarily, we based our placement by correlating the oil recoveries, gas velocities and the visuals obtained from time-lapsed photos. For the non-spreading system we identified three main flow regimes, namely the capillary-threshold regime, the viscous-bulk flow regime, and the gravity-wetting film regime. The spreading system exhibits the same regimes, except in the last part it is gravity-wetting/spreading flow regime.

In capillary-threshold regime, capillary pressure is building up to overcome pore-throat threshold pressure to allow gas invasion into smaller pores. This is followed by the viscous-bulk region where viscous forces become dominant and bulk of the oil in the column is displaced in this regime. After a prolonged time the displacement enters gravity-wetting/spreading film regime for the spreading oil case and gravity-wetting film regime for the non-spreading oil. Comparison between both cases allow us to assess qualitatively the relative dominance of particular forces and their corresponding contributions to oil recovery throughout the displacement history. As discussed previously, in non-spreading system almost half the oil is recovered under the first two regimes while the remaining half through the gravity-wetting film regime. In contrast, most of the oil recovery for spreading system occurs through the gravity-wetting/spreading film regime. These observations tie in with our discussion based on the experimental results earlier.

4.1.4 Comparison of wettability effect in secondary GAGD

To evaluate the effect of wettability on oil recovery we plot Figure 4.20 for FGD and secondary CGD experiments respectively. For the spreading system both FGD and sec-

ondary CGD experiments show that oil recovery is highest in water-wet sand. This is followed by oil-wet sand and the least recovery is in fractional-wet sand.

In water-wet sand spreading film flow helps to connect the residual oil bypassed initially by gas to the bulk oil phase. The water coated sand grains form a layer upon which the oil can spread and establish hydraulic path to link up oil elsewhere in the sand. In oil-wet and fractional-wet sand this mechanism is shown to be less effective in recovering additional oil for the spreading system. One possible explanation could be that water, now the non-wetting phase resides in the larger pores. Oil mobilization could be hindered because water is blocking the path. Consequently oil relative permeability would decrease and this affect the transport of the mobilized oil.

In non-spreading system Figure 4.20 shows that oil recovery is higher in oil-wet and fractional-wet sand compared to water-wet sand. This is because in both oil-wet and fractional-wet sand oil is transported through the wetting film flow instead of the spreading mechanism. There is evidence from experimental study using micromodel that support this observation (Sohrabi et al., 2004). At the core scale experimental results using oil-wet sand by Paidin and Rao (2007) also arrive at the same conclusion. The sand grains with oleophilic surface provides the hydraulic path for oil mobilization and transport. In oil-wet sand the wetting film connects pore bodies and pore throats filled with oil everywhere in the sand column. In fractional-wet sand oil in the larger pores displaced by gas in the water-wet regions is linked up with the oil wetting film in the oil-wet regions for subsequent transport. Another explanation for the high recovery as revealed from the analysis of gas velocity and time-lapsed photos is that the drainage of bulk oil occurred earlier and faster than its counterpart in the spreading system. Therefore most of the oil recovery is accounted for through bulk flow and the remaining oil is drained later through the wetting film.

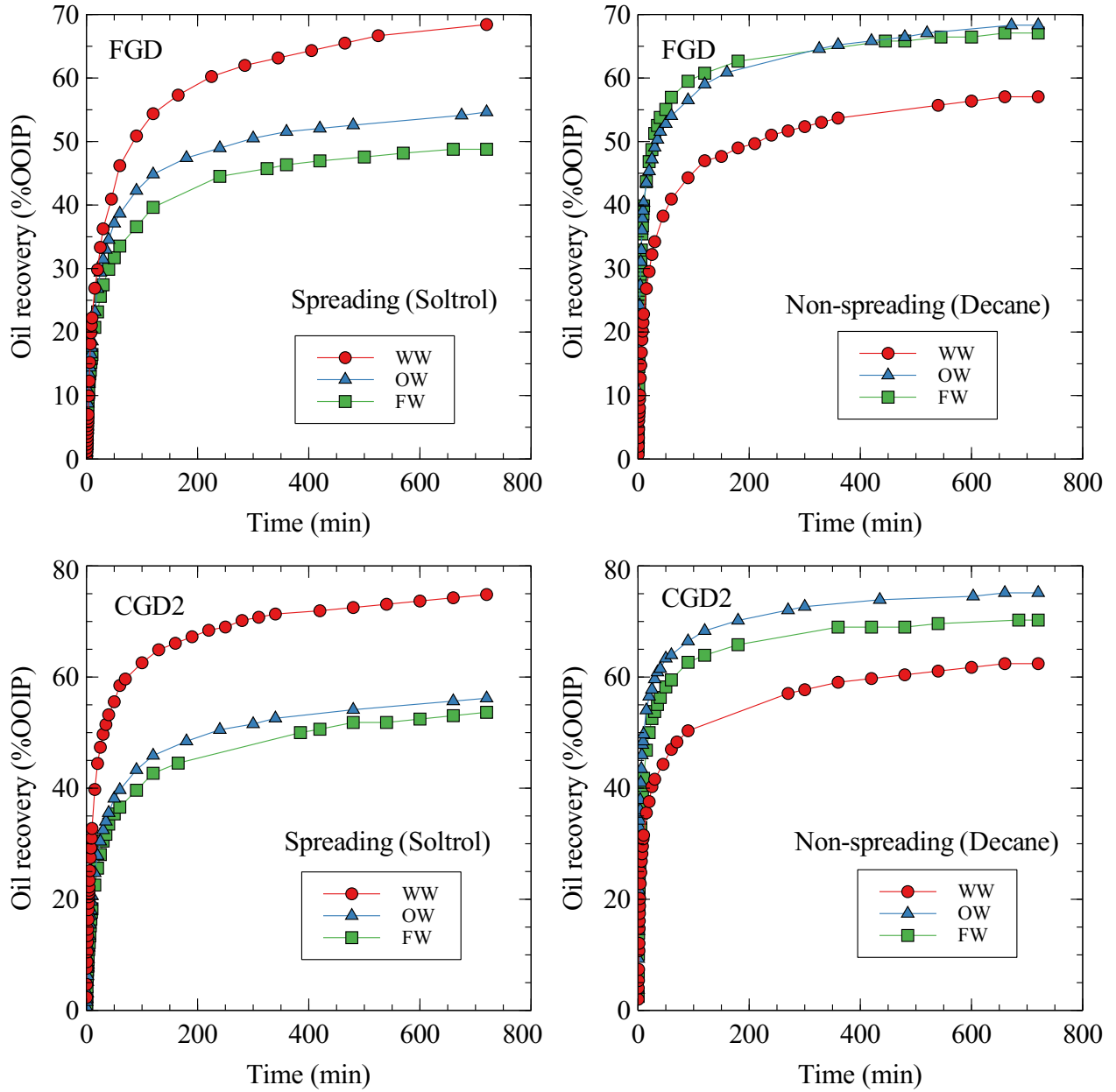


Figure 4.20: Oil recovery for GAGD under FGD and secondary CGD mode with all wet-
tability conditions.

4.1.5 Discussion of GAGD under tertiary mode

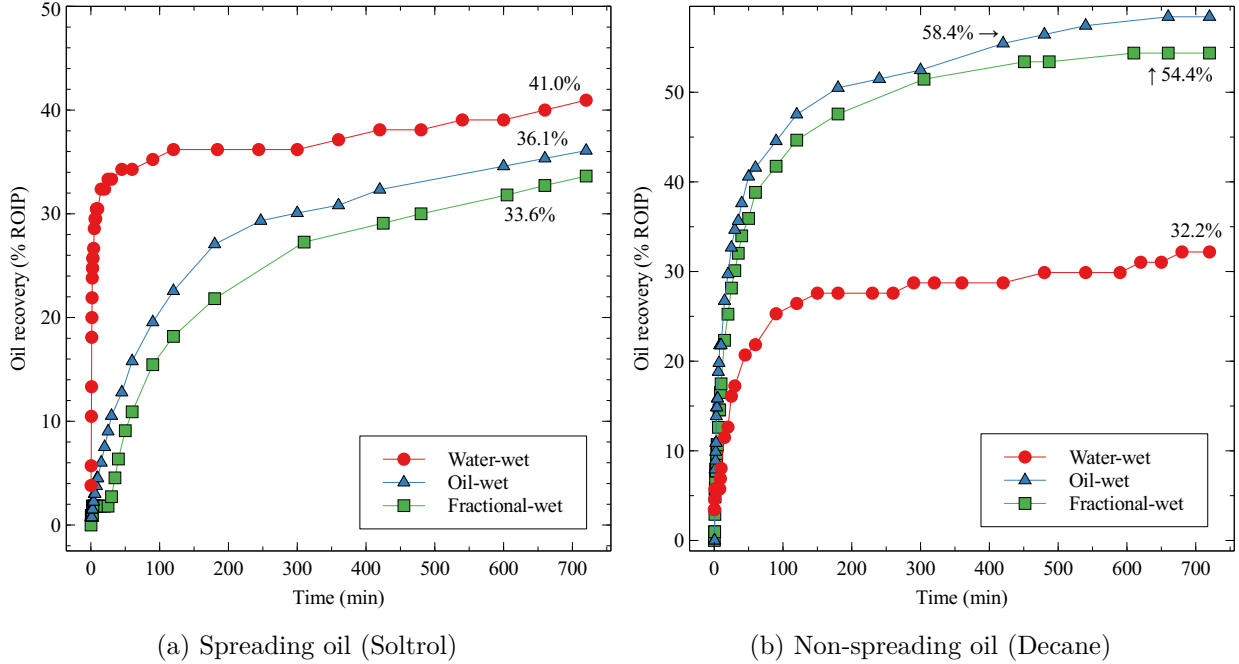


Figure 4.21: Oil recovery for GAGD under tertiary CGD mode with all wettability conditions

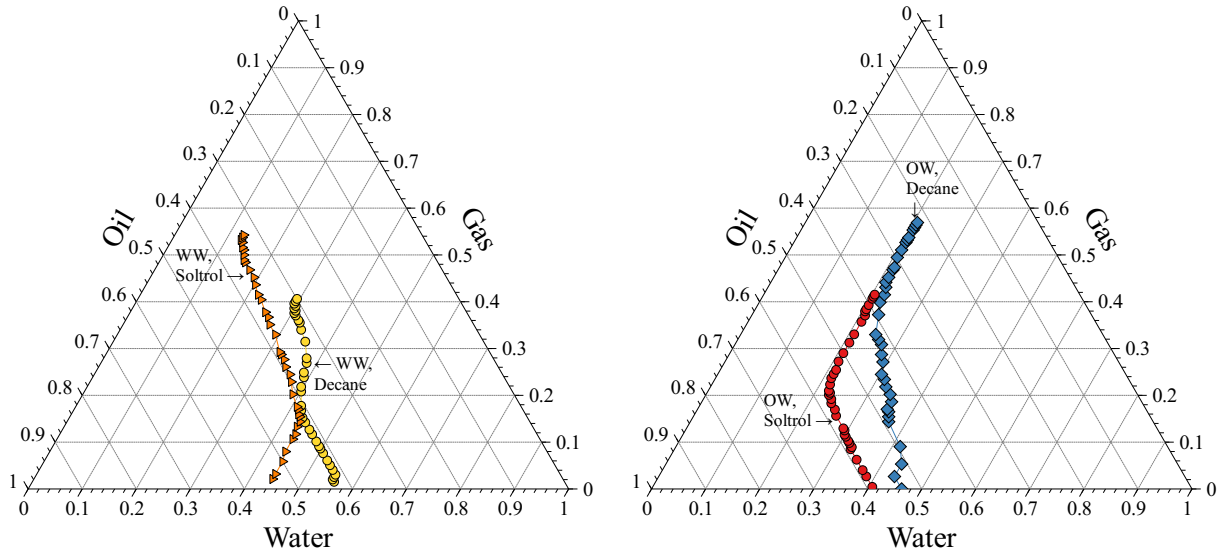
In tertiary CGD experiments Figure 4.21 shows that the oil recovery follows similar trend to that observed in the previous section for both spreading (4.21a) and non-spreading (4.21b) system. As expected the oil recovery is higher in the spreading system with water-wet sand compared to oil recovery in both oil-wet and fractional-wet sand. The underlying reason for the high recovery is similar to that discussed in the previous section. What is most remarkable is that oil recovery is almost twofold for non-spreading system in both oil-wet and fractional-wet sand compared to water-wet sand. Our results suggest that tertiary recovery of non-spreading oil with GAGD works best when the porous media is oil-wet or fractional-wet. This finding would serve as a useful guide to engineers when designing GAGD project in the field.

We plot ternary diagrams in Figure 4.22 to show the saturation paths taken by each phase during the course of the tertiary CGD experiments. In the water-wet experiment with Soltrol, Figure 4.22a shows that initially water saturation was constant because the injected

gas prefers to enter the larger pores and displaces the oil there rather than displacing water which resides in the smaller pores. The bend in the curve marks the point where gas started entering the smaller pores to displace the water until $S_w \approx 0.1$. At the same time the oil saturation changed very little from $S_o \approx 0.4$ at the beginning of the bend until the end of the experiment. Slight decrease during this period indicates that the residual oil reduction is attributed to the spreading mechanism.

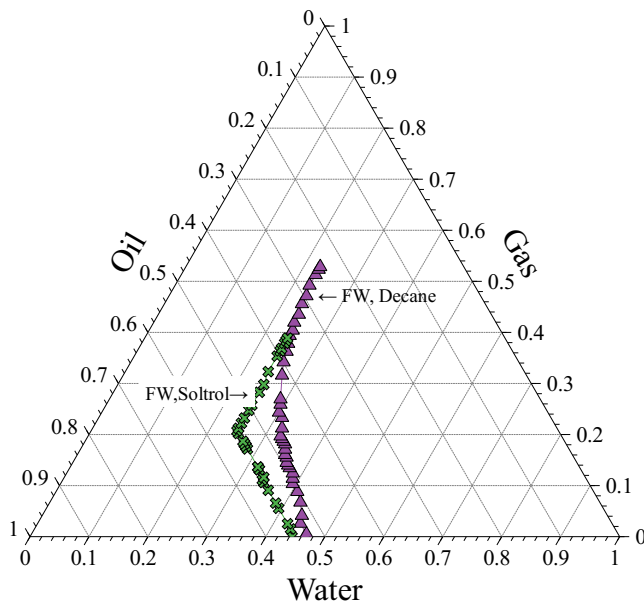
For the non-spreading system with Decane, at the beginning of the experiment water saturation was decreasing because gas prefers to enter the smaller pores containing water than displacing the oil. During this same period oil saturation remained at $S_o \approx 0.4$, possibly because gas bypassed the oil, and the stranded oil found no continuous path to outlet to be mobilized and produced. A point is reached which is marked by a bend in the Decane curve where oil eventually established a continuous path to the outlet. This can be seen where S_o gradually decreased from approximately 0.4 to 0.3. At the point beyond the bend, gas entered both smaller and larger pores to displace the water and oil there respectively. This is because during this period both S_o and S_w was decreasing simultaneously.

In oil-wet sand Figure 4.22b shows that for the spreading system (red curve), water saturation decreased steeply at the beginning of the experiment before the curve reached a bend. This is because water as the non-wetting phase in oil-wet sand resides in the larger pores, hence gas prefers to invade these pores and displaces the water within. At the same time oil saturation remained almost constant because oil resides in the smaller pores, thus it was more difficult for gas to enter the oil-filled pores. A bend in the Soltrol curve marks the point where oil saturation decreased precipitously while water saturation remained constant. The bend indicates that gas has started to invade the smaller pores containing oil and displace them. The oil saturation terminated at a point slightly less than



(a) Water-wet

(b) Oil-wet



(c) Fractional-wet

Figure 4.22: Ternary diagrams showing saturation paths for tertiary CGD experiments under all wettability conditions

$S_o \approx 0.4$ because gas could not penetrate even smaller pores or the path of oil mobilization was blocked by water.

In the non-spreading system (blue curve) water and oil was produced simultaneously in the beginning of the experiment. This is seen from the gradual decline of both water and oil saturation during this period. This means that gas entering the sand column simultaneously invaded both small and large pores filled with oil and water respectively. At some point a bend was reached where the water saturation settled on a constant value of approximately 0.2 while oil saturation continued to decrease steeply. During this time gas has invaded most of the larger pores and now displacing oil in the smaller ones. Residual oil saturation at the end of the experiment was significantly smaller than that of the spreading case. This is possibly because the wetting film in the non-spreading case has more transport capability due to having greater conductance than its counterpart in the spreading system. This will be elaborated further in Section 4.2.

The saturation paths in fractional-wet experiments is shown in Figure 4.22c. For the Soltrol curve water saturation decreased steeply in the beginning before the curve reached a bend whereby afterward water saturation remained almost constant. At the same time oil saturation appeared to be almost constant before the bend and decreased steeply afterward. This observation can be correlated with analysis of the gas velocity profile and time-lapsed photos previously (cf. Figures 4.15a and 4.18). Comparison with the saturation path for the spreading case in oil-wet sand in Figure 4.22b revealed similar pattern. Therefore the mechanism that operates during oil-wet experiment with Soltrol also applies in the fractional-wet case. The trend in the Decane curve is also similar to the one in oil-wet system. One notable difference however is that there appears to be no clear point where the curve bends and water saturation reached a constant value.

4.1.6 Summary of gravity drainage results

We have performed a series of gravity drainage experiments in water-wet, oil-wet and fractional-wet sand packs. Analysis of the results based on time-lapsed photos and gas-velocity profiles helps us to understand the internal mechanics of the displacement process. For gravity drainage in water-wet sand, higher oil recovery is achieved with Soltrol as the spreading oil. This is attributed to the spreading oil forming film when all three phases are present. In oil-wet sand, experiments using Decane as non-spreading oil resulted in higher recovery. The same trend is observed for experiments with fractional-wet sand. In both cases significant portion of oil in the column is recovered through bulk flow in the early time and subsequent recovery occurred through wetting film until termination of the experiments. In the next section we investigate the pore-scale dynamics to understand the underlying mechanisms, particularly for the cases where our results differed from findings in the literature.

4.2 Pore-scale mechanisms

To gain better understanding of the displacement mechanism, it is instructive to focus on the pore-level mechanism. This is because analysis of the core-level experiments has limitation particularly when explaining the behavior of our oil-wet and fractional-wet experiments. The pore-level mechanism would involve all three phases because in gravity drainage process the gas phase invades a vertical column saturated with water and oil. The introduction of a third phase to an existing two-phase system presents additional problem of determining the fluid distribution and pore occupancy, which altogether affect the displacement behavior. Although we did not perform experiments at the pore-scale, we used results from micromodel studies available in the literature to help us understand the pore-level mechanism.

In a three-phase process, the simultaneous interactions between fluid-fluid and fluid-rock influence the trapping and mobilization of the oil phase. The spreading behavior de-

scribes the fluid-fluid interaction while wettability affect the fluid-rock interaction. Therefore to enable direct comparison at the pore-level, we used micromodel studies with similar setup that match the spreading behavior and wettability system of our core-scale experiments.

In the literature, we found such studies from experiments and network model simulations conducted by Øren and Pinczewski (1991), Oren et al. (1992), Oren and Pinczewski (1994) and Oren (1994). Their work investigate the effect of spreading and wettability on a three-phase displacement during immiscible gas injection in water-wet and oil-wet systems. Later work by Øren and Pinczewski (1995) summarized their previous results and systematically characterized the pore-scale fluid configuration based on interfacial tension, contact angle and capillary pressure.

In order to relate their pore-level results to our core-level experiments, we will use their naming convention, whenever necessary for the fluid phases. Hence the non-wetting phase is fluid-1, the intermediate phase is fluid-2 and the wetting phase is fluid-3.

4.2.1 Pore-scale fluid configuration

In a two-phase system, one phase wets the rock surface while the other phase becomes the non-wetting phase. Based on capillary pressure requirement, the wetting phase tends to occupy the smaller pores while the non-wetting phase prefers to reside in larger pores. In a three-phase system, the fluid arrangement is less straightforward because the non-wetting, intermediate and wetting phase interact with spreading, wettability and capillary pressure to determine the pore occupancy. According to Blunt et al. (1994), the wetting phase (fluid-3) will occupy the smaller pores or the crevices and angularities in the larger pores. The other two phases (fluid-1 and fluid-2) will compete to occupy the larger pores. Although both fluids are non-wetting, for the same pore geometry, the fluid that has the larger capillary pressure difference relative to fluid-3 will occupy the larger pore space. Øren and Pinczewski (1995) simplify this condition as:

$$\sigma_{13} > \sigma_{23} \quad (4.2)$$

where σ refers to the interfacial tension and the subscripts refer to fluid-1-fluid-3 and fluid-2-fluid-3 pair respectively. The fluid that satisfies the condition in Equation 4.2 is the most non-wetting phase fluid-1, leaving the other phase as the intermediate phase fluid-2. For example using the fluid properties in Table 3.1 on page 33 for water-wet spreading system, fluid-3 is water, fluid-1 (non-wetting phase) is gas and fluid-2 (intermediate phase) is oil. To satisfy the capillary pressure requirement, the intermediate phase cannot occupy the larger pore if it already contained the non-wetting phase. From micromodel observation, Øren and Pinczewski (1995) noted that the intermediate phase tends to occupy the space between the pore throat and entrance to the pore body.

The intermediate phase in a three-phase system determines the spreading behavior. When the intermediate phase spreads over the wetting surface, the process is spontaneous due to decrease in free energy (Adamson and Gast, 1997). This is characterized by the spreading coefficient S_{23} :

$$S_{23} = \sigma_{31} - \sigma_{32} - \sigma_{12} \quad (4.3)$$

where σ is the interfacial tension and the subscripts refer to fluid 3-fluid 1, fluid 3-fluid 2, and fluid 1-fluid 2 interfaces respectively. In a water-wet system, this becomes

$$S_{ow} = \sigma_{wg} - \sigma_{wo} - \sigma_{go} \quad (4.4)$$

For all cases the intermediate phase can only spread when $S_{23} > 0$. Three-phase system that meets this condition is defined as having Configuration A according to Øren and Pinczewski (1995). This is shown in Figure 4.23 where fluid-2 the intermediate phase spreads between fluid-1 and fluid-3 and at the same time envelops fluid-1 completely.

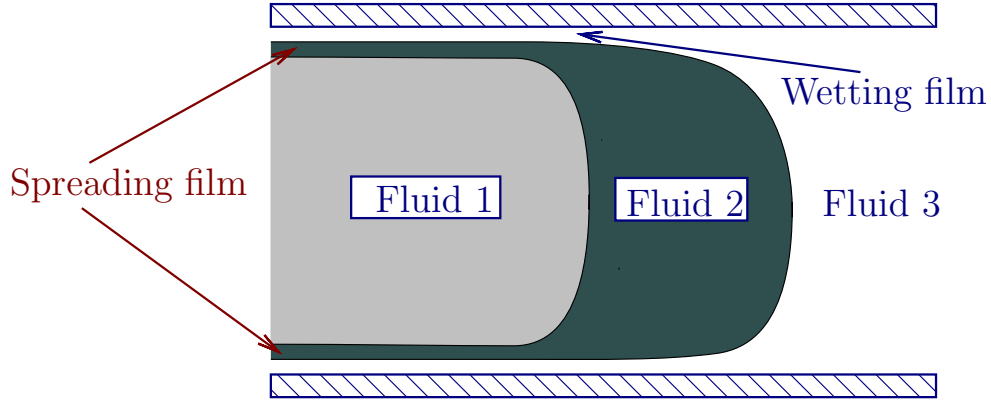


Figure 4.23: Configuration A

When the intermediate phase does not spread, $S_{23} < 0$. In this condition a three-phase contact line is formed at the point where all phases meet. If no stable three-phase contact line exist even though S_{23} is negative, the wetting film (fluid-3) spreads between fluid-1 and fluid-2.

We can define the condition for existence of stable three-phase contact line as

$$\frac{\sigma_{13}}{|\sigma_{12} - \sigma_{23}|} > 1. \quad (4.5)$$

The fluid system that satisfies the condition in Equation 4.5 is defined by Øren and Pinczewski (1995) as having Configuration B. This configuration is shown in Figure 4.24. Note that in Figure 4.24 both non-wetting phases fluid-1 and fluid-2 is linked together by three contact angles α , θ and δ . For a non-spreading water-wet system, α is θ_{ow} , θ is θ_{go} and δ is θ_{gw} .

What happens when the condition given in Equation 4.5 is not satisfied? This leads to the last configuration, shown in Figure 4.25 as Configuration C. In this configuration there is no three-phase contact line linking fluid-1 and fluid-2. Instead both phases are separated by a thin film of fluid-3.

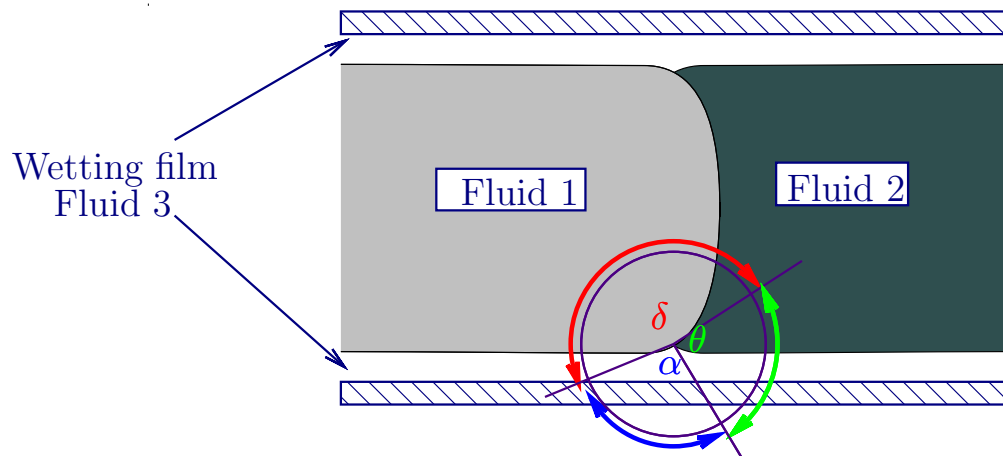


Figure 4.24: Configuration B

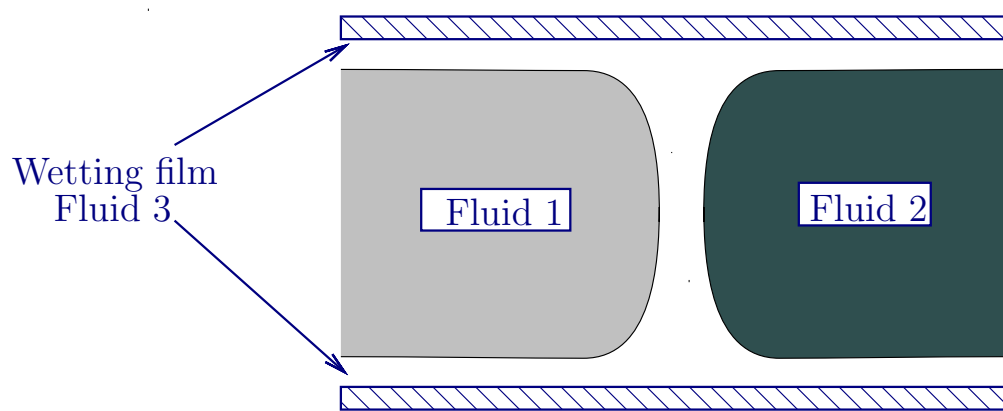


Figure 4.25: Configuration C

4.2.2 Dynamic three-phase pore-scale fluid displacement

The fluid configurations discussed above were observed to maintain their morphology during displacement (Øren and Pinczewski, 1995). Although three phases are involved, at any particular time only one interface is advanced. Pereira et al. (1996) in their network model simulations explained that based on micromodel experiments, the fundamental displacement occurring in a three-phase system actually consisted of sequences of two-phase displacement. This means the displacement process can be described using the familiar two-phase flow such as drainage and imbibition. More description on two-phase displacement process can be found in Lenormand et al. (1983) and Lenormand and Zarcone (1984). In a drainage process, a non-wetting fluid displaces the wetting fluid in a piston-like fashion when the interface capillary pressure is greater than the threshold pressure. During imbibition, the wetting fluid displaces the non-wetting fluid when the interface capillary pressure is smaller than the threshold pressure. The imbibition process allows the defending fluid to be displaced either through piston-like invasion or snap-off. When the fluid is intermediate phase it is non-wetting with respect to the wetting fluid but wetting with respect to the non-wetting fluid. Thus displacement process involving the intermediate phase (fluid-2) can be either drainage or imbibition process.

In our experiments the invading fluid is either fluid-1 (non-wetting) or fluid-2 (intermediate). When the invading fluid is a non-wetting phase its interface has greater capillary pressure, therefore it can fill a pore body that contains either wetting or intermediate fluid and displace them. However when the pore already contained fluid of the same phase, it will merge with the fluid. For invasion with intermediate fluid it will displace a pore that contains a wetting fluid. If the pore contains fluid of intermediate phase the fluids will merge. Its advance will be halted if the pore body is already occupied by a non-wetting fluid.

For actual displacement to take place, the invading fluid has to arrive at the invasion site (the pore) while the defending fluid has to move away from the invasion site. The transport

of invading or defending fluid occurs through bulk or film flow. The non-wetting fluid flows to an invasion site through a series of adjoining pore bodies and pore throats filled with the same phase (bulk flow). The wetting fluid is transported away from the site through a series of adjoining pore bodies and pore throats filled with the wetting phase (bulk flow) and linked by wetting film. This makes the wetting fluid to be hydraulically connected anywhere in the porous media. When the invading fluid is fluid-2 (intermediate phase), the manner in which it is transported depends on the sign of the spreading coefficient S_{23} . A positive spreading coefficient indicates a spreading film exists (Figure 4.23) therefore the fluid flow is similar to that of the wetting fluid, with bulk flow through adjoining pores and throats linked by spreading film. If the spreading coefficient is negative, there is no spreading film thus the fluid flow is through bulk flow similar to that of the non-wetting fluid.

Visualizations from micromodel experiments conducted by Øren and Pinczewski (1991), Oren and Pinczewski (1994) and Øren and Pinczewski (1995) have identified three displacement mechanisms operating in three-phase system: direct-drainage, double drainage and imbibition-drainage. These mechanisms are controlled by wettability, capillary pressure and the spreading behavior of the fluids. Direct drainage mechanism is a two-phase process where either fluid-1 (non-wetting) or fluid-2 (intermediate) directly displaces fluid-3 (wetting). Alternate course would be fluid-1 displacing fluid-2. Double drainage mechanism is a sequence of two drainage events: the non-wetting displacing intermediate fluid followed by the intermediate fluid displacing the wetting fluid. In imbibition-drainage mechanism, fluid-2 first displaces fluid-1. This is an imbibition event because fluid-2 is wetting relative to fluid-1 and the capillary threshold pressure is negative. This is followed by drainage event where the displaced fluid-1 then displaces fluid-3. In all drainage events the invading fluid can only advance when the capillary pressure is greater than the defending fluid's capillary threshold pressure. Note that all drainage mechanisms result in mobilization of fluid-3 because the wetting fluid is continuous throughout the system. When fluid-2 is the

defending fluid, it can only be mobilized through the double drainage mechanism because it depends on continuity of fluid-3 for transport.

Mobilization of fluids in Configuration A, B and C occur through the direct drainage and double drainage mechanism when fluid-1 is the injected fluid. In Configuration B and C for oil-wet system the injected fluid can be of intermediate phase (fluid-2). Fluids mobilization in this particular case occur through direct drainage and imbibition-drainage mechanism.

4.2.3 Discussion of pore-scale mechanisms in experimental results

Based on previous discussion, and using fluid properties in Table 3.1 on page 33 we have determined the pore-level fluid configurations in our experiments. This is shown in Table 4.2 on the next page. For comparison we also determined the pore-level fluid configuration for oil-wet case in Vizika and Lombard (1996) using their fluid properties. To facilitate the comparison, the result from additional oil-wet experiment we performed using the non-spreading fluid system of Vizika and Lombard (1996) is also shown. In Table 4.2 on the following page we can see which fluid is non-wetting (fluid-1), intermediate (fluid-2) and wetting (fluid-3) for each experiment. Note that for fractional-wet experiments the fluid that become the non-wetting, intermediate and wetting phase could interchange. This depends on the local spreading behavior and the local wettability of the sand grains. The table also listed the oil recoveries corresponding to each experiment in the free-fall mode (FGD).

There are several observations we can make in Table 4.2. For example the only instance when the intermediate phase (oil) is spreading is when the fluid configuration is A in water-wet system. This might affect the oil recovery because higher recovery is achieved for Configuration A than that for Configuration B. The oil recoveries in oil-wet experiments are similar when using spreading and non-spreading fluid system based on Soltrol, regardless the fluid configurations. However the oil recovery is significantly higher in oil-wet system

Table 4.2: Pore scale configurations and oil recoveries for gravity drainage experiments.

Wetting system	Experiment	Fluid system	S_{23}	Fluid 1	Fluid 2	Fluid 3	3-phase contact line	Config.	k (Darcy)	ϕ	Recovery (%OOIP)
WW	This study	spreading (Soltrol)	+12.0	gas	oil	water	x	A	3.8	0.346	68.4
	This study	non-spreading (Decane)	-3.4	gas	oil	water	✓	B	3.8	0.346	57.0
OW	This study	non-spreading (Decane)	-43.6	water	gas	oil	✓	B	3.2	0.346	68.3
	This study	non-spreading (Soltrol+isobutanol)	-41.5	gas	water	oil	✓	B	7.2	0.394	55.8±0.8
	This study	spreading (Soltrol)	-60.0	water	gas	oil	x	C	6.6	0.413	54.6
OW	Vizika and Lombard (1996)	spreading (Soltrol)	-61.5	water	gas	oil	x	C	9.5	0.334	74.8
	Vizika and Lombard (1996)	non-spreading (Soltrol+isobutanol)	-41.5	gas	water	oil	✓	B	9.5	0.327	73.3
FW	This study	non-spreading (Decane)	-3.4/ -43.6	gas/ water	oil/ gas	water/oil	✓	B	5.5	0.355	67.1
	This study	spreading (Soltrol)	+9.0/ -53.0	gas/ water	oil/ gas	water/oil	x	A,C	8.9	0.365	48.8

WW : water-wet
 OW : oil-wet
 FW : fractional-wet
 S_{23} : spreading coefficient, intermediate over wetting phase
 Config. : Configuration
 k : permeability
 ϕ : porosity

when Decane is used as the non-spreading fluid. In fractional-wet experiments, the non-spreading fluid system achieves higher oil recovery than spreading fluid system. We discuss these observations by considering the pore scale fluid configuration and displacement.

4.2.3.1 In water-wet media, higher oil recovery is achieved for spreading fluid system

In Table 4.2 for water-wet sand the spreading fluid system has Configuration A while non-spreading system has Configuration B.

The distribution of fluids in the water-wet sand is shown in Figure 4.26 for spreading system (Configuration A) and non-spreading system (Configuration B). In Figure 4.26a the existence of spreading film helps to reconnect isolated oil ganglia. The hydraulic path established by the film enabled the reconnected oil to be drained to very low saturation.

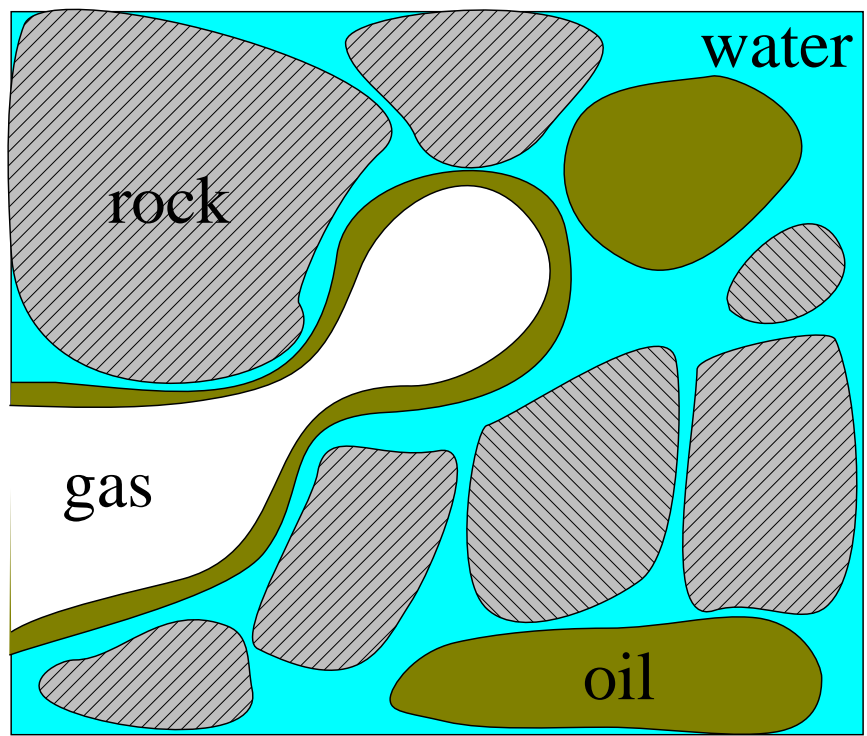
In contrast the non-spreading system in Figure 4.26b does not form spreading film. The absence of film prevents isolated oil ganglia from reconnecting and because there is no continuous path for the oil phase to the outlet, the ganglia remain trapped.

When GAGD is performed at condition where initial oil saturation is high, the path for the mobilized oil to drain to the outlet is through bulk flow (adjacent pores and throats filled with oil) interconnected with spreading film flow. For example this corresponds to the case at early time during gravity drainage experiment in free-fall mode (FGD) or secondary mode (sec. CGD). At low oil saturation the role of spreading film becomes more dominant. This is because the flow capacity through bulk flow decreases at later time when most of the pores and throats are filled with gas. Since the only path for flow is through the spreading film, the oil recovery at later time tends to extend for prolonged period. Sand pack experiments by Zhou and Blunt (1997) using hexane as spreading oil took about three weeks to attain 0.1% oil saturation. Likewise experiment with consolidated rock by Dumore and Schols (1974) using kerosene as spreading oil required three months to drain the oil to 3% saturation.

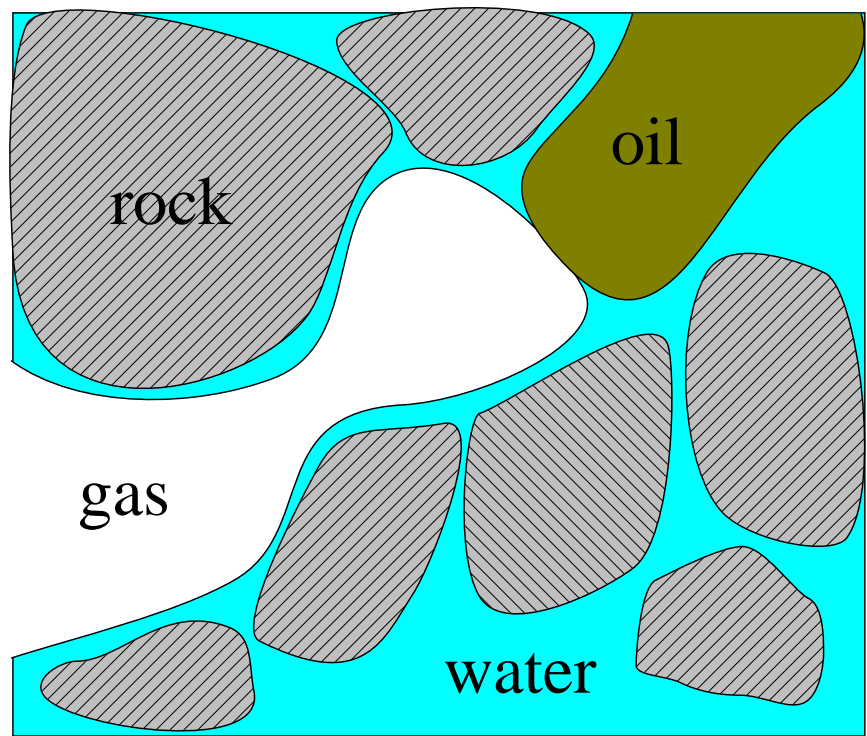
GAGD experiment performed where the initial condition is oil at residual saturation also has limited drainage path through bulk flow. This is because the pores and throats are filled with water and the oil phase is isolated, which makes spreading film flow the overall mechanism for transport of mobilized oil throughout the experiment. Such is the case for gravity drainage in tertiary mode (tert. CGD). Although the mechanism is slow it offers possibility for mature, waterflooded field to extend its production life.

4.2.3.2 Oil recovery is similar for spreading and non-spreading fluid system in oil-wet media

Comparison of results from oil-wet experiment in Vizika and Lombard (1996) showed that oil recoveries for both spreading and non-spreading system were similar. The same can be said for our oil-wet experiments using Soltrol and Soltrol + isobutanol pair. At the pore level the spreading system is represented by Configuration C while non-spreading system is



(a) Spreading fluid system



(b) Non-spreading fluid system

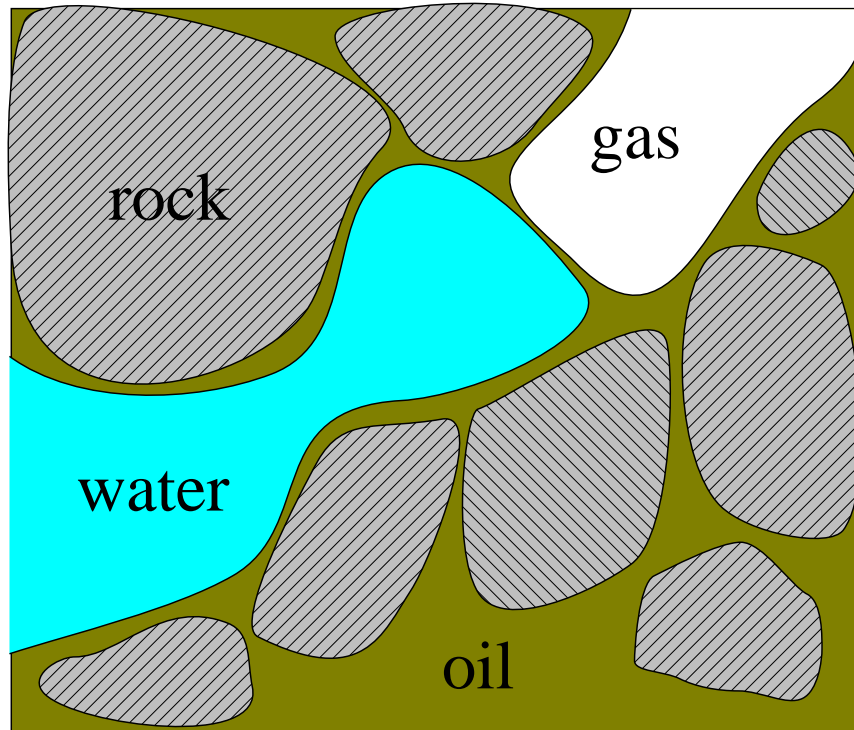
Figure 4.26: Pore scale fluid configuration in water-wet experiments

Configuration B. This is shown in Figure 4.27. The significant differences between the two systems are that water and gas is separated by a thin film of oil in the spreading system; while in non-spreading system both non-wetting phases are linked by a three-phase contact line. Oren and Pinczewski (1994) explained that for oil-wet system the fluid configuration at the pore level has little effect on the eventual oil recovery because oil is always the continuous phase. This means that oil is drained through both bulk flow (adjacent pores and throat filled with oil) and wetting film flow.

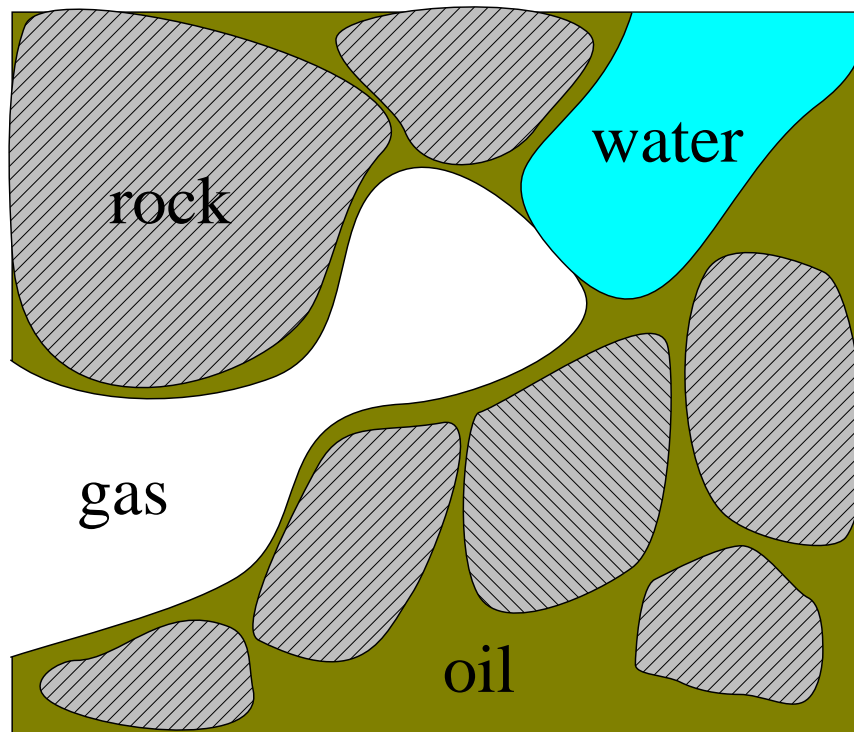
Given the same pore geometry, gas as the invading phase favors entry into oil-filled pores since the gas-oil interfacial tension is lower ($\sigma_{go} = 22$ mN/m for spreading, 25.5 mN/m for non-spreading) and the capillary threshold is smaller. For oil-wet GAGD at high initial oil saturation (free-fall and secondary mode) direct drainage of gas-oil interface is the mechanism that contributes to oil production. When GAGD in oil-wet media is performed after waterflooding (oil at residual saturation) high water saturation prevents the displaced oil to be transported through bulk flow because the adjacent pores and throats are filled with water. In this condition oil is displaced through wetting film either through double drainage mechanism when gas is the non-wetting phase (Configuration B) or imbibition-drainage mechanism when gas is the intermediate phase (Configuration C).

4.2.3.3 Oil recovery is higher for low viscosity, non-spreading fluid system in oil-wet media

Studies investigating the effect of spreading and wettability in three-phase flow such as those from Chatzis et al. (1988), Oren and Pinczewski (1994), Øren and Pinczewski (1995) and Vizika and Lombard (1996) used the same fluid pairs to model the spreading and non-spreading fluid system. Both Soltrol and Soltrol + isobutanol pair have similar density and viscosity. Their experimental designs used such fluid systems in order to highlight the effect of spreading and wettability; and at the same time minimize variations caused by changing fluid properties. This helps to provide clear interpretation of the results. Consequently the



(a) Spreading fluid system



(b) Non-spreading fluid system

Figure 4.27: Pore scale fluid configuration in oil-wet experiments with Soltrol-based fluid system

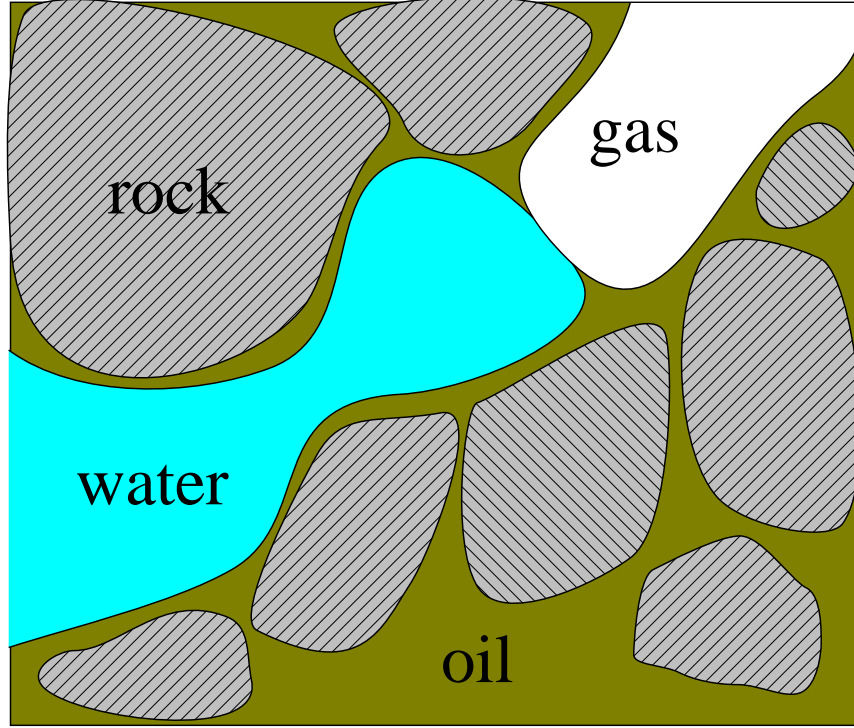


Figure 4.28: Pore scale fluid configuration in oil-wet experiments with low viscosity, non-spreading Decane

results from these experiments with oil-wet media share similar conclusion as that discussed in Section 4.2.3.2 previously.

In this study we used Decane as the non-spreading fluid. The fluid configuration at the pore scale is shown in Figure 4.28. The configuration is similar to that of Soltrol in oil-wet (Figure 4.27a) except that both water and gas is attached to a three-phase contact line. As discussed previously the fluid configuration at the pore scale has little effect on the eventual oil recovery in oil-wet media. However if we consider the pores and throats as bundles of capillary tubes and assume that the flow of the wetting phase follows Poiseuille's law, we can define its conductance as (Blunt, 1997)

$$g = \frac{Ar^2}{\beta\mu L} \quad (4.6)$$

where A is the area occupied by the wetting phase of contact angle θ in a pore of square cross-section, r is the curvature radius of the fluid interface, β is a dimensionless resistance

factor, μ is the wetting phase viscosity and L is length of the element. In Equation 4.6 by assuming all the terms are the same, oil that has higher viscosity (Soltrol, $\mu = 2.75$ cp) will have lower conductance than that for Decane ($\mu = 0.84$ cp). The conductance affects the drainage rate of the wetting phase (Blunt, 1997):

$$Q = g\Delta P \quad (4.7)$$

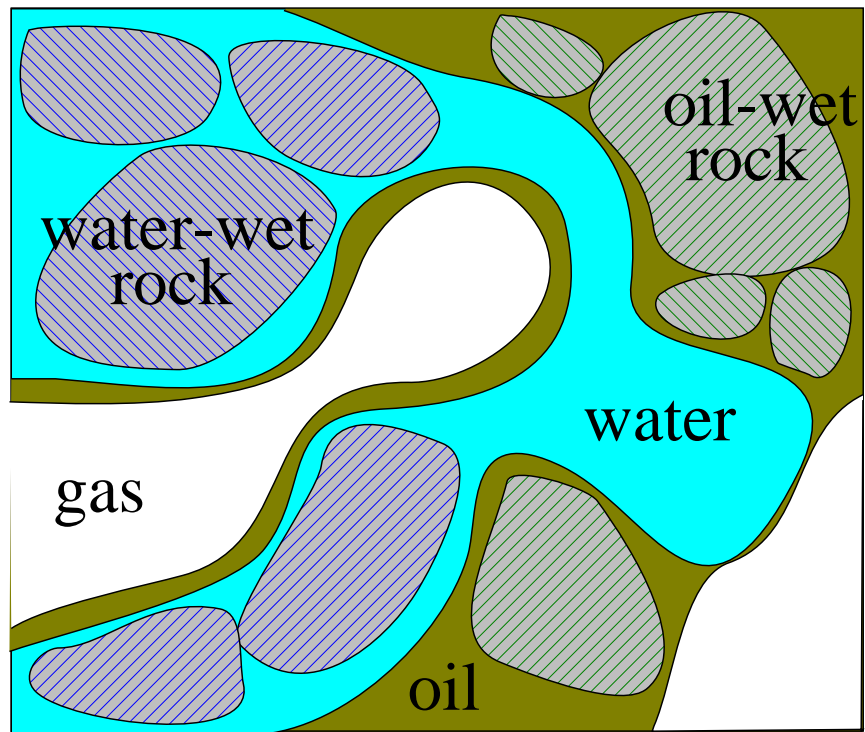
where Q is the volumetric flow of the wetting phase through pore or throat per unit time and ΔP is the pressure drop across the element. It is possible that the hydraulic path established by Decane through the wetting film has higher conductance than that of Soltrol, and consequently the drainage rate is faster. This eventually leads to higher oil recovery observed for non-spreading fluid system with Decane in oil-wet media.

4.2.3.4 In fractional-wet media oil recovery for non-spreading fluid system is higher

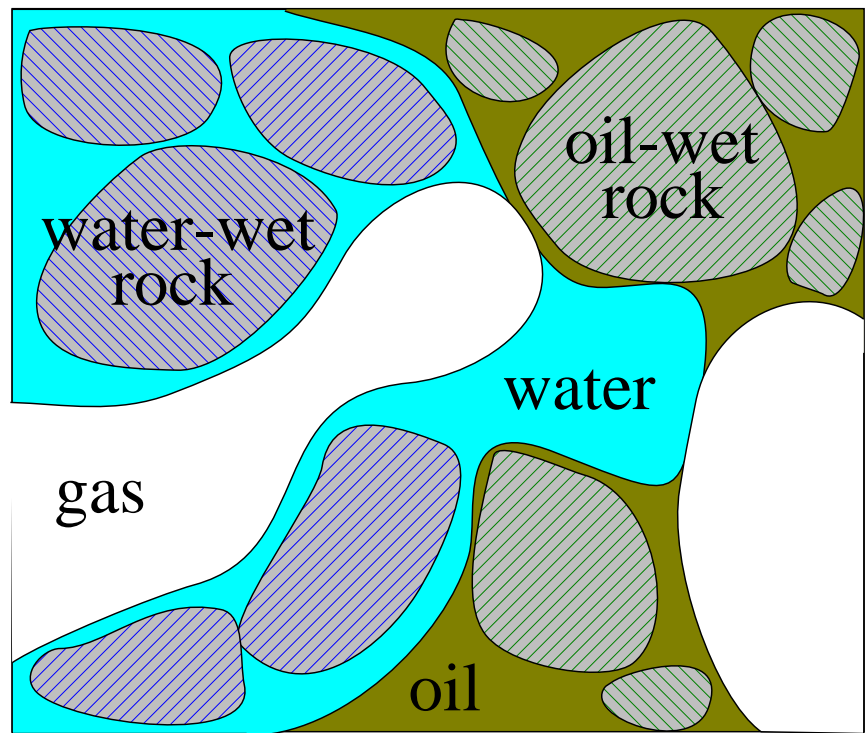
For the spreading system, in the water-wet regions oil is the intermediate phase and it becomes the wetting phase in oil-wet regions. The same applies for the non-spreading system.

The fluid configuration at the pore scale is shown in Figure 4.29. The spreading system has combinations of Configuration A and C in Figure 4.29a. The intermediate phase is spreading in regions of water-wet sand and non-spreading in regions of oil-wet sand. In non-spreading system Figure 4.29b shows the fluids assume Configuration B. This means both the non-wetting and intermediate phases in water-wet and oil-wet sand are linked by three-phase contact line.

Observations from our experiments indicate that recovery at early stage occurred mostly from bulk flow for both spreading and non-spreading system and wetting/spreading film at later stage. In non-spreading system the recovery is higher because gas as the non-wetting phase in water-wet regions prefers invading pores filled with oil since the capillary



(a) Spreading fluid system



(b) Non-spreading fluid system

Figure 4.29: Pore scale fluid configuration in fractional-wet experiments

threshold pressure is lower ($\sigma_{go} = 23.5$ mN/m). Hence the displacement mechanism is mostly through the direct drainage method. Although there is no spreading film to reconnect the displaced oil, the oil can still be mobilized through the wetting film in the oil-wet regions. Øren and Pinczewski (1991) shows in their micromodel experiments that the flow capacity through the wetting film is greater than that for the spreading film for the same oil phase since the wetting film is thicker. Thicker wetting film and smaller viscosity means the conductance through the wetting film is higher. This possibly accounts for the faster drainage rate observed in the non-spreading case.

In the spreading system, gas mobilized the oil through the double drainage mechanism. This mechanism is efficient if water as the wetting phase is continuous throughout the porous media. This is because this mechanism depends on the continuity of the water phase to advance the gas-oil interface. However, since the sand grains were distributed randomly, there were regions where water was disconnected. Consequently the oil mobilized in the water-wet regions were trapped, leaving the oil production coming mostly from the oil-wet regions.

4.3 Analysis of results with dimensionless groups

Dimensionless groups have been used by previous investigators to study the interplay of mechanisms operating in gravity drainage recovery. Grattoni et al. (2001) have identified capillary, viscous and gravity forces to be important in characterizing oil recovery under gravity drainage process. Ratios of these forces are used to define dimensionless parameters such as capillary and Bond numbers. Capillary number measures the relative strength of viscous over capillary forces and Bond number determines the relative strength of gravity over capillary. In their work they used capillary and Bond numbers to correlate the oil production in their gravity drainage experiments. Kulkarni et al. (2005) and Kulkarni and Rao (2006b) used gravity number (ratio of gravity over viscous) in addition to the other two to characterize field-scale gravity drainage projects. Their aim was to scale the mechanisms

operating at field-scale for gravity drainage experiments in laboratory. In this regard they attempted to reduce the unknown parameters that might affect oil recovery in larger scale down to a few parameters they could replicate in a laboratory setting. Subsequent work by Sharma and Rao (2008) and Mahmoud and Rao (2008) as well as Rostami et al. (2010) and Sadati and Kharrat (2013) further demonstrate the application of these numbers.

The dimensionless numbers used in the studies mentioned were derived assuming two-phase flow condition in water-wet media. Furthermore they were used to correlate with oil recovery at the end of the experiment. This means the entire dynamics of the displacement process is represented by a single number. It would lead to more insight if we could track the changes in the dimensionless numbers over the course of the experiment. In light of our understanding of pore and core scale mechanisms, the dimensionless numbers used to characterize gravity drainage process should incorporate three-phase flow mechanisms in porous media of varying wettability states. In this study we use dimensionless numbers developed by Grattoni et al. (2001) that address these issues. The capillary and Bond numbers used in Grattoni et al. (2001) are dynamic parameters, meaning they change values as function of time. This allows us to see the interplay of forces affecting gravity drainage recovery as the experiments progress. In their work Grattoni et al. (2001) used their dimensionless numbers to characterize gravity drainage in water-wet and oil-wet sand. We extend their results by including our dataset for water-wet, oil-wet, and fractional-wet experiments with spreading and non-spreading fluid.

4.3.1 Effect of Bond Number, N_B

Bond number is defined by Grattoni et al. (2001) as

$$N_B = \frac{\Delta\rho g Z R_a}{2\sigma} \quad (4.8)$$

where $\Delta\rho$ is the gas-oil density difference, g is the gravity acceleration constant, Z is the average position of the gas interface, R_a is the average pore throat radius and σ is

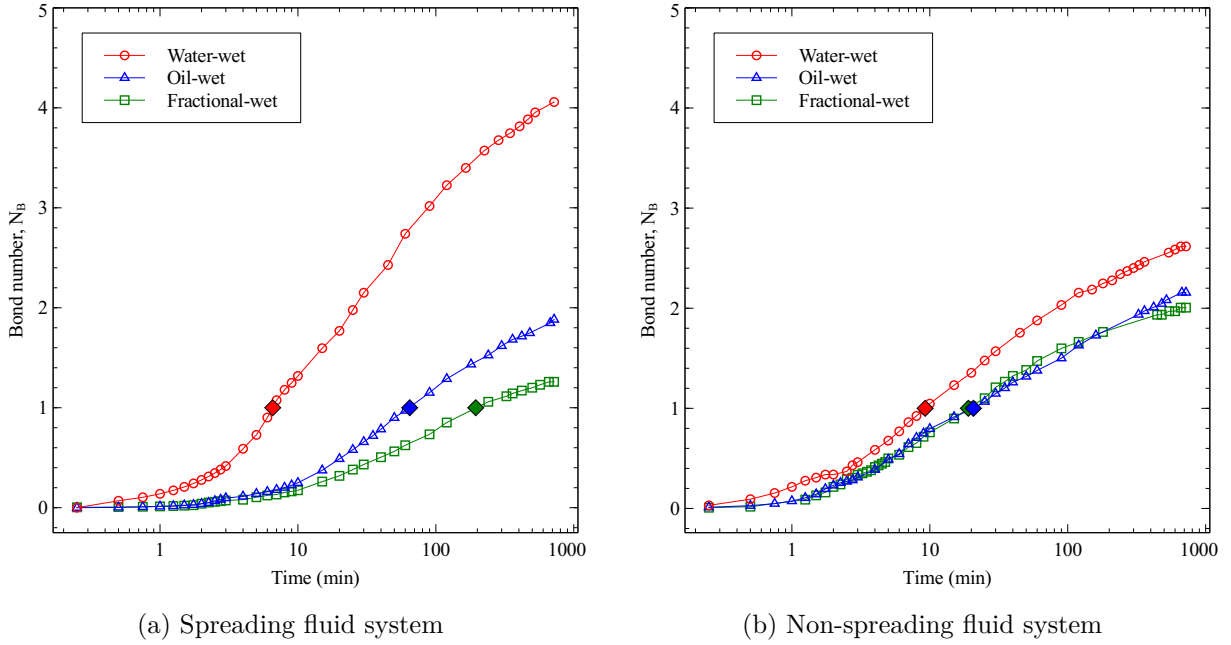


Figure 4.30: Profile of Bond Number, N_B for FGD experiments in water-wet, oil-wet and fractional-wet sand. The diamond marker indicates the time when $N_B=1$.

the gas-oil interfacial tension. R_a can be estimated from $R_a = 0.155R_b$ where R_b is the bead radius, assuming spherical beads with hexagonal packing. Equation 4.8 applies for water-wet experiments. In oil-wet experiments the term for density contrast is given as

$$\Delta\rho = (\Delta\rho_{go}S_g) + (\Delta\rho_{ow}S_w) \quad (4.9)$$

where ρ_{go} and ρ_{ow} are the gas-oil and oil-water density contrast; S_g and S_o are gas and oil saturations respectively. Equation 4.9 is used to account for the interaction between gas and water in Configuration B and C during displacement.

Figure 4.30 shows the profile of Bond number as a function of time for experiments conducted in free-fall mode. In general both spreading (4.30a) and non-spreading (4.30b) system show that the Bond number increases with time. This means that as the experiment progresses, gravity force becomes more dominant than capillary force in controlling the displacement behavior. In spreading system Figure 4.30a reveals that Bond number

increased almost fourfold since the beginning of the experiment with water-wet sand. In the same period Bond number increased less than twofold for experiments in oil-wet and fractional-wet sand. This indicates that gravity-dominated flow becomes more significant over the course of the experiment. Likewise in the non-spreading system Bond number also grows with time, although the maximum value attained was less than four.

It is instructive to determine the exact time the displacement process transitions from capillary-dominated flow to gravity-dominated flow. This transition happens when $N_B = 1$, which by definition means that gravity force is balanced by capillary force.

In Figure 4.30a and 4.30b this is marked by a diamond marker. Our calculation shows that for spreading system, it took about seven minutes for the transition to occur in water-wet sand. In oil-wet and fractional-wet sand the time became progressively longer, at 65 minutes and 195 minutes respectively. In non-spreading system our calculation shows that the transition occurred after nine minutes in water-wet sand, and 19 minutes and 21 minutes for fractional-wet and oil-wet sand respectively. This shows that gravity-dominated flow occurred earlier for spreading system in water-wet sand and was delayed significantly as the wettability became less water-wet.

The effect of Bond number in oil recovery for gravity drainage experiments is shown in Figure 4.31. In Figure 4.31a for the water-wet case the oil recovery increases linearly with Bond number. Similar trend is seen for water-wet experiment with non-spreading fluid in Figure 4.31b. This shows that oil recovery in gravity drainage experiment in water-wet sand is strongly influenced by gravity forces. In spreading system, gravity forces increases almost fourfold with respect to capillary forces. For non-spreading system in water-wet sand the increase is slightly over twofold.

The reason the final value for N_B is less in water-wet sand with non-spreading fluid system than its spreading counterpart is because of the term Z , the average position of gas interface in Equation 4.8. In spreading system during gas invasion, gas-oil and oil-water

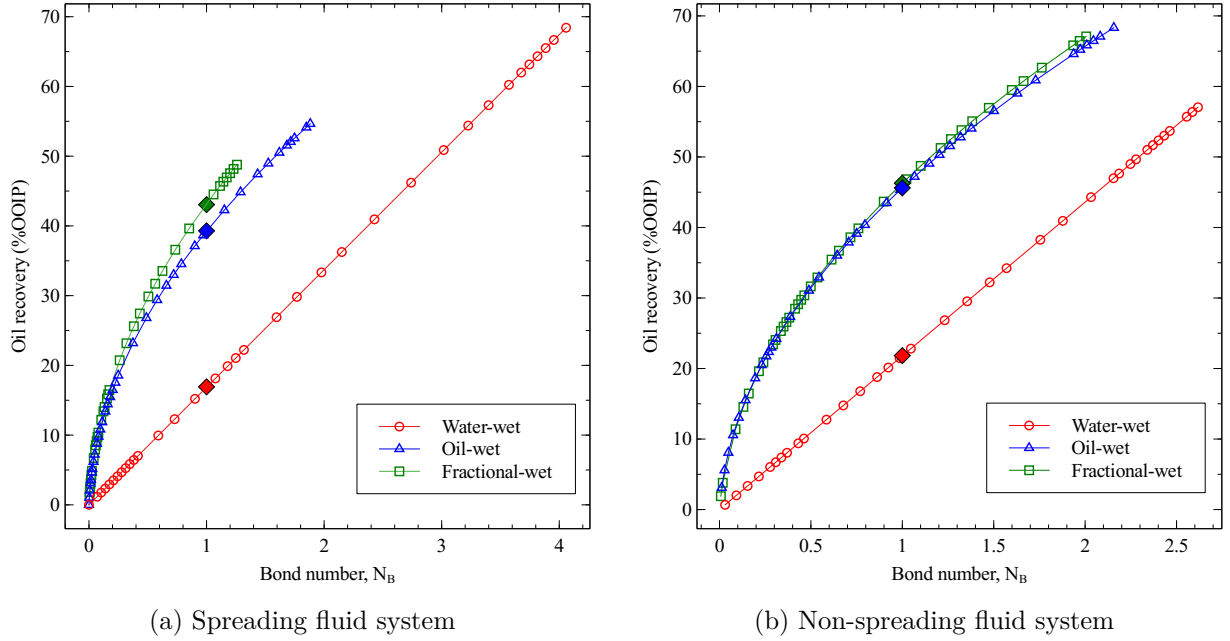


Figure 4.31: Effect of Bond Number, N_B on oil recovery for FGD experiments in water-wet, oil-wet and fractional-wet sand. The diamond marker indicates the oil recovery when $N_B=1$.

interfaces are formed and the advancement of these interfaces mobilize the oil phase. Since water is the continuous phase, propagation of the interfaces help to transport the oil phase all the way to the outlet. Therefore Z is increasing as the gas-oil and oil-water interfaces are advancing.

In non-spreading system since the oil phase does not spread, the invading gas contacts the water phase directly since there is no oil film separating them. This creates either gas-water, gas-oil or oil-water interfaces in the pores. The transport of the oil phase is retarded because the advancement of the interfaces do not directly lead to oil mobilization and eventual transport to the outlet. Although Z is increasing oil production is slowing.

As $N_B > 1$, the proportion of oil recovery contributed by gravity forces becomes greater. For example in Figure 4.31a oil recovered during capillary-dominated flow ($N_B < 1$) in water-wet sand is 16.9% OOIP. The remaining oil recovery (51.5%) occurred during gravity-dominated flow. As the sand pack becomes less water-wet, the contribution of gravity-dominated flow toward oil recovery is reduced. In Figure 4.31a the oil recovered

during capillary-dominated flow is 39.3% and 43.1% OOIP for oil-wet and fractional-wet sand respectively. For the same set of experiments the remaining 15.3% and 5.7% OOIP were recovered during gravity-dominated flow. In non-spreading system the oil recovered during capillary-dominated flow is 21.8%, 45.6% and 46.3% OOIP for experiments conducted in water-wet, oil-wet and fractional-wet sand respectively. From our calculations in both Figures 4.31a and 4.31b we can infer that in water-wet sand, the proportion of oil-recovery that is recovered during gravity-dominated flow is greater than those in oil-wet and fractional-wet sand. In oil-wet and fractional-wet sand significant portion of the oil is recovered during capillary-dominated flow.

Figures 4.31a and 4.31b also show that oil recovery has non-linear relationship with Bond number in experiments with oil-wet and fractional-wet sand. The non-linear behavior is caused by the term $\Delta\rho$ used in Equation 4.9 to obtain N_B in Equation 4.8. In oil-wet and fractional-wet sand the gas and water phase occupy the larger pores since they are non-wetting with respect to oil. During gas invasion all three phases are mobile. The mobilization and transport of the oil phase is accounted for by the term Z . For water, although it is at residual saturation, the water phase is redistributed along the column. Eventually water is accumulated at the bottom, albeit no production is reported. The tendency for the water phase to accumulate at the bottom of the column, during gravity drainage at residual water saturation in oil-wet and fractional-wet sand packs has been confirmed through CT study by Vizika and Lombard (1996). The $\Delta\rho$ term used in Equation 4.9 considers this fact by accounting the interaction between water and gas phase along the column, and their movement toward the bottom controlled by buoyancy effect.

In Figure 4.31 the end-point N_B value in spreading system is less than that for non-spreading system in oil-wet and fractional-wet sand. This is because after accounting for the gas and water interactions in the $\Delta\rho$ term, the end-point N_B value is ultimately determined by the movement of the gas front given by the Z term. As discussed in Section 4.2.3.3 for the same gas front advancement that directly leads to oil mobilization, the one

in non-spreading system transports more oil to the outlet. This is because the wetting film that provides the continuous path for oil mobilization in the non-spreading system has greater conductance. Thus for the same pressure gradient the volumetric flow through this path is greater in the non-spreading system. In the fractional-wet system our analysis of time-lapsed photos and gas velocity profiles revealed that significant portion of the oil was produced through bulk flow early on in the experiment. Our results also indicate that the bulk oil drainage in the non-spreading case occurred *earlier* than that for the spreading case. This is because the gas velocity was higher in the non-spreading case, which means the gas front was able to penetrate more smaller pores to displace the oil therein. The cumulative effect is that the increase in the Z term is associated with more oil recovery for the non-spreading case.

4.3.2 Effect of Capillary Number, N_C

Capillary number from Grattoni et al. (2001) is defined as

$$N_C = \frac{2v_g\mu_g}{P_c R_a} \quad (4.10)$$

where v_g and μ_g is the gas velocity and viscosity respectively, P_c is capillary pressure defined as $P_c = \frac{2\sigma_{go}}{r}$, and R_a is the average pore throat radius.

In Figure 4.32 Capillary Number, N_C is shown to decrease with time as the experiments progress. The same behavior is observed for spreading (4.32a) and non-spreading (4.32b) fluid systems. N_C is decreasing over time because during the experiment the gas front travels with varying velocity. The velocity of the gas front is controlled by interactions between capillary, viscous and gravity forces. From our plot of gas velocity profile in each experiment the gas velocity is seen to decrease with time. This indicates that over time the influence of viscous forces is counter-balanced by greater capillary forces.

Based on our calculations we put a diamond marker on each curve in Figures 4.32a and 4.32b to indicate the time and the corresponding N_C when $N_B = 1$. This marks

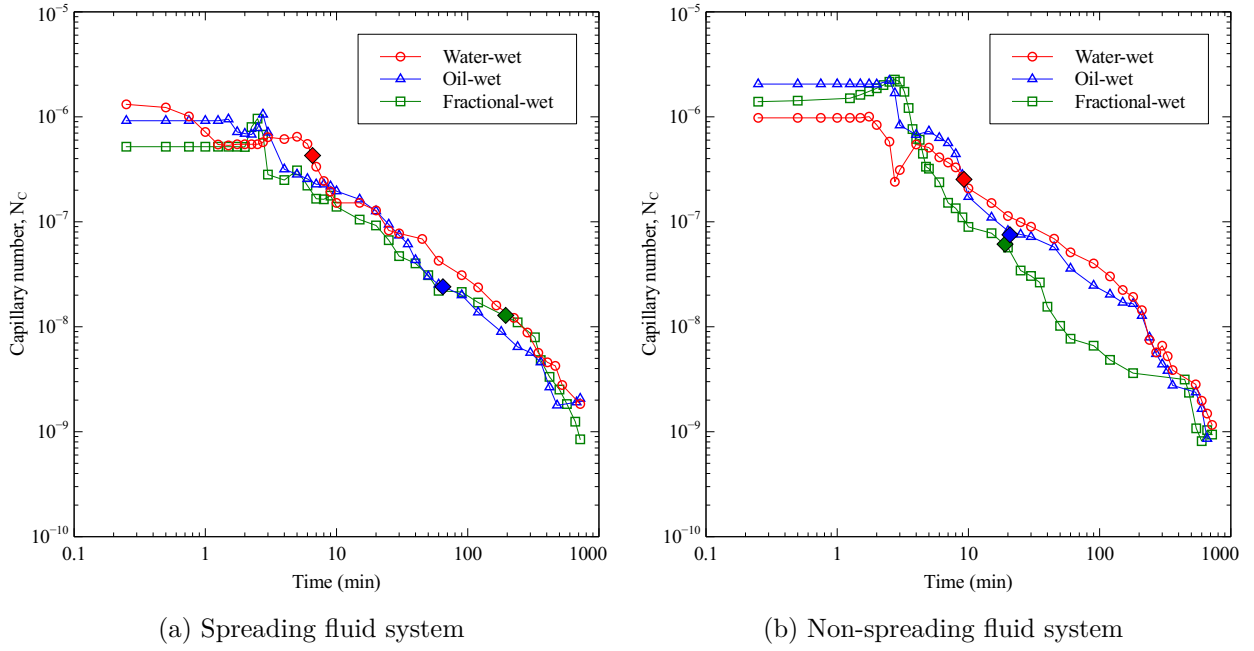


Figure 4.32: Profile of Capillary Number N_C for FGD experiments in water-wet, oil-wet and fractional-wet sand. The diamond marker indicates N_C when $N_B=1$.

the time when viscous and capillary-dominated flow transition to gravity-dominated flow. As discussed in the previous section for the spreading system the transition occurs earlier in the water-wet sand and much later in the oil-wet and fractional-wet sand. In non-spreading system the transition also occurs earlier in water-wet sand but the timespan for the transition happening in oil-wet and fractional-wet sand is very close.

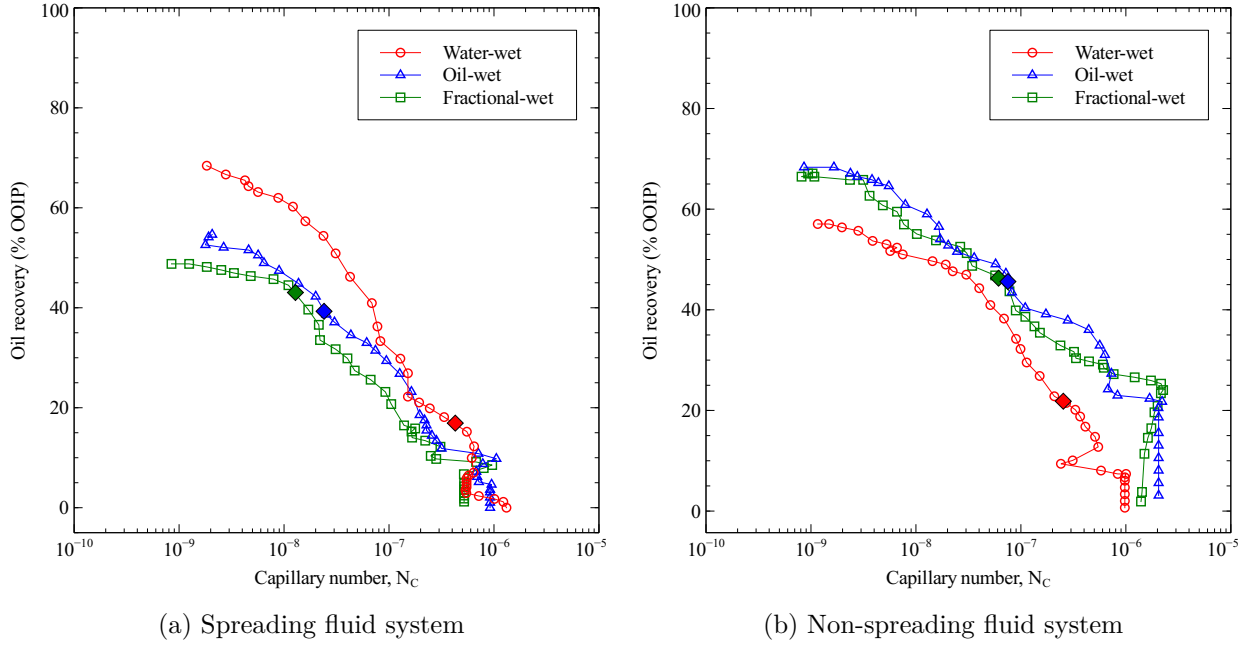


Figure 4.33: Effect of Capillary Number, N_C on oil recovery for FGD experiments in water-wet, oil-wet and fractional-wet sand. The diamond marker indicates the oil recovery when $N_B=1$.

In Figure 4.33 we plot the oil recovery as a function of N_C . We note that as the oil recovery increases N_C shows the opposite behavior. In both spreading and non-spreading system, experiments in water-wet, oil-wet and fractional-wet sand demonstrate that N_C decreases to a very small value as more oil is produced. In spreading system (4.33a) the changes in N_C is minimal given the steep gradient before $N_B = 1$, as indicated by the diamond marker. After $N_B > 1$, the gradient increases, meaning greater changes in N_C in the negative direction leads to corresponding changes in the positive direction for the oil recovery. This is because during this period gravity forces exert more influence on the overall displacement than capillary forces. The same trend is shown for non-spreading system in water-wet sand.

For the spreading system in the oil-wet and fractional-wet experiments (4.33a) when $N_B < 1$, the gradient is larger initially in the negative direction. As $N_B > 1$, the gradient is reduced in the negative direction. This means that when the flow is gravity-dominated for these experiments, a large decrease in N_C resulted in minimal increase in oil recovery.

In the non-spreading system for oil-wet and fractional-wet experiments (4.33b) we observe a steep gradient initially for both experiments. This indicates that viscous forces are active during this period since only a small reduction in N_C leads to significant jump in oil production. This observation is supported by our analysis with time-lapsed photos and gas velocity profiles for these experiments before. Later gas velocity slowed down which corresponds to greater reduction in N_C but oil production continued to increase because during this period most of the oil is still drained through bulk flow. When $N_B = 1$, 45.6% OOIP and 46.3% OOIP has been produced from the oil-wet and fractional-wet sand. After $N_B > 1$, the gradient continues its ascent in the negative direction. Although the flow is gravity-dominated at this stage only about 20% OOIP additional oil was produced in either experiments. Note that in the non-spreading system the curves for oil-wet and fractional-wet sand are consistently higher than that of water-wet sand, indicating that viscous forces are generally greater in these experiments.

4.3.3 Effect of Gravity Number, N_G

Gravity number, N_G is a measure of the relative strength of gravity to viscous force. According to Hagoort (1980) and Chatzis and Ayatollahi (1993) N_G is defined as

$$N_G = \frac{gK\Delta\rho_{og}}{\mu_o V_{pg}} \quad (4.11)$$

where g is the gravity acceleration, K is the absolute permeability, $\Delta\rho_{og}$ is the oil-gas density difference, μ_o is the oil viscosity and V_{pg} is the pore velocity of the gas-liquid interface. For oil-wet and fractional-wet experiments $\Delta\rho_{og}$ is calculated using Equation 4.9 on page 99 to account for the fact that gas and water are the non-wetting phases, thus they tend to occupy larger pores and move downward under gravity. Although in the original paper Chatzis and Ayatollahi (1993) measured V_{pg} in their experiments, they also suggested that this parameter can be calculated using production data, porosity of the sand pack and

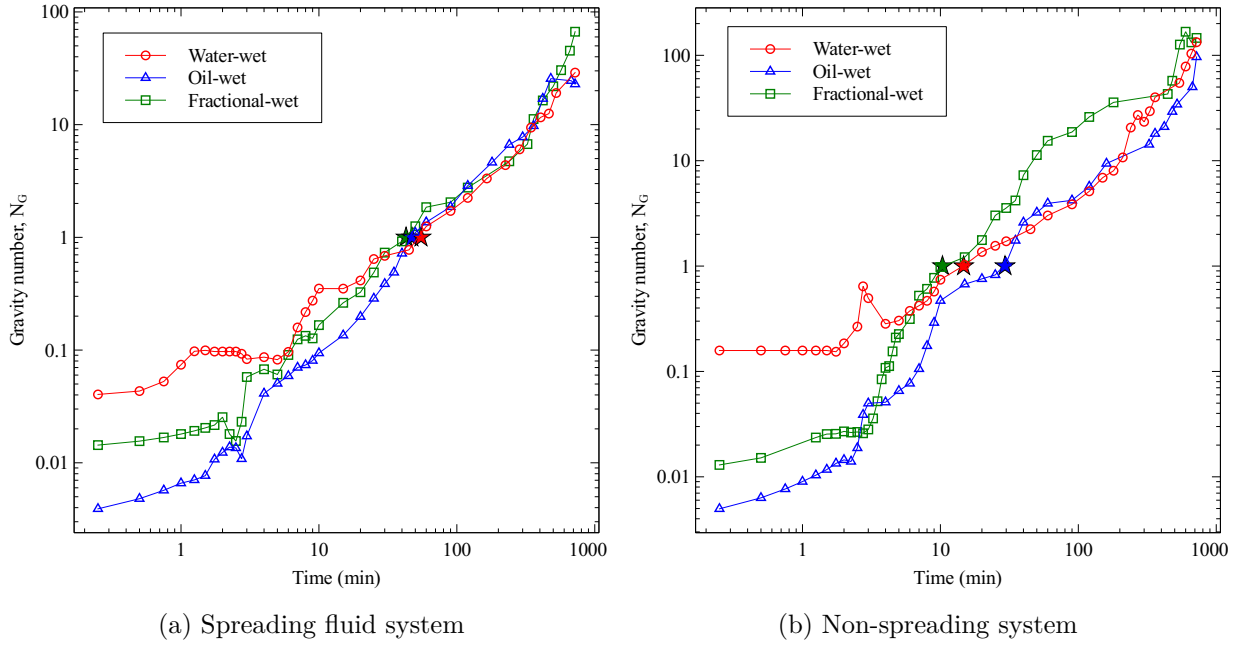


Figure 4.34: Profile of Gravity Number, N_G , for FGD experiments in water-wet, oil-wet and fractional-wet sand. The star marker indicates the time when $N_G=1$.

connate water saturation. In this study the gas velocity we calculated using the method presented in Grattoni et al. (2001) is used as V_{pg} .

Based on their previous study using square capillary tubes, Chatzis and Ayatollahi (1993) explained that the velocity of the oil film in the corners of the square during gas invasion is proportional to the permeability of the tube and also proportional to $\frac{\Delta\rho_{og}}{\mu_o}$. In their study they defined the term $\frac{K\Delta\rho_{og}}{\mu_o}$ to represent the action of gravity forces influencing the downward direction of average oil velocity by film flow as gas is invading the top of the column. In the denominator the term V_{pg} represents the action of viscous pressure gradient influencing the pore velocity of the oil bank at the gas-oil contact.

Figure 4.34 shows that N_G increases with time. This trend is observed for both spreading (4.34a) and non-spreading (4.34b) fluid systems in water-wet, oil-wet and fractional-wet sand packs. In the plot the time when $N_G = 1$ indicated by the star marker marks the point when the flow shifts from viscous-dominated to gravity-dominated flow. In the spreading system (4.34a) this transition occurred almost at the same time beginning with fractional-wet sand at 43 minutes, oil-wet sand at 47 minutes and water-wet sand at 55 minutes. It is

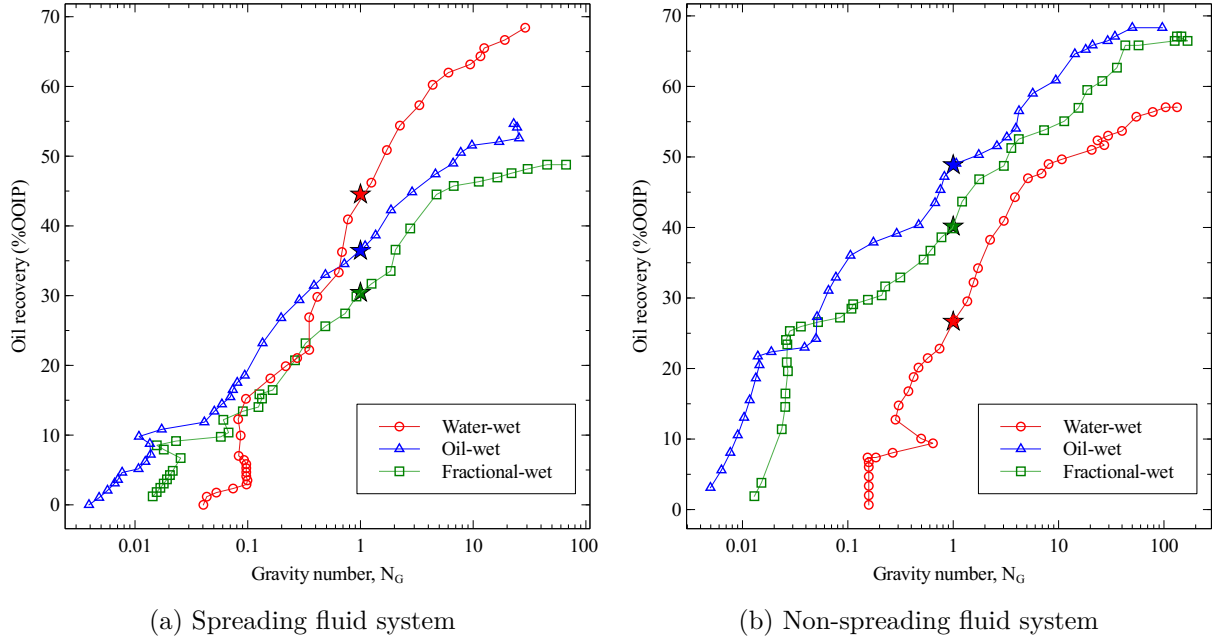


Figure 4.35: Effect of Gravity Number, N_G on oil recovery for FGD experiments in water-wet, oil-wet and fractional-wet sand. The star marker indicates the oil recovery when $N_G=1$.

notable that in spreading fluid system, beyond the point where gravity is dominating the flow, the curves for each experiment almost collapse into a single curve.

In non-spreading system (4.34b) the same pattern of increasing N_G with time is observed. The transition to gravity-dominated flow occurred earlier in fractional-wet sand, followed by water-wet sand and finally oil-wet sand at ten, 15, and 29 minutes respectively. In contrast to the spreading fluid system, the curves did not collapse into one curve after the transition to gravity-dominated flow.

The effect of N_G on oil recovery is shown in Figure 4.35. In general oil recovery is increasing as a logarithmic function of N_G . Both spreading (4.35a) and non-spreading (4.35b) fluid systems show the same trend. The one notable difference is the relative position of the curves. In spreading fluid system the water-wet curve was below the oil-wet and fractional-wet curves initially. However when $N_G > 1$, the oil recovery for the water-wet curve increased to surpass both oil-wet and fractional-wet curves and maintained its leading position until the end of the experiment. This is because after $N_G = 1$, the gravity forces grew stronger relative to viscous forces in water-wet sand. More oil was drained

through spreading film under the influence of gravity forces after this transition. Figure 4.35a clearly demonstrates the effectiveness of spreading film flow in recovering additional oil in water-wet sand.

Figure 4.35b shows the opposite trend. In the plot instead of water-wet curve, the oil-wet and fractional-wet curves were leading. Before and after $N_G = 1$, both oil-wet and fractional-wet curves consistently exceeded the water-wet curve. This is because gravity forces were stronger in this sand relative to viscous forces since the start of the experiment. Since the oil phase (Decane) has lower viscosity the drainage rate through the wetting film is greater because lower viscosity leads to higher conductance. As a result combination of stronger gravity forces and faster drainage rate helped to drain more oil downward through the wetting film.

4.3.4 Effect of dimensionless numbers in tertiary GAGD

Dimensionless numbers analysis discussed so far concerned mainly on gravity drainage experimental results performed at residual water saturation (FGD and secondary CGD). Since both FGD and secondary CGD experiments exhibited similar trends we chose to present in the previous sections analysis of FGD experiments only. In this section we performed the same analysis on tertiary CGD experiments. We would like to see whether the same observations hold for gravity drainage at residual oil saturation. The results are shown in Figure 4.36.

In Figure 4.36 the dimensionless numbers are plotted with total liquid production as the dependent variable (y-axis). This is because during gas invasion, both oil and water are produced. At the top of the figure liquid production exhibits linear trend with N_B for water-wet sand in both spreading and non-spreading fluid systems. In oil-wet and fractional-wet sand the trend with N_B is nonlinear. Comparing with Figure 4.31 we see similar trends.

The center of Figure 4.36 shows the liquid production as a function of N_C . Similar to Figure 4.33 the water-wet curve in spreading fluid system surpassed both oil-wet and fractional-wet curves. In non-spreading fluid system the oil-wet and fractional-wet curves were leading instead. In both plots as liquid production increases, N_c decreases spanning three to four orders of magnitude.

The effect of N_G on liquid production is shown at the bottom of Figure 4.36. The trends observed for spreading and non-spreading fluid systems are similar to that in Figure 4.35. In spreading fluid system the water-wet curve was leading ahead of oil-wet and fractional-wet curves. The trend is reversed in the non-spreading fluid system. Both plots show the liquid production increases as N_G increases over the span of more than three orders of magnitude.

Since the trends shown for liquid production when plotted against N_B , N_C , and N_G are similar to that observed in experiments at residual water saturation, the same discussions pertaining these experiments also apply to experiments at residual oil saturation.

4.3.5 Flow regime characterization based on dimensionless numbers

Earlier when discussing experimental results for fractional-wet experiments we presented the flow regime map in Figure 4.19. The shaded area delineating region where capillary, viscous and gravity force is dominant was placed arbitrarily to illustrate the interplay of forces influencing oil production in gravity drainage process.

Now with insights gained from analysis of dimensionless numbers we are able to refine the flow regime map by locating exactly the time when the transition between the forces occur. This has the benefit of clearly attributing which force is dominating the flow during the course of the experiment. In addition pinpointing the exact time for the transition enable us to correlate the amount of oil produced in each flow regime.

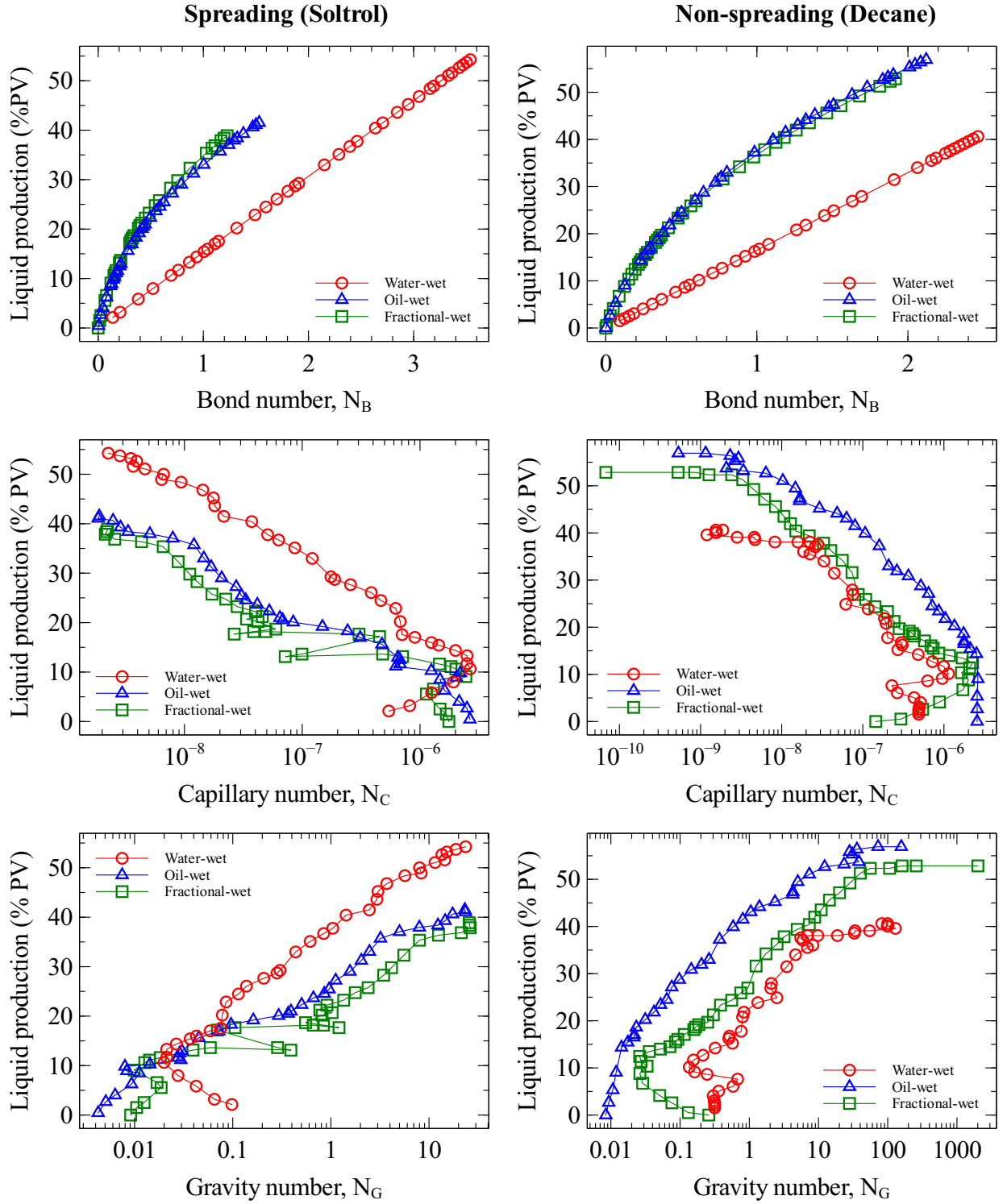


Figure 4.36: Effect of Bond number, N_B (top), Capillary number, N_C (center) and Gravity number, N_G (bottom) on liquid production in tertiary CGD experiments in water-wet, oil-wet and fractional-wet sand for both spreading (left column) and non-spreading (right column) fluid system.

The revised flow regime map is shown in Figure 4.37 for FGD experiments in water-wet, oil-wet and fractional-wet sand. We chose to show the flow regime map for only FGD experiments for the sake of brevity. It is expected that the flow regime map for experiments at residual oil saturation (tertiary CGD) would be similar since the forces interacting during the experiments exhibited similar trends (refer to Figure 4.36). However the width of each region might be different depending on interactions between the forces.

We plotted the gas velocity as the ordinate to track the movement of gas-oil interface with time. The time when $N_B = 1$ indicates the transition from capillary-dominated to gravity-dominated flow. When $N_G = 1$, this marks the transition from viscous-dominated to gravity-dominated flow. The set of times when the transition occurred was determined by interpolation of curves plotted previously in Figure 4.30 and Figure 4.34. The shaded area in each plot denotes the region where capillary (green), viscous (pink) or gravity force (cyan) is dominating. The transition time calculated earlier was also used to mark the extent of each flow region. For example when the time for $N_G = 1$ is greater than the time for $N_B = 1$ ($t_{NG=1} > t_{NB=1}$) an overlap of dominating forces is possible. This means that at $t_{NB<1}$ both capillary and viscous forces are dominating the flow. Between $t_{NB=1}$ and $t_{NG=1}$ both viscous forces and gravity forces are dominant and when $t_{NG>1}$ only gravity forces are controlling the flow. Overlap of dominating forces also happens when $t_{NG=1}$ occurs earlier than $t_{NB=1}$.

In water-wet experiments (top of Figure 4.37) the flow was dominated by capillary and viscous forces initially before the transition to viscous and gravity-dominated flow. This is followed by gravity-dominated flow which continued until the end of the experiment. In spreading system the time span for the viscous-dominated flow was wider than that in non-spreading system. In contrast the onset of gravity-dominated flow was earlier in non-spreading system. At the beginning of the experiment when the flow was capillary and viscous-dominated, gas was invading the larger pores to displace the oil within. The oil was retained by capillary force and viscous force set the pressure gradient required for

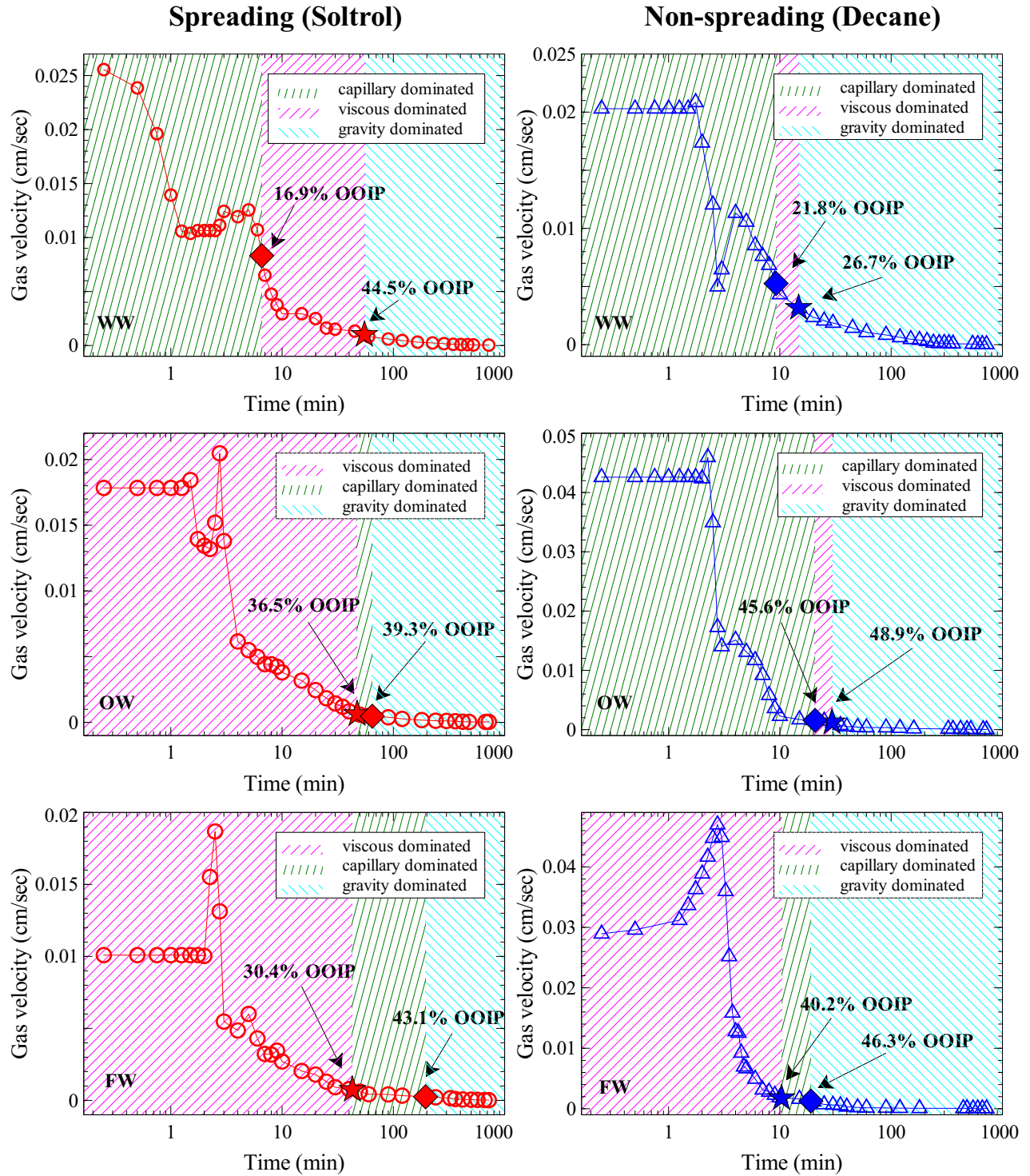


Figure 4.37: Gas velocity as a function of time during FGD experiments in water-wet (top), oil-wet (center) and fractional-wet (bottom) sand using spreading (left column) and non-spreading (right column) fluid systems. The diamond and star markers indicate the gas velocity, time and oil recovery when $N_B=1$ and $N_G=1$ respectively. The shaded area indicates the extent where flow is dominated either by capillary, viscous or gravity force.

gas to penetrate the pore and access the oil. The pressure gradient required to overcome pore capillary threshold depends on the interfacial tensions, wettability and pore geometry, with larger pore size having smaller capillary threshold; thus making it more amenable to gas invasion. In the viscous and gravity-dominated flow some oil was bypassed by the invading gas initially. In this region the bypassed oil which existed as isolated blobs started coalescing to form bigger blobs. In spreading system the span where viscous force is dominating was wider and started earlier to account for the effect of film flow reconnecting the stranded oil and providing continuous hydraulic path. This can be correlated with the time-lapsed photos during this period (see Figure 4.2a). In the gravity-dominated region the remaining oil was displaced either through the hydraulic path established earlier for spreading system or through interconnecting oil layer formed between the pore crevices and wedges for non-spreading system. The rate of oil drainage in this region is controlled by gas-oil density difference and the oil viscosity.

In oil-wet experiments (center of Figure 4.37) overlap of dominating forces is seen at the beginning of both spreading and non-spreading system. In spreading system viscous and capillary forces dominated the flow and accounted for 36.5% OOIP recovered. Between $t_{NG=1}$ and $t_{NB=1}$ both viscous and gravity forces were dominant while at $t_{NB>1}$ only gravity forces were dominant. In non-spreading system combination of capillary and viscous forces in the first stage accounted for 45.6% OOIP recovery. Higher recovery was attained in the first stage for the non-spreading system because the viscous pressure gradient was higher, which is evident from the higher initial gas velocity in the plot. In the spreading system lower initial gas velocity limited the viscous pressure gradient available to drain the oil. During gravity-dominated flow regime, residual oil in both systems was drained through the wetting layer. Since the density difference of the oil phase is about the same in the spreading and non-spreading system, the drainage rate is controlled by oil viscosity. More oil can be transported through the wetting layer in non-spreading system since it has greater conductance (refer to Equation 4.6 on page 94).

Flow regime maps for fractional-wet experiments are shown at the bottom of Figure 4.37. The difference with Figure 4.19 is that we did not know then the extent of capillary or viscous forces controlling the flow during the early part of the experiments. With analysis of dimensionless numbers this can be located easily. In spreading system the flow was dominated by both viscous and capillary forces until $t_{NB=1}$ at 43 minutes after the experiment began. Between $43 < t < 195$ minutes both capillary and viscous forces controlled the flow. At the onset of gravity-dominated flow ($t = 195$ minutes) about 43.1% OOIP has been recovered. In non-spreading system similar arrangement of flow regimes is observed. However the extent of viscous and capillary-dominated region was shorter and gravity-dominated region was longer but the amount of oil recovered at the beginning of gravity-dominated region was greater (46.3% OOIP). This observation ties in with visualizations of time-lapsed photos (cf. Figures 4.13a and 4.13b). Since gas velocity was higher in non-spreading system the viscous pressure gradient was greater. This helped to penetrate more pores and drained more oil than that in spreading system during the same period.

4.3.6 Summary of dimensionless groups analysis

In this section we analyzed the results of gravity drainage experiments using dimensionless groups to evaluate the effect of capillary, gravity and viscous forces on oil production. The forces are combined in dimensionless numbers to consolidate the parameters affecting the gravity drainage process. The dimensionless numbers are Bond number, N_B , Capillary number, N_C , and Gravity number, N_G .

It is shown that N_B increases with time for all experiments in spreading and non-spreading fluid systems. The increasing trend indicates that gravity forces grow stronger over capillary forces as the experiment progresses. The transition from capillary-dominated flow to gravity-dominated flow occurs when $N_B = 1$. In water-wet sand for spreading fluid system the transition occurs earlier while for oil-wet and fractional-wet sand the transition

takes longer time. In non-spreading system the transition time is located very close to each other for each experiment. Oil recovery is also shown to increase as a function of N_B . In water-wet sand for both spreading and non-spreading systems this relationship is linear. A nonlinear relationship is observed for oil-wet and fractional-wet sand in both fluid systems. A linear relationship is shown for water-wet sand because the oil production is strongly controlled by the average position of the gas interface. In oil-wet and fractional-wet sands the effect of N_B on oil recovery is nonlinear because the N_B in these sands is also a function of gas and water saturations. Since both phases are non-wetting relative to oil, they reside in the larger pores, thus have tendency to move. Their movement could advance or impede oil production, hence the nonlinear relationship with oil recovery.

Capillary number, N_C is shown to decrease with time for all experiments in both spreading and non-spreading fluid systems. In water-wet sand the decline starts at the onset when $N_B = 1$. In oil-wet and fractional-wet sand the decline is observed to occur earlier before $N_B = 1$. As oil recovery increases N_C decreases. For water-wet sand the decline happens when $N_B > 1$. In oil-wet and fractional-wet sand N_C is declining well before $N_B = 1$. In the spreading system water-wet sand shows it has stronger viscous forces to overcome capillary forces in the sand. In non-wetting system both oil-wet and fractional-wet sand show greater viscous forces relative to capillary forces. When viscous forces are stronger it resulted in higher oil recovery as more oil can be drained from the pores which was initially held by capillary forces.

Analysis using Gravity number, N_G shows it increases with time for all experiments in spreading and non-spreading fluid systems. This means gravity forces are growing stronger relative to viscous forces as the experiment continues. Oil recovery also increases as N_G increases. In spreading fluid system water-wet sand is shown to have a bump in oil production after the transition from viscous-dominated to gravity-dominated flow. In non-spreading system the curves for both oil-wet and fractional-wet sand are observed to surpass water-wet sand since the beginning. This is because gravity forces present in these sand packs

are relatively stronger than that of water-wet sands. Stronger gravity forces coupled with faster drainage rate through the wetting layer help to mobilize more oil in these sand packs.

All the above analyses are also performed on gravity drainage experiments at residual oil saturations. It is shown that relationship between N_B , N_C and N_G with oil recovery follow the same patterns as observed earlier for experiments under residual water saturation. Therefore it is expected that the explanations hitherto for the patterns observed in experiments at residual water saturation also applies to the set of results from experiments at residual oil saturation.

The final part of the analysis concerns application of dimensionless numbers to determine the extent of flow regime operating during the experiment. The exact time for the transition between the forces can be determined by setting $N_B = 1$ for the transition from capillary-dominated to gravity-dominated flow and $N_G = 1$ for the transition from viscous to gravity-dominated flow. It is observed that overlap of capillary and viscous forces occurs in the early stage of the experiment. In the middle stage there is overlap between viscous or capillary forces and gravity forces. Toward the end of the experiment gravity forces are dominating the flow. In the early stage viscous forces provide the pressure gradient to overcome capillary forces retaining the fluids in the pores. In the middle stage gravity forces started to grow in strength relative to capillary or viscous forces. Finally in the late stage gravity forces controlled the drainage of oil either through spreading or wetting film.

Chapter 5

Evaluation of Existing Gravity Drainage Models

In the previous chapter we have discussed the experimental results for gravity drainage in sand packs. The experiments were run with sand under water-wet, oil-wet and fractional wet conditions with the fluid system having positive or negative spreading coefficient. We explained the results based on interactions at the pore scale between the fluids themselves and between the fluids and sand surfaces. The results were then analyzed with dimensionless numbers to evaluate the extent of gravity, capillary and viscous forces in controlling the drainage behavior.

In this chapter we investigate the existing models in the literature for gravity drainage process. This is done by evaluating their performance in predicting the results based on the match between the model and experimental data. This is assessed objectively using goodness-of-fit statistics such as coefficient of determination (r^2) and root mean squared error ($RMSE$). By using these objective parameters as the model's performance marker, we can infer which model is capable of capturing the essential physics as discussed in the previous section. In addition the insights from this study provide guidance on how to select the best analytical model for gravity drainage, given the rock condition (wettability) and the fluid properties (interfacial tensions and spreading coefficient).

5.1 Goodness-of-fit parameter for gravity drainage models

When fitting analytical model to experimental data, we need to quantify the accuracy of the model. This will help in selecting the best model that characterize the experiments. In statistics this can be achieved by calculating the goodness-of-fit parameter. Although there are various metrics to assess goodness-of-fit (James et al., 2013), we will use the coefficient of determination (r^2) and root mean squared error ($RMSE$) since these parameters provide useful insight regarding the accuracy of the model.

In MATLAB (2018) r^2 is defined as

$$r^2 = 1 - \frac{SSE}{SST}, \quad (5.1)$$

where SSE is the sum of squared errors and SST is the total sum of squares. Given n data points for the experimental data y_i and \hat{y} is the value calculated from the model, SSE is

$$SSE = \sum_{i=1}^n (y_i - \hat{y}_i)^2, \quad (5.2)$$

and SST is given as

$$SST = \sum_{i=1}^n (y_i - \bar{y})^2, \quad (5.3)$$

with \bar{y} is defined as

$$\bar{y} = \frac{1}{n} \sum_{i=1}^n y_i. \quad (5.4)$$

Evaluating a model based on r^2 is intuitive because the output ranges from zero to one, with one indicating the model is the best fit for the experimental data. This is because a value of r^2 closer to one means the model is more successful in accounting for the proportion of variance in the experimental data. Therefore according to Equation 5.1, r^2 can be maximized by minimizing the sum of squared errors, SSE in Equation 5.2. Since SSE measures how far the experimental data (y_i) from the model's predicted value (\hat{y}), a model that is able to minimize the distance between y_i and \hat{y} will show higher r^2 value.

However, since the models that we use in the curve fitting are nonlinear, certain authors have expressed caution against using r^2 as the best-fit parameter to evaluate nonlinear model. Kvalseth (1983) explained that in a linear model, SST or the total variance is always equal to the sum of SSE , the error variance and regression variance, $\sum_{i=1}^n (\hat{y} - \bar{y})^2$. This arrangement leads to r^2 value between zero to one. In a nonlinear model, the sum of

error variance and the regression variance often do not add up to the total variance, thus negating the validity of Equation 5.1.

Furthermore Spiess and Neumeyer (2010) evaluated the validity of using r^2 to assess the goodness-of-fit for nonlinear models. After running thousands of simulations, they found that using r^2 does not necessarily lead to the best model although its r^2 value is high. This is because r^2 is shown to consistently give a high value regardless whether the model is best or mediocre. The studies from Kva°Lseth (1983) and Spiess and Neumeyer (2010) underscore the need to use another goodness-of-fit parameter to complement the value given by r^2 .

In the literature (James et al., 2013) another measure of the model’s accuracy is given by the mean squared error (MSE). This is the sum of squared error (SSE) over the total number of data points, n . Thus $MSE = SSE/n$. Based on the definition, root mean squared error ($RMSE$) is the square root of MSE , thus $RMSE = \sqrt{MSE}$. This parameter is also known as the standard error of the regression. For both linear and nonlinear models $RMSE$ gives the absolute measure of fit to the experimental data. This contrasts with r^2 which only gives the relative measure of fit. This means the parameter $RMSE$ indicates how close the observed experimental data points to the model’s predicted values. Since it has the same unit as the dependent variable, lower value of $RMSE$ is desirable because this shows smaller deviation of the model’s value from experimental data.

In this work $RMSE$ values are shown to gauge the performance of the model. Since the models used are nonlinear, $RMSE$ values will be used primarily to rank the model.

5.2 Dykstra model

Dykstra (1978) model incorporates previous work by Cardwell and Parsons (1949) in calculating the advance of the demarcator gas-oil interface. In formulating the model they noted that gravity drainage models that came after Cardwell and Parsons are mostly suitable for the case where the operation mode is at constant rate. Model such as the

one used in experimental study from Terwilliger et al. (1951) suits this purpose since it used the Buckley and Leverett (1942) solution to calculate the saturation profile. The calculation procedures usually require the production rate to be known a priori or obtained from historical data in order to determine the oil recovery.

For reservoirs under pressure maintenance, the operation mode is constant pressure. Over time a condition emerges where it is advantageous to employ gravity force to assist the oil recovery. When coupled with high effective oil permeability, low oil viscosity and steep formation dip, the oil recovery can be improved substantially. In their paper they argued that a model for gravity drainage developed for such condition under constant pressure would help engineer to calculate the oil recovery as a function of time even when there is no historical production data available. Such knowledge can be used to justify economically the continued operation under gravity force.

In their work they modify the relative permeability expression used in Cardwell and Parsons paper to allow the oil relative permeability to go to zero at residual oil saturation instead of zero saturation by defining a normalized saturation variable. This definition enables them to come out with a new expression to calculate oil recovery, which was absent in the original Cardwell and Parsons paper. The governing equations are given below:

Demarcator equation:

$$\frac{dZ_d}{dt} = \frac{\rho g k}{\mu \phi'} \left[\frac{K_r(S_i) \left(1 - \frac{H}{L - Z_d}\right) - \left(\frac{m Z_d}{t}\right)^{\frac{B}{B-1}}}{S_i - \left(\frac{m Z_d}{t}\right)^{\frac{1}{B-1}}} \right] \quad (5.5)$$

where Z_d is the distance of demarcator or gas-liquid interface from the top of the column, t is time, ρ the oil density, g the gravity acceleration constant, k the absolute permeability, μ the oil viscosity, ϕ' the adjusted porosity, K_r the oil relative permeability, H the equilibrium height of capillary rise, L the column length, B the exponent in oil relative permeability equation and S_i the initial oil saturation. In Equation 5.5, m is the

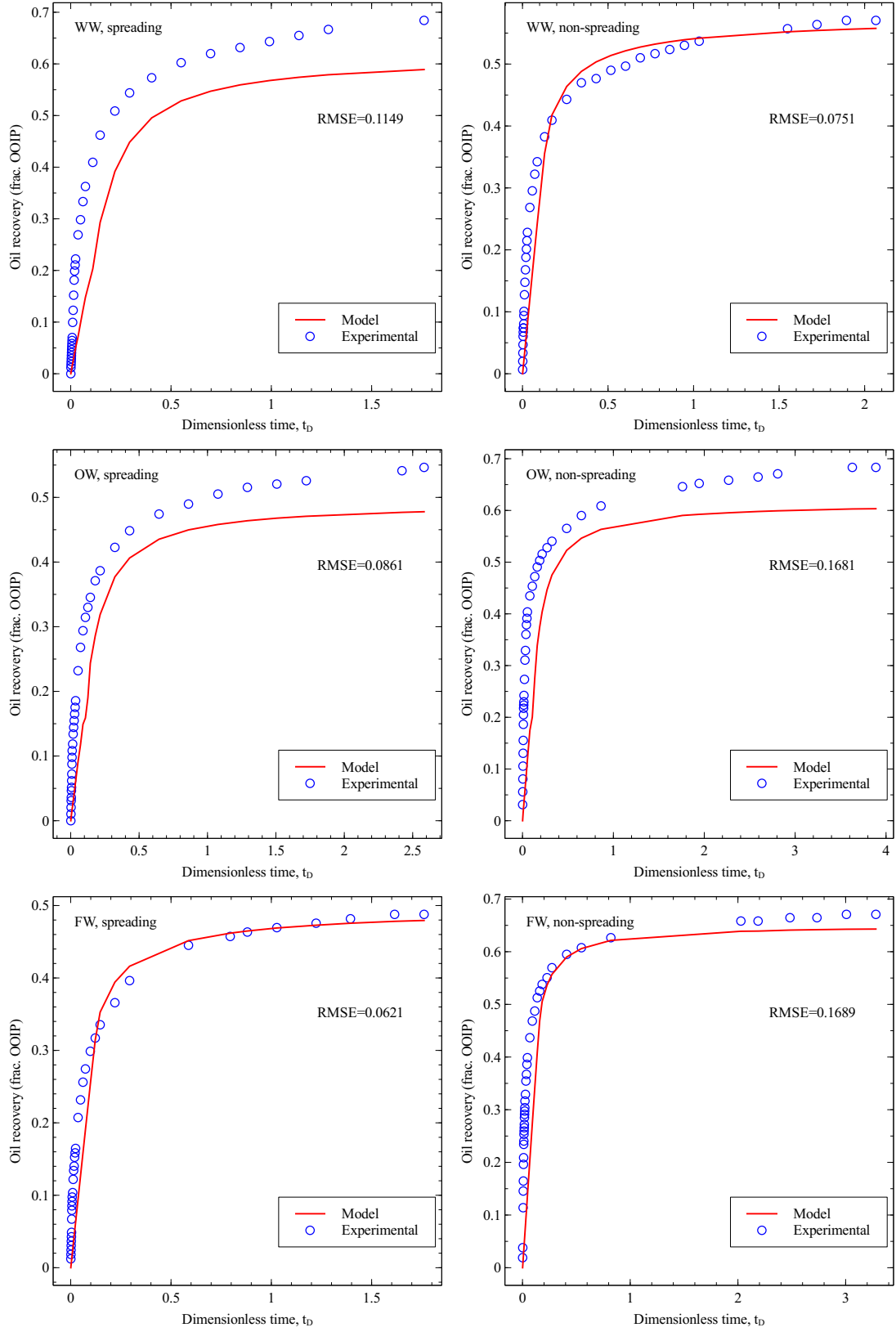


Figure 5.1: Curve fit results using data from FGD experiments for Dykstra model.

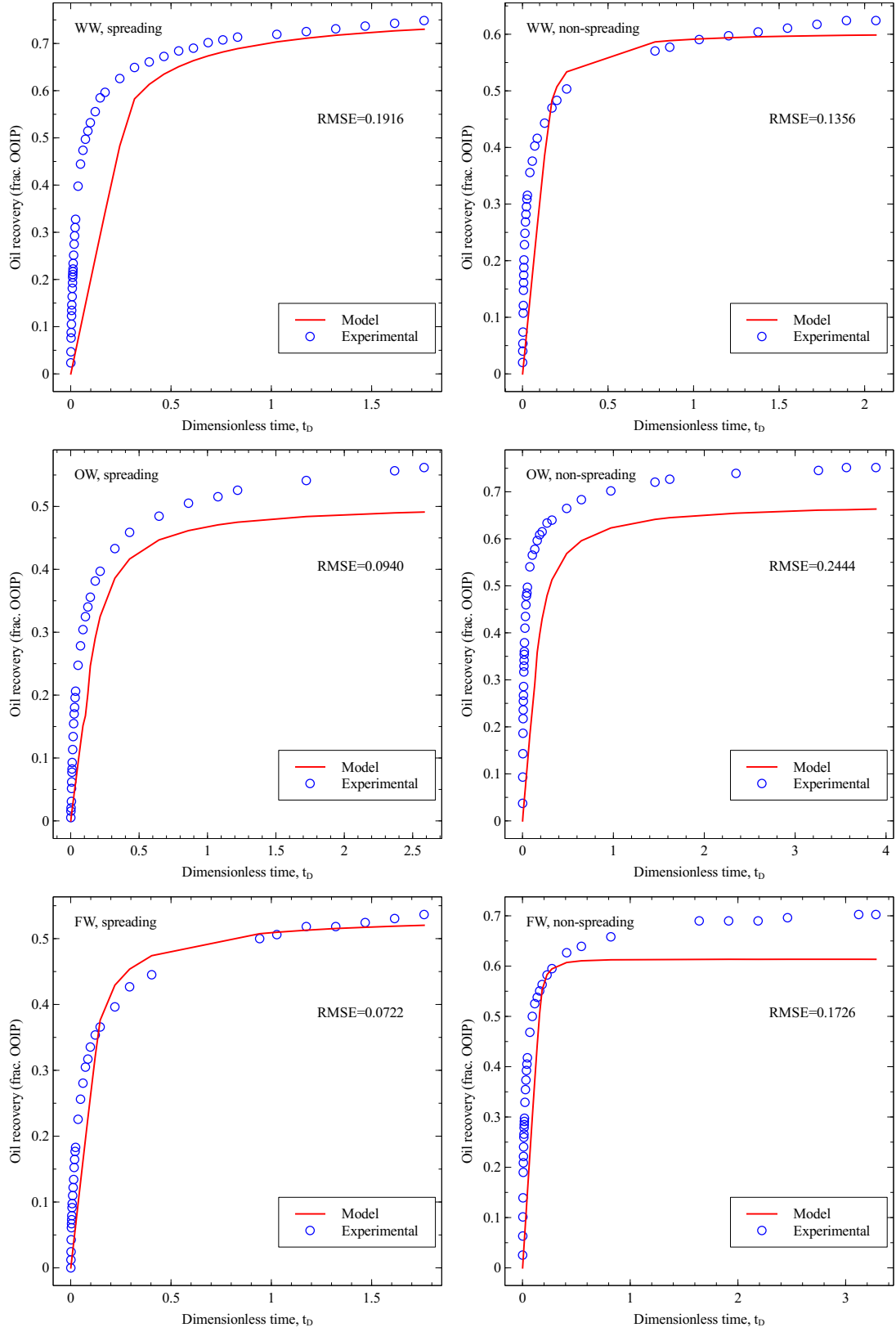


Figure 5.2: Curve fit results using data from secondary GAGD experiments for Dykstra model.

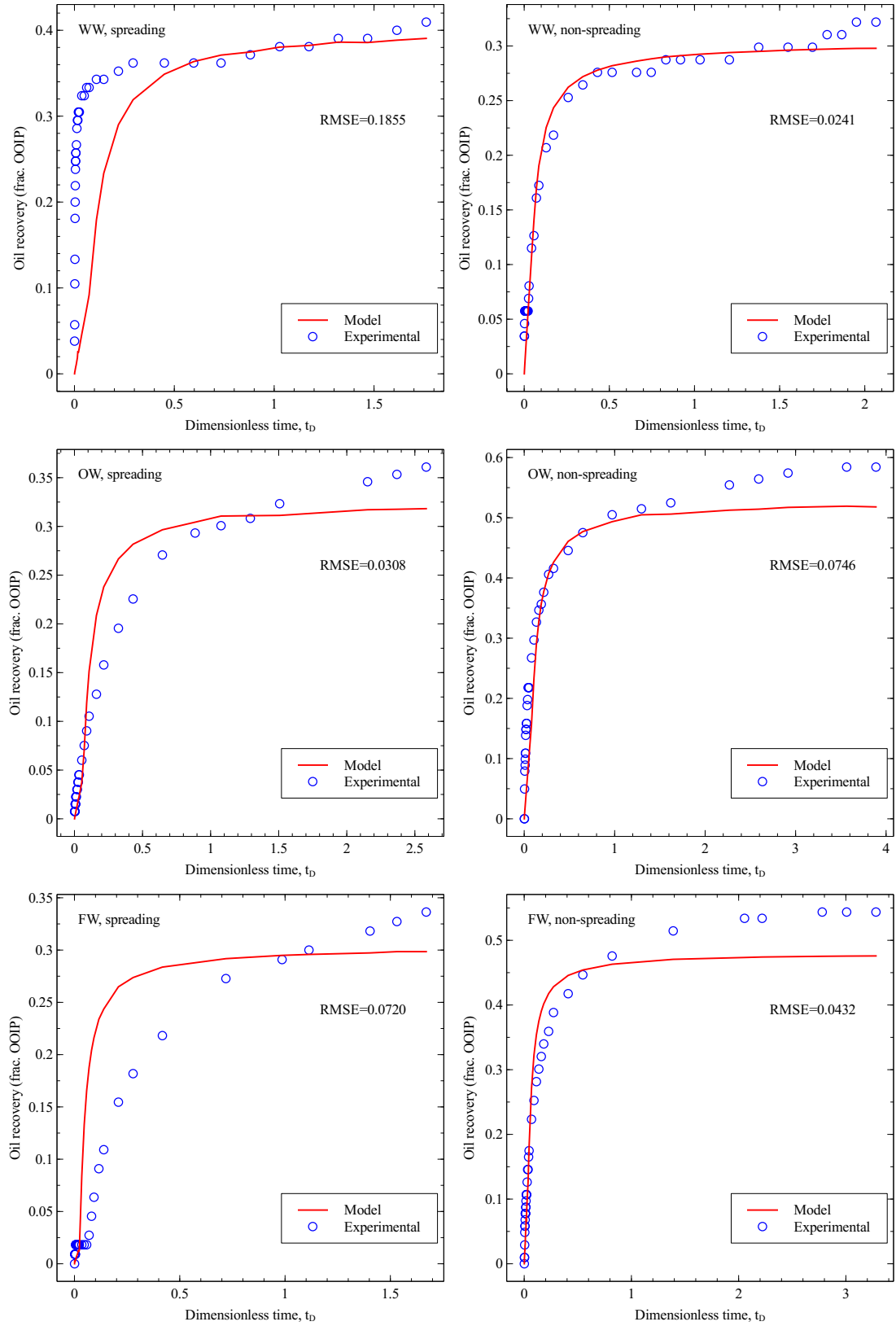


Figure 5.3: Curve fit results using data from tertiary GAGD experiments for Dykstra model.

constant defined as $\frac{\mu\phi'}{Bk\rho g}$ where ϕ' , the adjusted porosity is $\phi(1 - S_{or})$ for a two-phase system and $\phi(1 - S_{or} - S_{wc})$ for a three-phase system.

Oil recovery equation:

$$R = \frac{Z_d}{L} \left[\left(1 - \frac{B_{oi}S_{or}}{S_{oi}B_o} \right) - \frac{B_{oi}}{S_{oi}} \left(\frac{1 - S_{or}}{B_o} \right) \left(\frac{B - 1}{B} \right) \left(\frac{mZ_d}{t} \right)^{\frac{1}{B-1}} \right] \quad (5.6)$$

where R is the oil recovery, B_o is the oil formation volume factor, S_{oi} the initial oil saturation and S_{or} the residual oil saturation.

In order to fit Equation 5.6 to the experimental data, first we have to solve the demarcator Equation 5.5 to obtain Z_d . This is because the term Z_d is required in Equation 5.6 to calculate the oil recovery, R . In order to find Z_d from Equation 5.5 we used MATLAB built-in solver *ode45* or *ode113* to ensure fast convergence since Equation 5.5 is a nonlinear ordinary differential equation. The actual matching to experimental data is achieved by using the MATLAB function *lsqcurvefit* from the Optimization Toolbox with B , H and S_i set as the fitting parameters.

In Appendix B on page 158 we have included a working *.m* files with the associated functions for this model. The program was developed initially to be used in *Octave* version 4.2.1, a MATLAB-compatible open-source program before the codes were migrated to MATLAB in order to use the proprietary toolboxes. The earlier program written for *Octave* used Euler's method to obtain Z_d . When the codes were migrated to MATLAB and used together with *lsqcurvefit* it lead to erroneous results, particularly in the early time with fluctuations in the predicted recovery. After rewriting the codes to solve Equation 5.5 with *ode45* or *ode113* and fitting Equation 5.6 to recovery data using *lsqcurvefit* we successfully removed the unphysical fluctuations from the model output.

The curve fit results are shown in Figures 5.1, 5.2 and 5.3 for free-fall gravity drainage (FGD), secondary GAGD and tertiary GAGD respectively. The experimental results are plotted with the horizontal axis using dimensionless time, t_D from Equation 5.9 on page 128 in Schechter and Guo model.

In Figure 5.1 under free-fall mode, the predicted values for oil recovery at the end of the experiment tend to be lower than the experimental values. Performance of the model varies with experiments. For example the best match for this set of experiments came from fractional-wet, spreading case with $RMSE = 0.0621$. This is followed by water-wet, non-spreading experiment with $RMSE = 0.751$ and oil-wet, spreading experiment with $RMSE = 0.0861$. The greater the value of $RMSE$ than zero, the more the prediction of terminal oil recovery differs from experimental value. The results for this group indicate that Dykstra model works best to predict oil recovery from experiment in fractional-wet, spreading condition.

Table 5.1: Performance of Dykstra model in FGD, secondary GAGD and tertiary GAGD experiments.

Experiment mode	Wettability condition	Spreading condition	$RMSE$
FGD	fractional-wet	spreading	0.0621
	water-wet	non-spreading	0.0751
	oil-wet	spreading	0.0861
	water-wet	spreading	0.1149
	oil-wet	non-spreading	0.1681
	fractional-wet	non-spreading	0.1689
Secondary GAGD	fractional-wet	spreading	0.0722
	oil-wet	spreading	0.0940
	water-wet	non-spreading	0.1356
	fractional-wet	non-spreading	0.1726
	water-wet	spreading	0.1916
	oil-wet	non-spreading	0.2444
Tertiary GAGD	water-wet	non-spreading	0.0241
	oil-wet	spreading	0.0308
	fractional-wet	non-spreading	0.0432
	fractional-wet	spreading	0.0720
	oil-wet	non-spreading	0.0746
	water-wet	spreading	0.1855

The results for secondary GAGD experiments are shown in Figure 5.2. Similar to free-fall mode, Dykstra model is also shown to underpredict the oil recovery at late time. The best match came from fractional-wet, spreading case with $RMSE = 0.0722$. The second

and third best match for this group came from oil-wet, spreading experiment and water-wet, non-spreading experiment respectively at $RMSE = 0.0940$ and 0.1356 each. The top three results are consistent with that to the previous group of experiments in free-fall mode. In both free-fall and secondary GAGD (both performed at residual water saturation) the results again demonstrate that Dykstra model can be used to predict oil recovery from fractional-wet, spreading experiment.

In tertiary GAGD experiments the results in Figure 5.3 indicate that the model also underpredict the oil recovery at late time. In tertiary mode the model exhibits best match for experiment performed in water-wet, spreading condition ($RMSE = 0.0241$). This is followed by oil-wet, spreading experiment and fractional-wet non-spreading experiment at $RMSE = 0.0308$ and 0.0432 respectively. The results for experiments performed in this group show that Dykstra model works best to predict oil recovery in water-wet, non-spreading condition.

We tabulate the experimental results for each group and arrange them according to increasing $RMSE$ values in Table 5.1. As mentioned earlier, results with $RMSE$ values approaching zero would show better match between the model and experimental data. From Table 5.1 we can infer that for FGD and secondary GAGD experiments under varying wettability and spreading conditions, Dykstra model performs better in fractional-wet, spreading system. In tertiary GAGD under varying wettability and spreading, Dykstra model is found to match reliably oil recovery from water-wet, non-spreading experiment.

5.3 Schechter and Guo model

The Schechter and Guo model is considered in this study because it takes into account the effect of film flow in gravity drainage displacement. In their model they divided a tall column where gravity drainage takes place into saturated and unsaturated zone. This approach is similar to that taken by Cardwell and Parsons (1949) and Dykstra (1978) when developing their gravity drainage models. In the saturated zone Darcy velocity is assumed

to be valid while in the top, unsaturated zone they consider the volume contributed by bulk and film flow. They derived a differential equation by equating the volume change due to Darcy flow in the saturated zone with the volume change due to bulk and film flow in the unsaturated zone. The resulting set of equations were solved numerically to obtain the demarcator (gas-oil interface) and the oil recovery. Below are the equations used:

Demarcator equation:

$$\Delta z_D = \frac{-\frac{\phi z_D}{3t_D} \sqrt{\frac{F_s \phi z_D}{5t_D}} + \left[1 - \frac{H_D}{1-z_D}\right]}{\phi \left[S_{oi} - S_{or} - \sqrt{\frac{F_s \phi z_D}{5t_D}}\right]} \Delta t_D \quad (5.7)$$

where z_D is the dimensionless demarcator depth, t_D is the dimensionless time, ϕ is porosity, F_s is the Kozeny correction factor, H_D is the dimensionless capillary pressure threshold, S_{oi} is the initial oil saturation and S_{or} is the residual oil saturation respectively.

Oil recovery equation:

$$R = \left(1 - \frac{S_{or}}{S_{oi}}\right) z_D - \frac{2z_D}{3S_{oi}} \sqrt{\frac{F_s \phi z_D}{5t_D}}. \quad (5.8)$$

The dimensionless time t_D is given as

$$t_D = \frac{k_e \Delta \rho g t}{\mu L} \quad (5.9)$$

where k_e is the effective permeability, $\Delta \rho$ is the density difference, g is the gravity acceleration constant, t is time, μ is viscosity and L is the column length respectively.

In this model the film flow effect is accounted by considering the volume contributed by the film. This is possible because they used earlier work by Nenniger and Storow (1958). In their paper Nenniger and Storow derived a gravity drainage model for a column of packed bed and solved the differential equation using a series solution. The effect of film drainage on the packed bed is incorporated using integration of Navier-Stokes approximate solution for film drainage down a vertical plane. The phase volume in the film is given as

$$V_f = \frac{2}{3}b\sqrt{\frac{\mu z_d^3}{\Delta\rho g t}} \quad (5.10)$$

where further down in the derivation the breadth of the film, b , is estimated using Kozeny equation

$$\frac{b\sqrt{k_e}}{A} = \sqrt{\frac{F_s\phi^3}{5}}. \quad (5.11)$$

In order to test this model using our experimental dataset, we have developed a GUI in MATLAB. The interface is shown in Figure 5.4. The GUI takes an input data in the form of .csv file and fits the oil recovery model from Equation 5.8 to the experimental data. Equation 5.7 and 5.8 are solved numerically using the Euler's method. We used the *lsqcurvefit* function from MATLAB's Optimization toolbox for the curve fitting. In performing the curve fitting the parameters F_s , H_D and S_{oi} were used as the tuning parameters. A .m script file developed for use in *Octave* software for Schechter and Guo model is included in Appendix A.

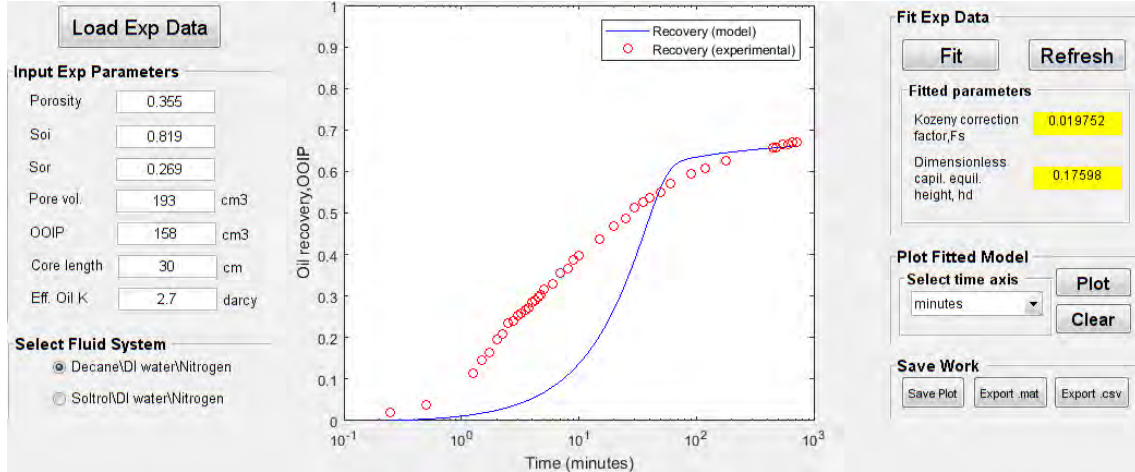


Figure 5.4: MATLAB GUI for solving Schechter and Guo (1996) model

We tested the model to fit our water-wet, oil wet and fractional-wet experiments. Figures 5.5, 5.6 and 5.7 show the results comparing the model with experimental data from free-fall, secondary GAGD and tertiary GAGD respectively.

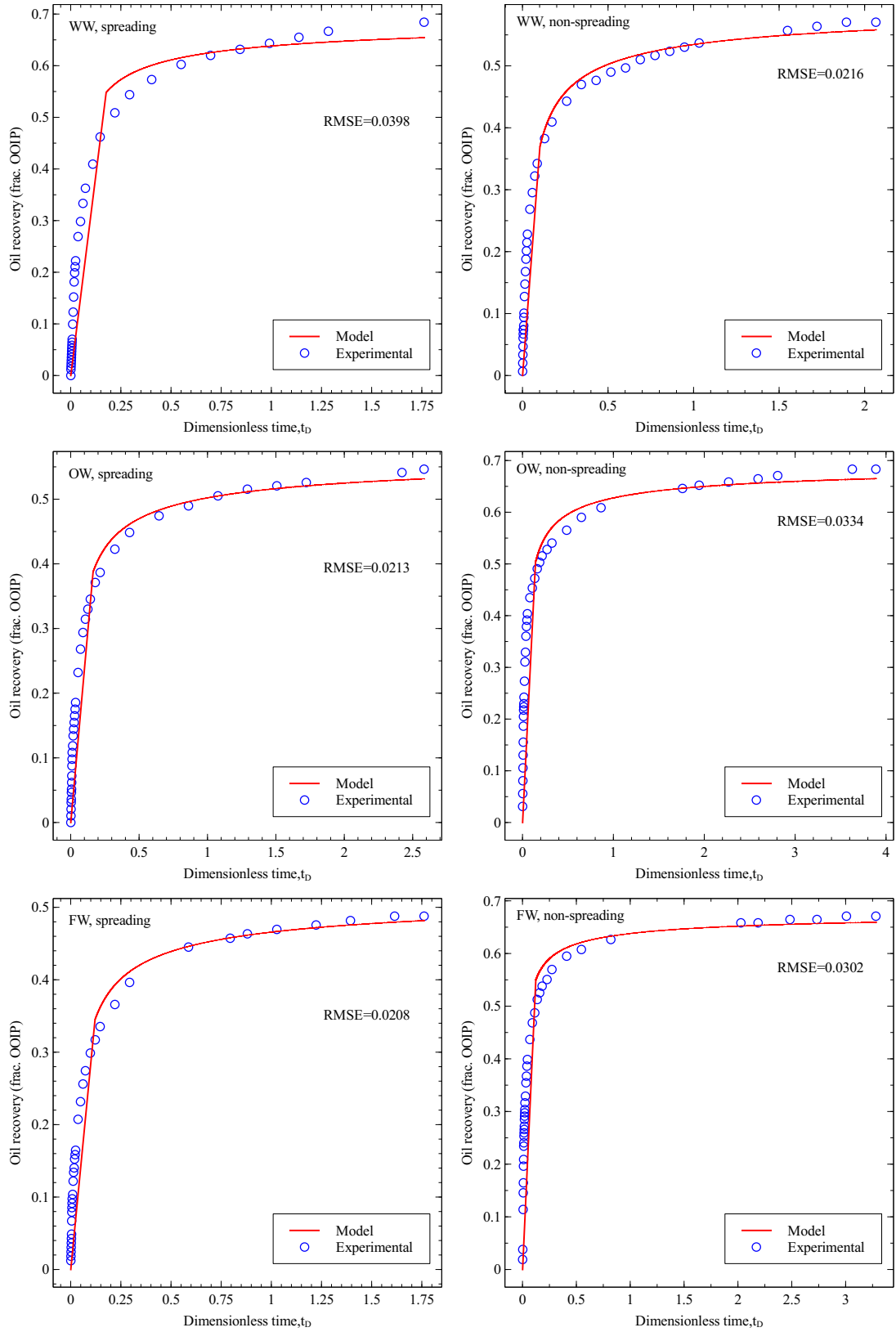


Figure 5.5: Curve fit results using data from FGD experiments for Schechter and Guo model.

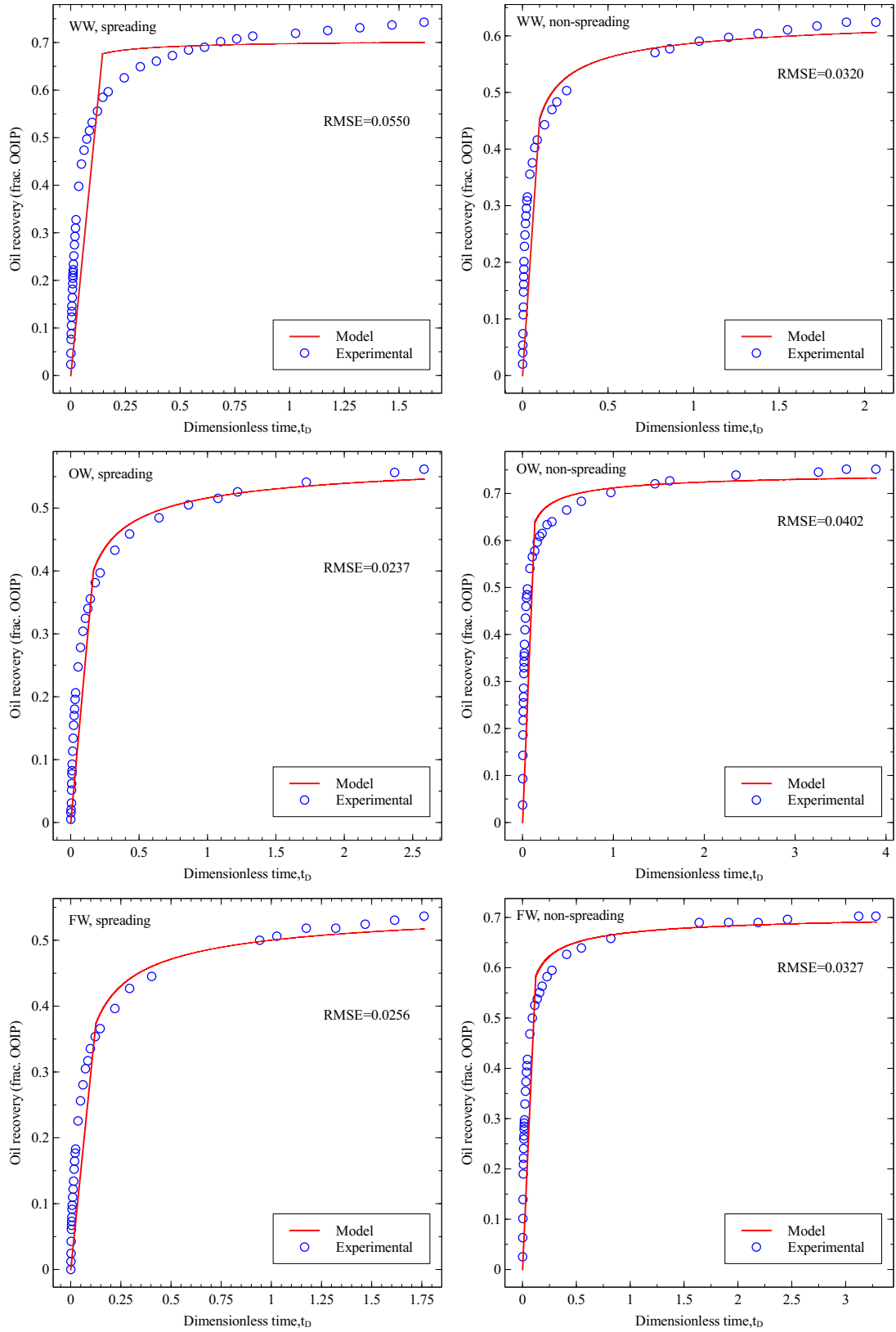


Figure 5.6: Curve fit results using data from secondary GAGD experiments for Schechter and Guo model.

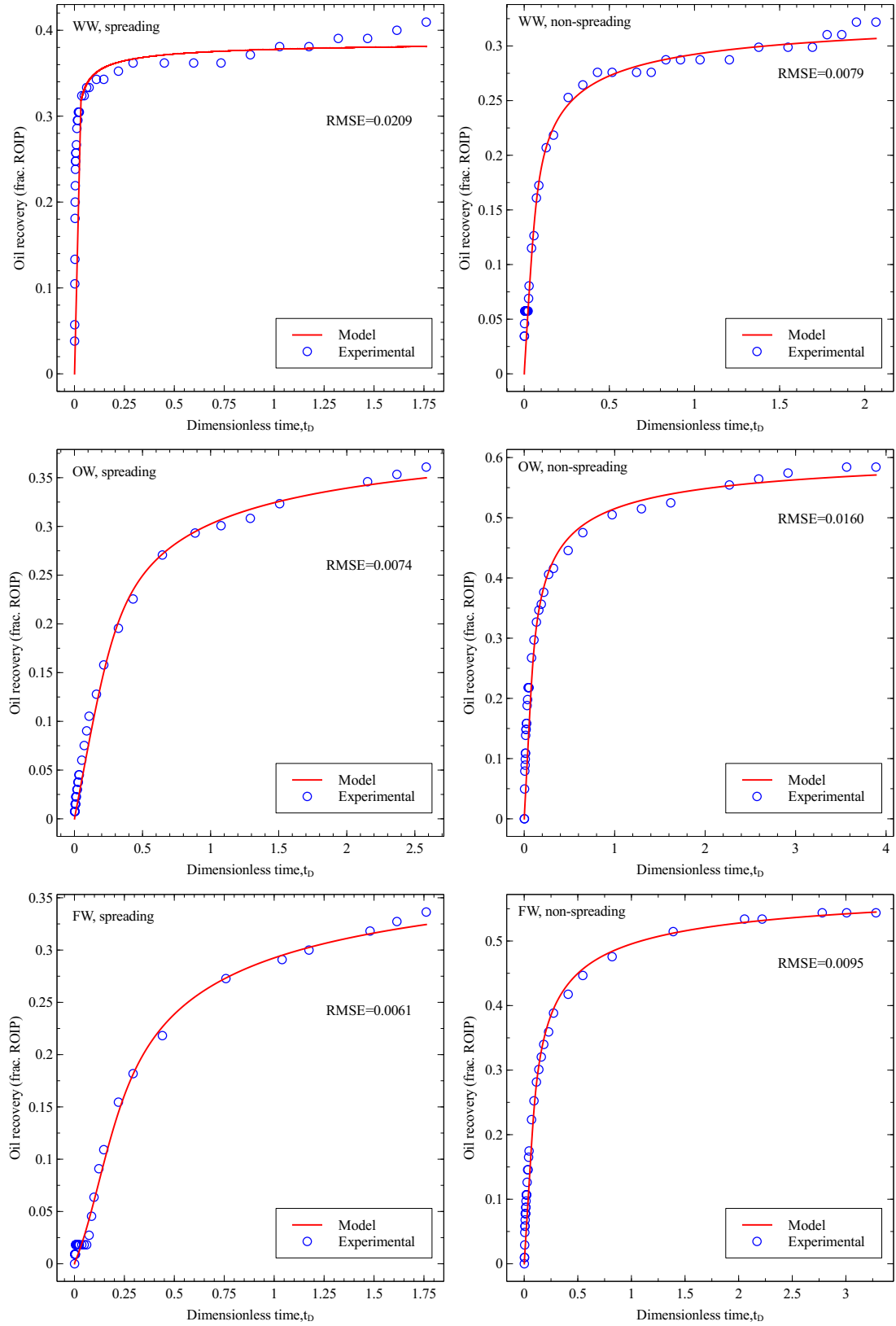


Figure 5.7: Curve fit results using data from tertiary GAGD experiments for Schechter and Guo model.

From the results in Figure 5.5 Schechter and Guo model is shown to achieve very close match with experimental data from fractional-wet, spreading system ($RMSE = 0.0208$). This is followed by oil-wet, spreading system ($RMSE = 0.0213$) and water-wet, non-spreading system ($RMSE = 0.0216$). In this set of experiments notable difference between oil recovery from experimental data and that predicted by the model is seen for the case of water-wet, spreading experiment with $RMSE = 0.0398$. Based on our results for this group Schechter and Guo model performs best in predicting oil recovery from fractional-wet, spreading experiment.

In Figure 5.6 for secondary GAGD, Schechter and Guo model is able to match closely experimental data from oil-wet, spreading system ($RMSE = 0.0237$). However the predicted oil recovery from the model is slightly less than that of the experimental data at late time for this experiment. Observations of other experimental data from this group also show the Schechter and Guo model underpredicts the oil recovery at late time, with the difference between model and experimental data increasing the higher the value of $RMSE$. This is clearly shown for matching of the model to water-wet, spreading experiment with $RMSE = 0.0550$. Results from this group indicate that the model works best for predicting oil recovery in oil-wet, spreading system.

For the set of experiments performed under tertiary mode the results in Figure 5.7 show that the model demonstrates satisfactory match overall with the experimental data as indicated by the very low $RMSE$ values. The best matching achieved by the model comes from fractional-wet, spreading system with $RMSE = 0.0061$. This infers that in tertiary experiments the model works best to predict the oil recovery from fractional-wet, spreading experiment. In the same group the prediction of the oil recovery at late time from the model is seen to deviate from the experimental data the greater the $RMSE$ value is from zero. This is shown for example with water-wet, spreading system with $RMSE = 0.0209$.

Table 5.2: Performance of Schechter-Guo model in FGD, secondary GAGD and tertiary GAGD experiments.

Experiment mode	Wettability condition	Spreading condition	<i>RMSE</i>
FGD	fractional-wet	spreading	0.0208
	oil-wet	spreading	0.0213
	water-wet	non-spreading	0.0216
	fractional-wet	non-spreading	0.0302
	oil-wet	non-spreading	0.0334
	water-wet	spreading	0.0398
Secondary GAGD	oil-wet	spreading	0.0237
	fractional-wet	spreading	0.0256
	water-wet	non-spreading	0.0320
	fractional-wet	non-spreading	0.0327
	oil-wet	non-spreading	0.0402
	water-wet	spreading	0.0550
Tertiary GAGD	fractional-wet	spreading	0.0061
	oil-wet	spreading	0.0074
	water-wet	non-spreading	0.0079
	fractional-wet	non-spreading	0.0095
	oil-wet	non-spreading	0.0160
	water-wet	spreading	0.0209

We have compiled the performance of Schechter and Guo model in terms of the best-fit with experimental data in Table 5.2. Table 5.2 summarizes the results for all experiments under different wettability and spreading conditions. To recapitulate in FGD experiments the model works best to predict oil recovery in fractional-wet, spreading system. In secondary GAGD curve fitting results indicate that the model can be used best for oil-wet, spreading system. In tertiary mode Table 5.2 shows that the *RMSE* values for all experiments in this group are significantly lower than the best matching results from FGD and secondary GAGD experiments. Thus it can be inferred that Schechter and Guo model works particularly well for experiments conducted in tertiary mode. Furthermore the model seems to perform well under all wettability and spreading conditions for this group. Although we recommended earlier to use Schechter and Guo model to predict oil recovery in fractional-wet, spreading experiment we would like to point out that based on the lower

$RMSE$ values overall, Schechter and Guo model can be used to predict gravity drainage recovery in all tertiary GAGD experiments.

5.4 Li and Horne model

Li and Horne (2003) derived gravity drainage model in free-fall mode by assuming that free-fall drainage mechanism is similar to that of spontaneous imbibition. Their model was based on earlier work from Aronofsky et al. (1958) for spontaneous imbibition. In Aronofsky et al. model a single fit parameter called rate constant is used in the exponential expression to obtain match with experimental data.

Li and Horne (2003) proposes the following equation to match oil recovery of FGD system:

$$R = \frac{1 - S_{wi} - \overline{S_{or}}}{1 - S_{wi}} (1 - e^{-\beta t}) \quad (5.12)$$

where R is the recovery, S_{wi} is the initial water saturation, $\overline{S_{or}}$ is the average residual oil saturation and β is the constant used as parameter to give the rate of convergence in Equation 5.12.

Compared to Aronofsky et al. model they used two parameters, $\overline{S_{or}}$ and β to fit the experimental data. The value $\overline{S_{or}}$ is different from the values of residual oil saturation in the core because in the latter the value changes with depth. $\overline{S_{or}}$ is calculated assuming equilibrium between gravity and capillary forces after completion of gravity drainage experiment.

In their model they relaxed the assumption that the oil saturation at the top of the column is at residual oil saturation. The derivation of the model aims to find the ultimate oil recovery by assuming that gravity force is balanced by capillary force everywhere in the column.

For a given data of gravity drainage experiment, we perform a nonlinear regression analysis to obtain the matching parameter $\overline{S_{or}}$ and β . According to Li and Horne (2003)

parameter β can be used to calculate p_e , the entry capillary pressure and both $\overline{S_{or}}$ and β can be used to obtain λ , the pore size distribution index. A working computer program for this model is included in Appendix C.

The curve fit results are shown in Figures 5.8, 5.9, and 5.10 for FGD, secondary GAGD and tertiary GAGD respectively. In free-fall mode the model typically matches the recovery at early time but underpredicts at late time. The best matching for this group comes from fractional-wet, spreading experiment with $RMSE = 0.0230$ followed by oil-wet, spreading experiment with $RMSE = 0.0257$ and fractional-wet, non-spreading experiment with $RMSE = 0.0289$. Results from this group show that for FGD experiments, the model can be used to match the oil recovery from fractional-wet, spreading experiment. However we caution against using it for predicting the oil recovery since the matched result was lower than the experimental data.

In secondary GAGD experiments Figure 5.9 shows that the model underpredicts oil recovery at late time. The best match is obtained for oil-wet, spreading experiment with $RMSE = 0.0280$. Within the same group the model's prediction of oil recovery differs greatly from experimental data as shown by the increasing $RMSE$ values. This can be seen for the case of water-wet, non-spreading experiment which has $RMSE$ value of 0.0368. Based on the results the model is suitable to be used to match the experimental data from oil-wet, spreading experiment. However since the matching result for this particular experiment does not reproduce the experimental data exactly, we again caution against using it for prediction of oil recovery.

For tertiary GAGD experiments Figure 5.10 shows that the model underpredicts the late time recovery overall and matches the early time recovery on select cases. The best match in this set of experiments goes to fractional-wet, spreading experiment with $RMSE = 0.0085$. This is followed by oil-wet, spreading experiment and water-wet non-spreading experiment with $RMSE$ values of 0.0117 and 0.0140 respectively. Although the results indicate that the model can be used to match experimental data from fractional-wet,

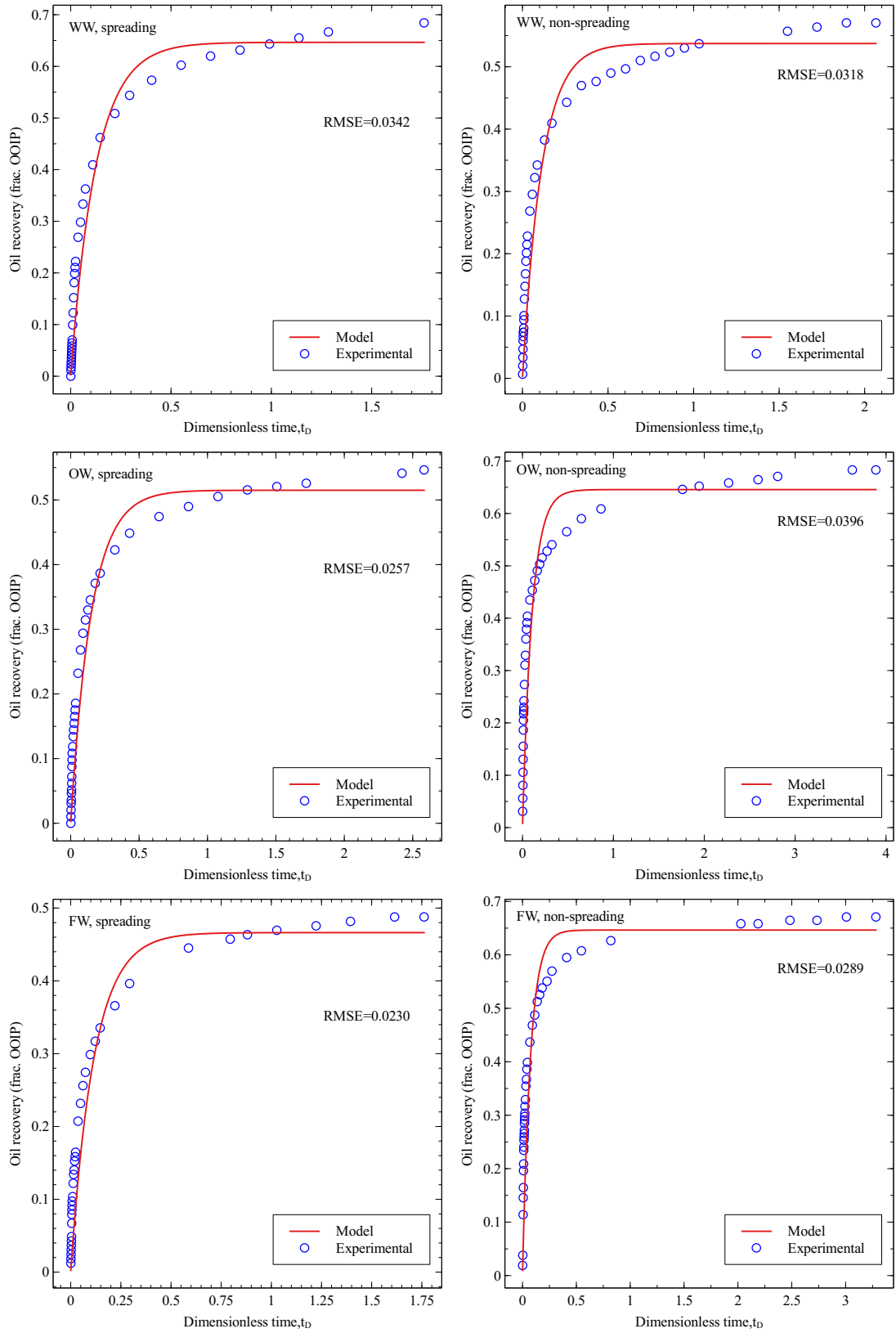


Figure 5.8: Curve fit results using data from FGD experiments for Li and Horne model.

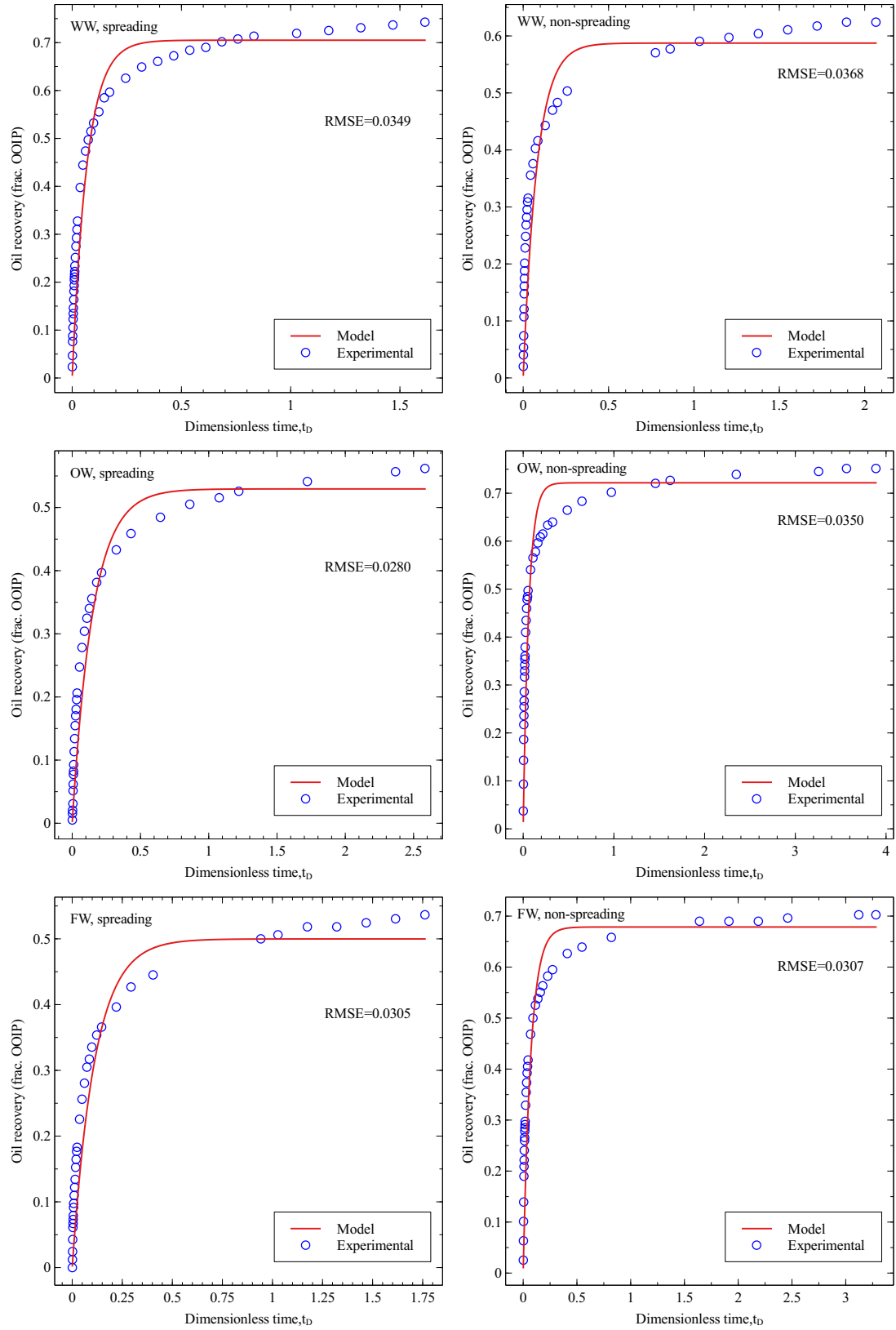


Figure 5.9: Curve fit results using data from secondary GAGD experiments for Li and Horne model.

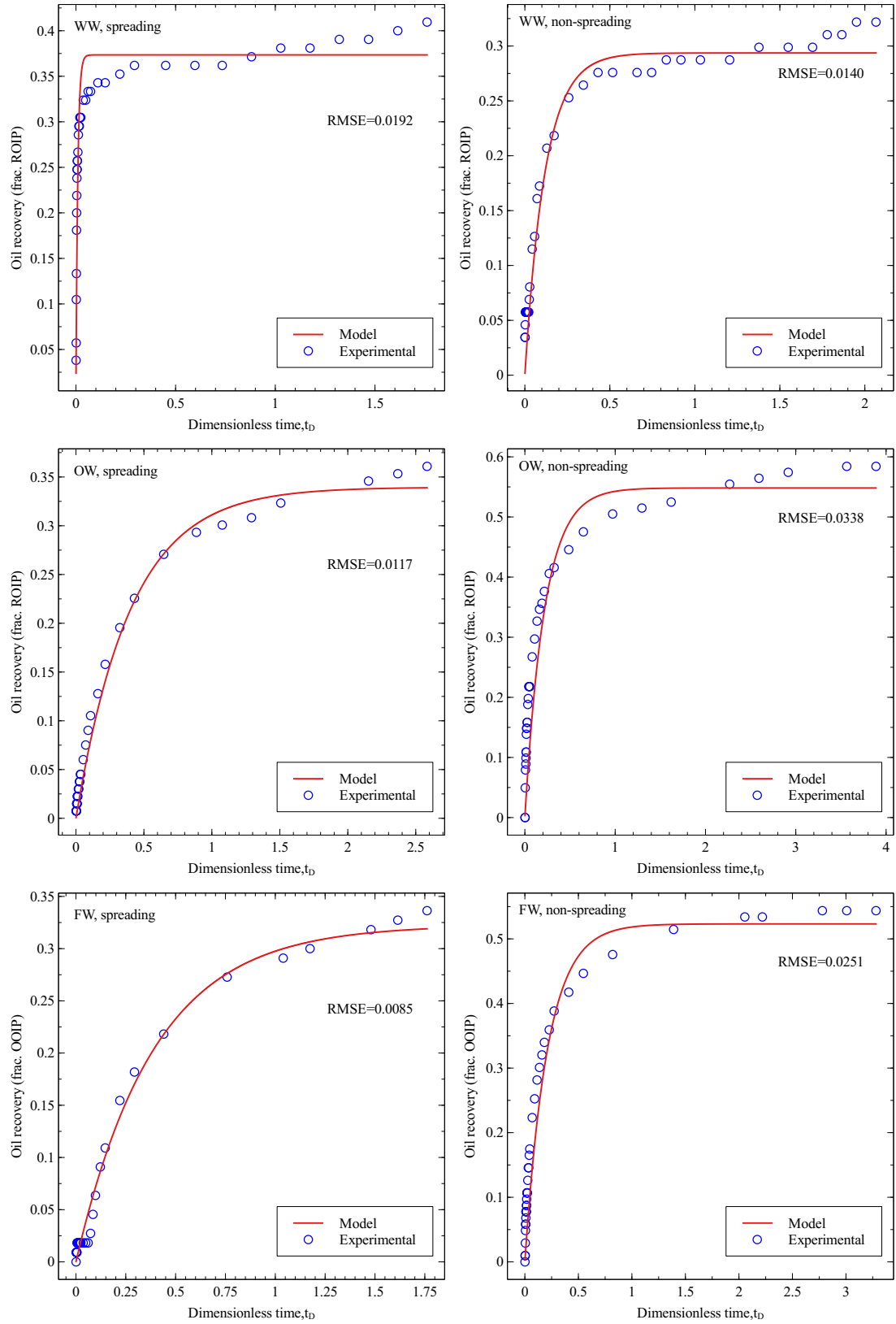


Figure 5.10: Curve fit results using data from tertiary GAGD experiments for Li and Horne model.

Table 5.3: Performance of Li and Horne model in FGD, secondary GAGD and tertiary GAGD experiments.

Experiment mode	Wettability condition	Spreading condition	$RMSE$
FGD	fractional-wet	spreading	0.0230
	oil-wet	spreading	0.0257
	fractional-wet	non-spreading	0.0289
	water-wet	non-spreading	0.0318
	water-wet	spreading	0.0342
	oil-wet	non-spreading	0.0396
Secondary GAGD	oil-wet	spreading	0.0280
	fractional-wet	spreading	0.0305
	fractional-wet	non-spreading	0.0307
	water-wet	spreading	0.0349
	oil-wet	non-spreading	0.0350
	water-wet	non-spreading	0.0368
Tertiary GAGD	fractional-wet	spreading	0.0085
	oil-wet	spreading	0.0117
	water-wet	non-spreading	0.0140
	water-wet	spreading	0.0192
	fractional-wet	non-spreading	0.0251
	oil-wet	non-spreading	0.0338

spreading experiment, the matched result is still lower than the experimental data at late time. Thus the user is advised to compare prediction result of this particular experiment from this model with other models (Dykstra and Schechter and Guo) to decide on the best model to use.

Table 5.3 shows the performance of Li and Horne model in matching the experimental data from FGD, secondary GAGD and tertiary GAGD experiments under different wettability and spreading conditions. In Table 5.3 the curve fit results from tertiary GAGD experiments exhibit the least $RMSE$ values compared to that of FGD and secondary GAGD experiments. This seem to indicate that the model would be suitable to use for matching experimental data from tertiary experiments. However caution is advised when using this model for predicting oil recovery because the model consistently underpredicts the late time recovery. This pattern of underprediction of oil recovery at late time is also observed for the best matching result from FGD (fractional-wet, spreading) and secondary

Table 5.4: Best curve fit results from Dykstra, Schechter and Guo and Li and Horne models for FGD, secondary GAGD and tertiary GAGD experiments.

Experiment mode	Model	Experiment	$RMSE$
FGD	Schechter and Guo	fractional-wet, spreading	0.0208
	Li and Horne	fractional-wet, spreading	0.0230
	Dykstra	fractional-wet, spreading	0.0621
Secondary GAGD	Schechter and Guo	oil-wet, spreading	0.0237
	Li and Horne	oil-wet, spreading	0.0280
	Dykstra	fractional-wet, spreading	0.0722
Tertiary GAGD	Schechter and Guo	fractional-wet, spreading	0.0061
	Li and Horne	fractional-wet, spreading	0.0085
	Dykstra	water-wet, non-spreading	0.0241

GAGD (oil-wet, spreading) experiments. Although Li and Horne (2003) intended this model for free-fall gravity drainage, our results further clarify that in FGD mode the model demonstrates best matching for experiment under fractional-wet condition with spreading oil.

5.5 Discussion and summary

In this chapter we have evaluated the performance of gravity drainage models from Dykstra (1978), Schechter and Guo (1996) and Li and Horne (2003). Using root mean squared error ($RMSE$) as the metric for comparison, we were able to rank the performance of each model according to closeness of the model fit to the experimental data. It is assumed that a close fit overall would infer that the model successfully capture the pore-scale physics discussed in Section 4.2 on page 81. According to Grattoni et al. (1997) the core-scale displacement is affected by many small events occurring at the pore-scale. Depending on wettability and three-phase fluid distribution, the pore-scale events when taken as average, would affect the residual oil saturation.

We have compiled the best matching results for each model and sorted them according to the mode of gravity drainage experiment in Table 5.4. In Table 5.4 the results for curve fit in FGD experiments indicate that all models can be used to match experiment from

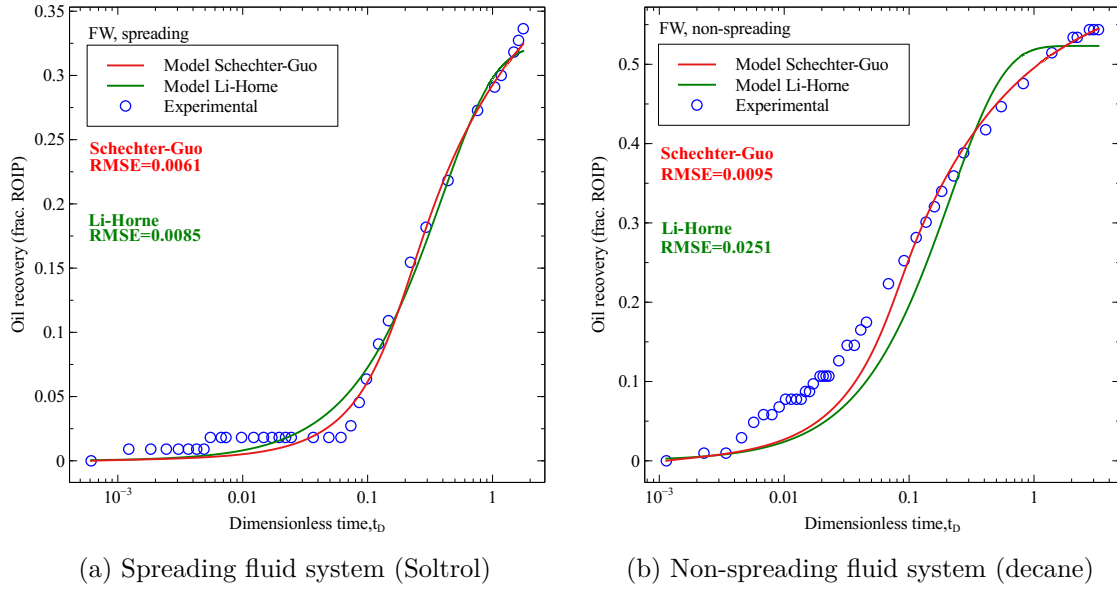


Figure 5.11: Performance comparison between Schechter-Guo and Li-Horne model in tertiary GAGD of fractional-wet sand for both spreading and non-spreading system

fractional-wet sand with spreading oil. Since Schechter and Guo model achieved the lowest $RMSE$ value for this group it can also be used for predicting oil recovery from the same experiment. In secondary GAGD group, Schechter and Guo and Li and Horne models both show that they were able to model experiment from oil-wet sand with spreading oil. In the same group, Dykstra model is shown to work best with experiment from fractional-wet, spreading system. Using $RMSE$ value as the criterion we determined that in secondary GAGD experiments, Schechter and Guo model is chosen as the model that is suitable to match and subsequently predict the oil recovery from experiment using oil-wet sand with spreading oil. For tertiary GAGD experiments Table 5.4 show that fractional-wet, spreading experiment can be modeled by both Schechter and Guo and Li and Horne models. Within the same group Dykstra model shows that it can best be used with water-wet, non-spreading experiment. Again using $RMSE$ values we determined that in tertiary mode, experiment from fractional-wet sand with spreading oil can be modeled best with Schechter and Guo model.

The model that is able to fit early time data is inferred to be better at capturing the bulk flow mechanism successfully. Likewise for late time, the model that successfully match the experiment during this period can be assumed to capture the spreading and wetting film flow behavior. In Figure 5.11 we plot the recovery profiles for tertiary GAGD experiments in fractional-wet sand packs for both spreading and non-spreading fluid system. We include the curve fit results from Schechter and Guo and Li and Horne models to observe their performance at early and late time. Thus the horizontal axes are in log scale to highlight the early time behavior. The fractional-wet experiment is selected for comparison because this wettability system could represent reservoir condition since a typical reservoir rock is neither strongly water-wet or oil-wet. More over tertiary mode is chosen since the effect of spreading or wetting film flow is readily manifested at late time under residual oil condition. We omitted comparison of both experiments with Dykstra model since Figure 5.3 showed that the curve fitting of the model to both experiments were not satisfactory.

For the spreading system it is observed that both Schechter and Guo and Li and Horne models capture the early time behavior. However in the middle time both models overpredict the recovery. Between the middle time and late time both models match the experimental data and track each other until the end of the experiment. At late time the modeled oil recoveries from Schechter and Guo and Li and Horne are both below the experimental value. Even though the predicted terminal oil recovery is lower than actual, Schechter and Guo model managed to capture the behavior at late time because it is observed to track the trajectory of the experimental data closely.

For the non-spreading system both models start out matching the experiment at early time but underpredict the experiment in the middle time. Between the middle time and late time both models track each other but Schechter and Guo model is observed to better match the experimental data than Li and Horne model. Finally at late time Schechter and Guo model fits the data well but Li and Horne model tapers off and underpredicts the recovery.

By comparing the performance of both models in Figure 5.11 we can observe that both models successfully capture the early time behavior in spreading and non-spreading experiments. Both models overpredict the middle time recovery in spreading system but the modeled oil recovery is below the experimental value in non-spreading system. At late time when additional recovery is obtained with the help of spreading or wetting film mechanism, Schechter and Guo model shows that it managed to capture the behavior during this time for both spreading and non-spreading system.

Our evaluation of the models and their performance in matching experimental data from diverse set of experiments encompassing varying wettability and spreading conditions demonstrate that in most cases Schechter and Guo is found to be suitable model to be used. This is possibly because the model incorporates film flow mechanism in its derivation. Whether the experiment is conducted in FGD, secondary GAGD or tertiary GAGD mode, comparison of results from this model in Table 5.2 indicates that this model can be expected to match and subsequently predict the oil recovery. Although the model seems to give satisfactory match for most of the experiments, this does not mean that the model should be the default option to be used. This is because the performance of the model at early, middle or late time varies according to experiments. Hence it is suggested to match the target experiment with several models before deciding on the best model since some models work best for a given wettability, spreading and injection conditions.

Our results in this chapter using models available in the literature underscore the need for gravity drainage model that is able to capture the behavior at early, middle and late time. Even though Schechter and Guo appears to be the best choice the model does not always capture the behavior at each time segment. As mentioned the early and middle time represent the period where bulk flow is dominant. In late time the spreading or wetting film flow mechanism is most active recovering additional oil. Since the matching of each model to experimental data varies given wettability and spreading condition, a new model

for gravity drainage that aims to capture the physical behavior should be able to achieve satisfactory match during each time segment.

Chapter 6

Conclusions and Recommendations

In this study we have accomplished the following:

1. Performed gravity drainage experiments using spreading and non-spreading fluid system in water-wet, oil-wet and fractional-wet sand.
2. Analyzed and compared the results with existing literature.
3. Discussed the pore level mechanisms affecting oil recovery at the core scale.
4. Performed analysis with dimensionless numbers to investigate the effect of gravity, capillary and viscous forces.
5. Evaluated and ranked the performance of gravity drainage models in matching experimental data.

We conclude our findings so far as follows:

The experimental results show that oil recovery is higher in spreading fluid system in water-wet sand. In oil-wet sand recovery from non-spreading fluid system is higher than that of spreading fluid. For fractional-wet sand, the recovery trend is similar to that of oil-wet experiments in that the non-spreading fluid produces more oil than spreading fluid system.

At the pore level oil recovery is higher for spreading fluid system in water-wet experiments because the spreading film reconnects isolated oil ganglia. Oil recoveries in oil-wet experiments are similar for both spreading and non-spreading fluid system because regardless the pore-level fluid configurations, the oil is drained through the continuous wetting phase. Oil-wet experiment with Decane shows higher recovery for non-spreading fluid system due to improved drainage rate from higher conductance path established by low viscosity wetting film. In fractional-wet experiments the non-spreading fluid system achieved higher recovery because oil is drained through higher conductance wetting film.

Oil recovery for spreading fluid system is lower because the displaced oil in the water-wet regions was trapped due to discontinuous water phase, and oil is produced mostly from the oil-wet regions.

Using a modified Bond number it is seen that the role of gravity force is significant very early in gravity drainage displacement. This is particularly so in water-wet experiment with spreading fluid system. In the spreading fluid system for water-wet experiment the transition from capillary-dominated to gravity-dominated flow occurs early in the experiment. In oil-wet and fractional-wet experiments the transition occurs much later. In non-spreading system the time for the transition to happen is early in the experiment and the exact time for its occurrence is almost the same for each experiment. Oil recovery is shown to have linear relationship with Bond number in water-wet experiments and non-linear relationship in oil-wet and fractional-wet experiments. In water-wet experiments for both spreading and non-spreading system the contribution of gravity-dominated flow toward oil recovery is significant. However in oil-wet and fractional-wet experiments a greater proportion of oil recovery comes from the capillary-dominated flow. In water-wet, oil-wet and fractional-wet experiments Capillary number decreases with time. The results also show that as the oil production increases, Capillary number decreases. Viscous forces are more dominant in experiment with spreading fluid in water-wet sand, which resulted in higher recovery. In experiments with non-spreading fluid, viscous forces are relatively stronger than capillary forces in both oil-wet and fractional-wet sand; which helped to mobilize and produce more oil. Analysis with Gravity number demonstrates that gravity forces increase with time. Oil recovery is also shown to be increasing with Gravity number. In experiments with spreading fluid, gravity forces become more dominant in water-wet sand after transition from viscous-dominated flow. Consequently this resulted in higher oil recovery. In non-spreading fluid system the presence of gravity forces are more dominant in oil-wet and fractional-wet sand. We also used dimensionless numbers to analyze experimental results from tertiary CGD. It is shown that the trend for total liquid production

exhibits similar relationship with Bond, Capillary and Gravity numbers as shown earlier for experiments conducted at residual water saturation. This means the same forces are also in effect for gravity drainage experiments at residual oil saturation. We also propose flow regime map for gravity drainage experiments based on analysis of dimensionless numbers. By calculating the time for transition from capillary-dominated and viscous-dominated to gravity-dominated flow we are able to determine the extent to which each force is dominant over the course of the experiment. In general the early stage is marked by overlap of capillary and viscous forces. At middle stage either capillary or viscous forces and gravity forces are dominant. At late stage gravity forces are dominating the flow regime.

Curve fitting the experimental data are performed with Dykstra, Schechter-Guo and Li-Horne models. In FGD experiments all three models are shown to work best in matching experimental data from fractional-wet, spreading system. Among the three models Schechter-Guo model gives the best matching and hence can be used to predict oil recovery for this experiment. In secondary mode Schechter-Guo model again shows the best match to experimental data from oil-wet sand with spreading system. In tertiary mode the results show that fractional-wet, spreading experiment can be best modeled with Schechter-Guo model. In addition comparison of fractional-wet experiments in tertiary mode between Schechter-Guo and Li-Horne model again exhibits that Schechter-Guo model is able to capture the drainage behavior at early and late time. However both models overpredict the recovery during middle time for spreading system and underpredict the recovery during the same time segment in non-spreading system. Our results demonstrate that Schechter-Guo model is possibly the model that can be used for all gravity drainage experiments under various wetting and spreading conditions. However opportunity exists to develop a better gravity drainage model since the current models do not capture fully the behavior during early, middle and late time.

From this study we recommend the following:

1. Further experiments to evaluate the fractional-wet system. In this study the fractional-wet sand was 50% water-wet and 50% oil-wet. Additional experiments is recommended to understand the performance of gravity drainage process in fractional-wet system under different mixing ratio.
2. A new set of experiments based on the same experimental design but implemented with fluids at high pressure and temperature. This is because experimental data with similar condition in the reservoir evaluating the effect of wettability and spreading condition is scarce.
3. Development of gravity drainage model that incorporates the wetting and spreading flow mechanism. Although this mechanism has been applied in three-phase network modeling, there is opportunity to develop similar model at the core scale.

References

- Adamson, A. W. and A. P. Gast (1997). *Physical Chemistry of Surfaces* (6 edition ed.). New York: Wiley-Interscience.
- Aronofsky, J. S., L. Masse, and S. G. Natanson (1958). A Model for the Mechanism of Oil Recovery from the Porous Matrix Due to Water Invasion in Fractured Reservoirs. *Petroleum Transactions, AIME* 213, 17–19.
- Blunt, M., D. Fenwick, and D. Zhou (1994). What Determines Residual Oil Saturation in Three-Phase Flow? In *SPE/DOE Improved Oil Recovery Symposium*, SPE. Society of Petroleum Engineers.
- Blunt, M., D. Zhou, and D. Fenwick (1995). Three-phase flow and gravity drainage in porous media. *Transport in Porous Media* 20(1), 77–103.
- Blunt, M. J. (1997). Effects of Heterogeneity and Wetting on Relative Permeability Using Pore Level Modeling. *SPE Journal* 2(01), 70–87.
- Boinovich, L. and A. Emelyanenko (2009, March). Wetting behaviour and wetting transitions of alkanes on aqueous surfaces. *Colloids, polymers and surfactants. Special Issue in honour of Brian Vincent* 147–148, 44–55.
- Buckley, S. E. and M. C. Leverett (1942). Mechanism of Fluid Displacement in Sands. *Transactions of the AIME* 146(01), 107–116.
- Cardwell, W. and R. Parsons (1949). Gravity Drainage Theory. *Transactions of the AIME* 179(01), 199–215.
- Catalan, L. J. and F. A. Dullien (1995). Application of gravity drainage to the recovery of residual LNAPL in homogeneous and lensed sand packs. *Journal of Contaminant Hydrology* 18(4), 279–306.
- Catalan, L. J., F. A. Dullien, and I. Chatzis (1994). The Effects of Wettability and Heterogeneities on the Recovery of Waterflood Residual Oil With Low Pressure Inert Gas Injection Assisted by Gravity Drainage. *SPE Advanced Technology Series* 2(02), 140–149.
- Chatzis, I. and S. Ayatollahi (1993). The Effect Of Gas Injection Rate On The Recovery Of Waterflood Residual Oil Under Gravity Assisted Inert Gas Injection. In *Technical Meeting / Petroleum Conference of The South Saskatchewan Section*, PETSOC. Petroleum Society of Canada.
- Chatzis, I., A. Kantzas, and F. Dullien (1988). On the Investigation of Gravity-Assisted Inert Gas Injection Using Micromodels, Long Berea Sandstone Cores, and Computer-Assisted Tomography. Society of Petroleum Engineers.
- DiCarlo, D., S. Akshay, and M. Blunt (2000). Three-Phase Relative Permeability of Water-Wet, Oil-Wet, and Mixed-Wet Sandpacks. *SPE Journal* 5(01), 82–91.

- Dong, M., F. A. Dullien, and I. Chatzis (1995). Imbibition of Oil in Film Form over Water Present in Edges of Capillaries with an Angular Cross Section. *Journal of Colloid and Interface Science* 172(1), 21–36.
- Dullien, F. A., L. Catalan, I. Chaizis, and A. Collins (1991). Recovery Of Waterflood Residual Oil With Low Pressure Inert Gas Injection, Assisted By Gravity Drainage From Water-Wet And Oil-Wet Cores. In *Annual Technical Meeting*, PETSOC. Petroleum Society of Canada.
- Dumore, J. and R. Schols (1974). Drainage Capillary-Pressure Functions and the Influence of Connate Water. *Society of Petroleum Engineers Journal* 14(05), 437–444.
- Dumore, J. M. (1964). Stability Considerations in Downward Miscible Displacements. *Society of Petroleum Engineers Journal* 4(04), 356–362.
- Dykstra, H. (1978). The Prediction of Oil Recovery by Gravity Drainage. *Journal of Petroleum Technology* 30(05), 818–830.
- Essley, Jr., P., G. Hancock, Jr., and K. Jones (1958, January). Gravity Drainage Concepts in a Steeply Dipping Reservoir. *SPE-1029-G*.
- Fenwick, D. and M. Blunt (1995, May). Pore Level Modelling of Three Phase Flow in Porous Media. Volume 1, Vienna, Austria, pp. 211–218.
- Grattoni, C., M. P. Almada, and R. Dawe (1997). Pore and Core-Scale Displacement Mechanisms with Spreading and Wetting Effects During Three-Phase Flow. In *Latin American and Caribbean Petroleum Engineering Conference*, SPE. Society of Petroleum Engineers.
- Grattoni, C., X. Jing, and R. Dawe (2001). Dimensionless groups for three-phase gravity drainage flow in porous media. *Journal of Petroleum Science and Engineering* 29(1), 53–65.
- Hagoort, J. (1980). Oil Recovery by Gravity Drainage. *Society of Petroleum Engineers Journal* 20(03), 139–150.
- Hayden, N. J. and T. C. Voice (1993). Microscopic observation of a NAPL in a three-fluid-phase soil system. *Journal of contaminant hydrology* 12(3), 217–226.
- Herzberg, W. J. and W. R. Erwin (1970, May). Gas-chromatographic study of the reaction of glass surfaces with dichlorodimethylsilane and chlorotrimethylsilane. *Journal of Colloid and Interface Science* 33(1), 172–177.
- Holbrook, O. C. and G. G. Bernard (1958). Determination of Wettability by Dye Adsorption. *Transactions of the AIME* 213, 261–264.
- James, G., D. Witten, T. Hastie, and R. Tibshirani (2013). *An Introduction to Statistical Learning: with Applications in R*. Springer Texts in Statistics. New York: Springer-Verlag.

- Kalaydjian, F.-M. and M. Tixier (1991, August). Effect of the Spreading Coefficient on Gas/Oil Capillary Pressure Curves in Presence of Connate Water. In *SCA paper No. 9106*, San Antonio, TX.
- Kalaydjian, F.-M., O. Vizika, J.-C. Moulu, and P. K. Munkerd (1995). The role of wettability and spreading in gas injection processes under secondary conditions. *Geological Society, London, Special Publications* 84(1), 63–71.
- Kantzas, A., I. Chatzis, and F. Dullien (1988a). Enhanced Oil Recovery by Inert Gas Injection. In *SPE Enhanced Oil Recovery Symposium*, SPE. Society of Petroleum Engineers.
- Kantzas, A., I. Chatzis, and F. Dullien (1988b). Mechanisms of Capillary Displacement of Residual Oil by Gravity-Assisted Inert Gas Injection. In *SPE Rocky Mountain Regional Meeting*, SPE. Society of Petroleum Engineers.
- Keller, A. A., M. J. Blunt, and A. P. V. Roberts (1997). Micromodel Observation of the Role of Oil Layers in Three-Phase Flow. *Transport in Porous Media* 26(3), 277–297.
- Kulkarni, M. and D. Rao (2006a, November). Analytical Modeling of the Forced Gravity Drainage GAGD Process. San Francisco, California.
- Kulkarni, M., A. Sharma, and D. Rao (2005, August). Use of Dimensional Analysis for Scaling Immiscible Gas Assisted Gravity Drainage (GAGD) Experiments. In *SCA2005-50*, Toronto, Canada.
- Kulkarni, M. M. and D. N. Rao (2006b). Characterization of Operative Mechanisms in Gravity Drainage Field Projects Through Dimensional Analysis. In *SPE Annual Technical Conference and Exhibition*, SPE. Society of Petroleum Engineers.
- Kva^Lseth, T. O. (1983, January). Note on the R² measure of goodness of fit for nonlinear models. *Bulletin of the Psychonomic Society* 21(1), 79–80.
- Lenormand, R. and C. Zarcone (1984). Role Of Roughness And Edges During Imbibition In Square Capillaries. In *SPE Annual Technical Conference and Exhibition*, SPE. Society of Petroleum Engineers.
- Lenormand, R., C. Zarcone, and A. Sarr (1983). Mechanisms of the displacement of one fluid by another in a network of capillary ducts. *Journal of Fluid Mechanics* 135(-1), 337–353.
- Lewis, J. O. (1944). Gravity Drainage in Oil Fields. *Transactions of the AIME* 155(01), 133–154.
- Li, K. and R. N. Horne (2003). Prediction of Oil Production by Gravity Drainage. In *SPE Annual Technical Conference and Exhibition*, SPE. Society of Petroleum Engineers.
- Li, K. and R. N. Horne (2008). Modeling of oil production by gravity drainage. *Journal of Petroleum Science and Engineering* 60(3–4), 161–169.

- Maeda, H. and K. Okatsu (2008). EOR Using Thin Oil Film Drainage Mechanism In Water Wet Oil Reservoir. In *SPE Asia Pacific Oil and Gas Conference and Exhibition*. Society of Petroleum Engineers.
- Mahmoud, T. and D. N. Rao (2008). Range of Operability of Gas-Assisted Gravity Drainage Process. In *SPE Symposium on Improved Oil Recovery*, SPE. Society of Petroleum Engineers.
- Marx, J. (1956, January). Determining Gravity Drainage Characteristics on the Centrifuge. *SPE-545-G*.
- MATLAB (2018). Evaluating Goodness of Fit - MATLAB & Simulink.
- Matthews, C. and H. Lefkovits (1956, January). Gravity Drainage Performance of Depletion-Type Reservoirs in the Stripper Stage. *SPE-665-G-P*.
- Nenniger, E. and J. A. Storrow (1958). Drainage of packed beds in gravitational and centrifugal-force fields. *AIChE Journal* 4(3), 305–316.
- Oliviera, I. B., A. H. Demond, and A. Salehzadeh (1996). Packing of sands for the production of homogeneous porous media. *Soil Science Society of America Journal* 60(1), 49–53.
- Oren, P., J. Billiotte, and W. Pinczewski (1992). Mobilization of Waterflood Residual Oil by Gas Injection for Water-Wet Conditions. *SPE Formation Evaluation* 7(01), 70–78.
- Oren, P. and W. Pinczewski (1994). The Effect of Wettability and Spreading on the Recovery of Waterflood Residual Oil by Immiscible Gasflooding. *SPE Formation Evaluation* 9(02), 149–156.
- Oren, P.-E. (1994). Pore-Scale Network Modelling of Waterflood Residual Oil Recovery by Immiscible Gas Flooding. In *SPE/DOE Improved Oil Recovery Symposium*, SPE. Society of Petroleum Engineers.
- Paidin, W. R. and D. N. Rao (2007, September). Physical Model Experiments to Evaluate the Effect of Wettability and Fractures on the Performance of the Gas Assisted Gravity Drainage (GAGD) Process. In *SCA2007-48*, Calgary.
- Parsaei, R. and I. Chatzis (2011). Experimental Investigation of Production Characteristics of the Gravity-Assisted Inert Gas Injection (GAIGI) Process for Recovery of Waterflood Residual Oil: Effects of Wettability Heterogeneity. *Energy & Fuels* 25(5), 2089–2099.
- Pereira, G. G., W. V. Pinczewski, D. Y. C. Chan, L. Paterson, and P. E. Øren (1996). Pore-scale network model for drainage-dominated three-phase flow in porous media. *Transport in Porous Media* 24(2), 167–201.
- Rao, D., S. Ayirala, M. Kulkarni, and A. Sharma (2004). Development of Gas Assisted Gravity Drainage (GAGD) Process for Improved Light Oil Recovery. In *SPE/DOE Symposium on Improved Oil Recovery*, SPE. Society of Petroleum Engineers.

- Ren, W., R. Bentsen, and L. Cunha (2004). Pore-Level Observation of Gravity-Assisted Tertiary Gas-Injection Processes. *SPE Reservoir Evaluation & Engineering* 7(03), 194–201.
- Ren, W., R. Bentsen, and L. Cunha (2005). A Study of the Gravity Assisted Tertiary Gas Injection Processes. *Journal of Canadian Petroleum Technology* 44(02).
- Ribe, J. M., S. Nils R., K. Ole-Andreas K., H. Armend G., B. Henrik, and S. Bjorn T. (2016, July). Simple and Low-cost Contact Angle Measurements Using a Smartphone with a PDMS-Lens – Chips and Tips.
- Richmond, P., B. W. Ninham, and R. H. Ottewill (1973, October). A theoretical study of hydrocarbon adsorption on water surfaces using Lifshitz theory. *Journal of Colloid and Interface Science* 45(1), 69–80.
- Rostami, B., R. Kharrat, M. Pooladi-Darvish, and C. Ghotbi (2010). Identification of Fluid Dynamics in Forced Gravity Drainage Using Dimensionless Groups. *Transport in Porous Media* 83(3), 725–740.
- Sadati, S. E. and R. Kharrat (2013). The Scaling of the Gas-assisted Gravity Drainage Process Using Dimensionless Groups. *Energy Sources, Part A: Recovery, Utilization, and Environmental Effects* 35(2), 164–172.
- Schechter, D. and B. Guo (1996). Mathematical Modeling of Gravity Drainage After Gas Injection into Fractured Reservoirs. In *Permian Basin Oil and Gas Recovery Conference*, SPE. Society of Petroleum Engineers.
- Seed, B. (2001). Silanizing Glassware. In *Current Protocols in Cell Biology*. John Wiley & Sons, Inc. DOI: 10.1002/0471143030.cba03es08.
- Sharma, A. and D. N. Rao (2008). Scaled Physical Model Experiments to Characterize the Gas-Assisted Gravity Drainage EOR Process. In *SPE Symposium on Improved Oil Recovery*, SPE. Society of Petroleum Engineers.
- Skurdal, H., O. St. Hustad, and T. Holt (1995). Oil Recovery by Gravity Drainage during Gas Injection. In *IOR 1995 - 8th European Symposium on Improved Oil Recovery*, Vienna, Austria. EAGE Publications BV.
- Sohrabi, M., D. Tehrani, A. Danesh, and G. Henderson (2004). Visualization of Oil Recovery by Water-Alternating-Gas Injection Using High-Pressure Micromodels. *SPE Journal* 9(03), 290–301.
- Soll, W. E., M. A. Celia, and J. L. Wilson (1993). Micromodel studies of three-fluid porous media systems: Pore-scale processes relating to capillary pressure-saturation relationships. *Water Resources Research* 29(9), 2963–2974.
- Spieß, A.-N. and N. Neumeyer (2010, June). An evaluation of R2 as an inadequate measure for nonlinear models in pharmacological and biochemical research: a Monte Carlo approach. *BMC Pharmacology* 10, 6.

- Stahl, R. F., W. Martin, and R. Huntington (1943). Gravitational Drainage of Liquids from Unconsolidated Wilcox Sand. *Transactions of the AIME* 151(01), 138–146.
- Takii, T. and Y. H. Mori (1993, November). Spreading Coefficients of Aliphatic Hydrocarbons on Water. *Journal of Colloid and Interface Science* 161(1), 31–37.
- Terwilliger, P., L. Wilsey, H. N. Hall, P. Bridges, and R. Morse (1951). An Experimental and Theoretical Investigation of Gravity Drainage Performance. *Journal of Petroleum Technology* 3(11), 285–296.
- Thanh-Khac Pham, D. and G. J. Hirasaki (1998). Wettability/spreading of alkanes at the water–gas interface at elevated temperatures and pressures. *Journal of Petroleum Science and Engineering* 20(3–4), 239–246.
- Vizika, O. (1993, April). Effect of the spreading coefficient on the efficiency of oil recovery with gravity drainage. In *Proceeding of Symposium on Enhanced Oil Recovery, presented before Division of Petroleum Chemistry, Inc., American Chemical Society, Denver, CO*.
- Vizika, O. and J.-M. Lombard (1996). Wettability and Spreading: Two key Parameters in Oil Recovery With Three-Phase Gravity Drainage. *SPE Reservoir Engineering* 11(01), 54–60.
- Vizika, O., E. Rosenberg, and F. Kalaydjian (1998). Study of wettability and spreading impact in three-phase gas injection by cryo-scanning electron microscopy. *Journal of Petroleum Science and Engineering* 20(3–4), 189–202.
- Zhou, D. and M. Blunt (1997). Effect of spreading coefficient on the distribution of light non-aqueous phase liquid in the subsurface. *Journal of Contaminant Hydrology* 25(1), 1–19.
- Øren, P. E. and W. Pinczewski (1991). The effect of film-flow on the mobilization of waterflood residual oil by gas flooding. In *IOR 1991 - 6th European Symposium on Improved Oil Recovery*. EAGE Publications BV.
- Øren, P. E. and W. V. Pinczewski (1995). Fluid distribution and pore-scale displacement mechanisms in drainage dominated three-phase flow. *Transport in Porous Media* 20(1-2), 105–133.

Appendix A

Program Codes for Schechter-Guo Model

```
1 %Another way to code Schechter and Guo 1996 Eq.5
2 %1/21/2017 Modify for 20/40 FFGD
3 clear all
4 close all
5 % Set global variables
6
7 global Fs theta hd soi sor
8
9 % Model parameters
10 Fs=3100;
11 theta=0.386740331;
12 hd=0.1;
13 soi=0.804761905;
14 sor=0.123809524;
15 td_fgd=csvread('td_fgd.csv');
16 recovery_fgd=csvread('recovery_fgd.csv');
17
18 % Initial conditions
19
20 dt = input("Give time step size: ");          %Usually 1e-4
21 T = input("Give time simulation ends (dimensionless): "); %
    Usually 10
22 zd0 = 0;
23 zdnew=1;
24 R=0;
25
26 N_t = floor(T/dt);
27 u = zeros(N_t+1, 1);
28 t = linspace(dt, N_t*dt, length(u));
29 u(1) = zd0;
30 for n = 1:N_t
31 u(n+1) = u(n) + dt*@func_dzdt2(u(n), n);
32
33 R=(1-sor/soi).*u .-(2 .*u/(3*soi)).*sqrt((Fs*theta.*u)/(5 .*n)
    );
34 end
35 sol = u;
36 time = t;
37 zdnew=[1 .-sol];
38
39
40 % Plot results
```

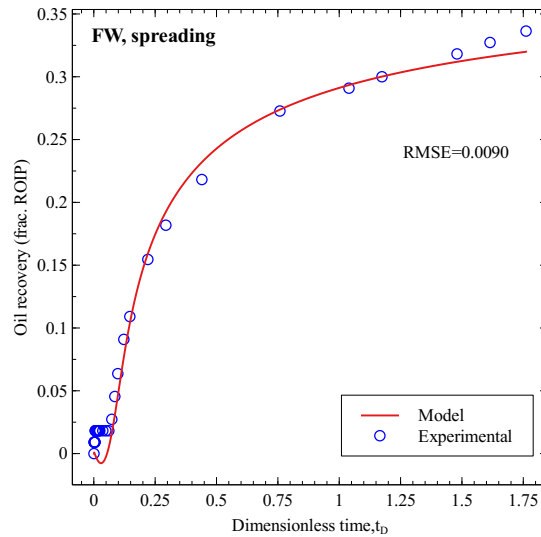


```

41 graphics_toolkit("gnuplot");
42 hold on
43 figure( 1 )
44 semilogx(time,zdnew,' b ') ;
45 semilogx(time,R,' r ') ;
46 semilogx(td_fgd,recovery_fgd,'g*','markersize',3);
47 xlabel (' Dimensionless time,t_{D} ') ;
48 ylabel ('1-z_{D}') ;
49 title (' Demarcator equation ') ;
50
51 %Save functions
52 filestem = 'Schechter_Guo_1996_v7_fgd';
53 print(filestem, '-dpng'); print(filestem, '-dpdf');

```

When using this model care must be exercised in selecting the tuning parameters for matching with experimental data. Initially the author used only two parameters, F_s and H_D . This worked for matching the model to most experiments. However problem arose when matching experimental data from tertiary GAGD experiment under fractional-wet, spreading system. We obtained the figure below which shows unphysical oil production at early time. Only after using three parameters F_s, H_D , and S_{oi} were we able to obtain satisfactory result from this particular experiment.



Appendix B

Program Codes for Dykstra Model

```

1      % Main script file to demonstrate Dykstra (1978) Eq. 21
      and Eq. 24
2      % Plot demarcator over time and recovery over time
3      %Use parameters for free-fall gravity drainage 50/70
4
5      clear all
6      close all
7
8      % Set global variables
9      global theta si sr rho kabs krsi g mu B H L Boi Bo
10
11     %Use data from experiment 50/70 free-fall GD
12     theta=0.346224678;          %porosity
13     si=0.936170213;             %So initial
14     sr=0.393617021;             %So residual
15     rho=0.734;                  %density of displaced phase (
      oil), g/cm3
16     kabs=6.91E-08;              %Abs perm,cm2
17     krsi=0.57;                  %Kro @ Swi
18     g=980;                      %gravity constant 980 cm/s2
19     mu=0.0084;                  %viscosity of displaced phase
      (oil), g/cm.s
20     B=2;                        %exponent in relperm r/ship
21     H=3;                        %equilibrium height of
      capillary rise, cm
22     L=30;                       %length of column
23     Boi=Bo=1;                   %oil FVF
24     t_fgd=csvread('t_fgd.csv');
25     recovery_fgd=csvread('recovery_fgd.csv');
26     recovery_in_percent_fgd=100 .*recovery_fgd;
27     %recovery2_ffgd=csvread('recovery2_ffgd.csv');
28
29     % Initial conditions
30
31     dt = input("Give time step size (in seconds): ");
32     T = input("Give time simulation ends (in seconds): ");
33     zd0 = 0;
34
35     [zd,zdnew,R,t] = dykstra2(zd0, dt, T);
36
37     % Plot functions
38     graphics_toolkit("gnuplot");

```

```

39 semilogx(t, zdnew, 'b-',t,R,'r--');
40 hold on
41 %semilogx(t_ffgd, recovery_ffgd, 'g-',t_ffgd,
    recovery2_ffgd,'m-');
42 semilogx(t_fgd, recovery_in_percent_fgd, 'g*', 'markersize '
    ,3);
43 xlabel ('Drainage time (seconds)') ;
44 ylabel ('Demarcator height (cm)') ;
45 title (' Dykstra Demarcator equation ') ;
46 legend('Gas-oil interface','Recovery','location','
    northeast');
47
48 %save results for plotting in veusz
49 csvwrite('recovery_model_50_70_fgd.csv',R);
50 csvwrite('model_time_50_70_fgd.csv',t);
51 csvwrite('demarcator_50_70_fgd.csv',zdnew);
52
53 %Save functions
54 filestem = 'demo_dykstra2_50_70_fgd';
55 print(filestem, '-dpng'); print(filestem, '-dpdf');

```

```

1 %Function call to Dykstra (1978)
2 %Includes Eq.21 and Eq.24
3 %Code use Euler method to step forward in time.
4 %To call function: [zd,zdnew,t] = dykstra(zd0, dt, T)
5 %Typically zd0=0,dt=1 (secs), T=10k to 100k (secs)
6
7 function [zd,zdnew,R,t] = dykstra2(zd0, dt, T)
8
9 % Set global variables
10 global theta si sr rho kabs krsi g mu B H L Boi Bo
11
12 N_t = floor(T/dt);
13 zd = zeros(N_t+1, 1);
14 R = zeros(N_t+1, 1);
15 t = linspace(dt, N_t*dt,length(zd));
16
17 % Initial condition
18 zd(1) = zd0;
19 R(1) = [0];
20 zdnew(1)=[L]; %Set initial zd to height of column or
    formation
21
22
23 % Step equations forward in time

```

```

24     for n = 1:N_t
25         zd(n+1) = zd(n) + dt*@func_dzdyk(zd(n), n);
26         R(n+1)=100*@func_recov_dyk(zd(n),n);
27         zdnew(n+1)=zdnew(1)-zd(n+1);
28     end
29 end

```

```

1 function dz = func_dzdyk(zd,t)
2
3 %Eq. 21 of Dykstra 1978 "The Prediction of Oil Recovery by
4   Gravity
5 %Drainage"
6 %zd is not dimensionless.Its unit is cm; t is also no
7   dimensionless.
8 %t is in seconds
9
10 %Declare global variables.
11
12 global theta si sr rho kabs krsi g mu B H L
13
14 %theta=porosity (dimensionless)
15 %si=initial saturation of the displaced phase (dimensionless)
16 %sr=residual saturation of the displaced phase (dimensionless)
17 %rho=density of the displaced phase (g/cm3)
18 %g=gravity acceleration (980 cm/s2)
19 %kabs=absolute permeability of rock (cm2)
20 %krsi=end point rel perm of displaced phase at initial
21   saturation
22 % Kro @ Swir
23 %mu=viscosity of displaced phase (cp or g/cm.sec)
24 %B=exponent in relative permeability equation
25 %H=equilibrium height of capillary rise (cm)
26 %L=length of draining column or formation (cm)
27 %For three phase - replace sr with sor, introduce swc
28
29 ptheta=theta*(1-sr); %Eq. 9a for 2 phase
30 %ptheta=theta*(1-sor-swc) %Eq. 9b for 3 phase.
31   Uncomment to use
32
33 m=mu*ptheta/(B*kabs*rho*g); %Eq. 20
34 n=rho*g*kabs/(mu*ptheta); %constants in Eq. 21
35 o=(1-H/(L.-zd)); %First term, numerator,
36   in Eq. 21
37 p=m.*zd/t; %Second term, num and
38   den, in Eq. 21

```

```

33 q=B/(B-1);
34 r=1/(B-1);
35
36 dz=n.*((krsi.*o.-p.^q)/(si.-p.^r));      %Eq. 21
37
38
39
40 end

```

```

1  function R = func_recov_dyk(zd,t)
2
3  %Eq. 24 of Dykstra 1978 "The Prediction of Oil Recovery by
4  Gravity
5  %Drainage"
6  %zd is not dimensionless.Its unit is cm; t is also no
7  dimensionless.
8  %t is in seconds
9
10 %Declare global variables.
11
12 global theta si sr rho kabs krsi g mu B H L Boi Bo
13
14 %theta=porosity (dimensionless)
15 %si=initial saturation of the displaced phase (dimensionless)
16 %sr=residual saturation of the displaced phase (dimensionless)
17 %rho=density of the displaced phase (g/cm3)
18 %g=gravity acceleration (980 cm/s2)
19 %kabs=absolute permeability of rock (cm2)
20 %krsi=end point rel perm of displaced phase at initial
21 saturation
22 % Kro @ Swir
23 %mu=viscosity of displaced phase (cp or g/cm.sec)
24 %B=exponent in relative permeability equation
25 %H=equilibrium height of capillary rise (cm)
26 %L=length of draining column or formation (cm)
27 %Boi,Bo=initial and current displaced phase formation volume
28 factor
29 %For three phase - replace sr with sor, introduce swc
30
31 ptheta=theta*(1-sr);      %Eq. 9a for 2 phase
32 %ptheta=theta*(1-sor-swc) %Eq. 9b for 3 phase.
33     Uncomment to use
34
35 m=mu*ptheta/(B*kabs*rho*g);      %Eq. 20
36 a=1-Boi*sr/(si*Bo);      %First term in Eq. 24

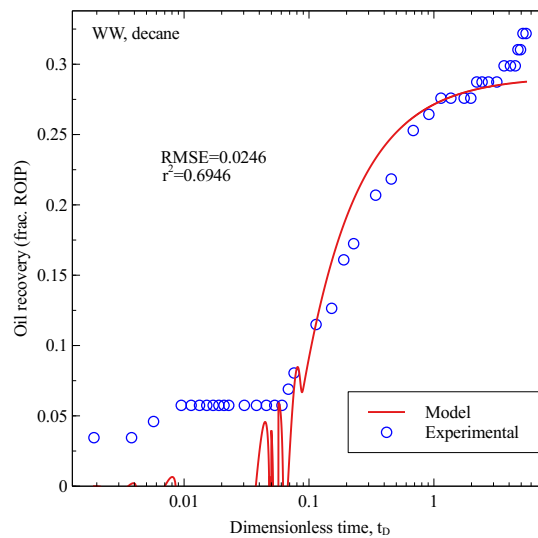
```

```

32 b=Boi/si*(1-sr)/Bo*((B-1)/B);           %Second term Eq. 24
33 c=m.*zd/t;                               %Third term Eq. 24
34 %q=B/(B-1);
35 d=1/(B-1);
36
37 R=zd/L.*(a-b.*c.^d);                     %Eq. 24
38
39
40
41 end

```

In Dykstra model initially we solved the expression for Z_d using Euler's method before calculating the oil recovery, R . When *lsqcurvefit* function from MATLAB is used for matching to experimental data this resulted in unphysical behavior in early time as shown in figure below. To eliminate the fluctuations we solved the nonlinear ordinary differential equation using MATLAB's built-in *ode45* or *ode113* solver before using *lsqcurvefit*.



Appendix C

Program Codes for Li-Horne Model

```

1 %Demo of Eq. 2 from Li & Horne 2003 and 2008 "Modeling of oil
  production
2 %by gravity drainage
3 %Use leasqr function to find Sor average and beta
4 %Use for free-fall drainage 50_70 sand
5 clear,clc
6 t=csvread('t_fgd.csv'); %load time data in csv
  format
7 recovery=csvread('recovery_fgd.csv'); %load recovery data in
  csv format
8 global swi
9 swi=0.063829787; %initial water saturation or
  connate water
10 p=[0.1 0.1]; %initial guess for sor average
  and beta
11
12 function r=ffun_r(t,p) %fitting function (from Eq.2
  in the paper)
13 global swi
14 r=((1-swi-p(1))./(1-swi)).*(1.-exp(-p(2).*t));
15 end
16
17 pkg load optim; %initialize optim package (octave) to use
  leasqr function
18
19 [yfit pfit cvg iter r2]=leasqr(t,recovery,p,"ffun_r");
20
21 %write results in csv data - for plotting later in veusz
22 %csvwrite('model_time_fgd.csv',t);
23 %csvwrite('recovery.csv',recovery);
24 %csvwrite('model_recovery_fgd.csv',yfit);
25
26 %plot results within octave
27 cvg, iter, pfit,r2
28 plot(t,recovery,'r*',t,yfit,'b-');
29 xlabel('Time (seconds)');
30 ylabel('Recovery (fraction OOIP)');
31 legend('Experiment','Model')
32
33 %save plot with the specified name
34 %filestem = 'Li_Horne_2008_50_70_fgd';
35 %print(filestem, '-dpng'); print(filestem, '-dpdf');

```

```
36 |%print(filestem, '-dsvg');
```


Vita

Iskandar Dzulkarnain, son of Dzulkarnain Abdullah and Rashidah Ismail was born in 1984 in the state of Johore, south of Malaysia. He started his B.Eng study in Electrical and Electronics Engineering at University of Technology PETRONAS and obtained his diploma in 2007. He continued his study in Petroleum Engineering through the joint-degree program offered by University of Technology PETRONAS and Heriot-Watt University and graduated with M.S. in 2010. He worked as a lecturer in the same university before joining the doctoral program in 2013 in Craft and Hawkins Department of Petroleum Engineering at Louisiana State University. He is expected to receive his degree of Doctor of Philosophy in Petroleum Engineering in December 2018.